Exploring the Role of ZnT8 in Islet Beta Cell Function and Type 2 Diabetes

By

Kristen Elizabeth Syring

Dissertation

Submitted to the Faculty of the

Graduate School of Vanderbilt University

in partial fulfillment of the requirements

for the degree of

DOCTOR OF PHILOSOPHY

in

Molecular Physiology and Biophysics

August 11, 2017

Nashville, Tennessee

Approved:

Owen P. McGuinness, Ph.D. (Chair)

Maureen A. Gannon, Ph.D.

David A. Jacobson, Ph.D.

Douglas P. Mortlock, Ph.D

ACKNOWLEDGMENTS

To begin, I must first thank the members of the O'Brien lab, both past and present for not only contributing to the work, but for the continuous support as well. I cannot thank Ken Oeser enough for his help with everything in the lab, for all the experiments and for the countless genotyping reactions. He has provided endless hours of entertainment and become a true friend. Ken was a constant reminder of the amazing places that need to be explored outside of the lab, and I will truly miss working with him. Next, to thank Karin Bosma, thank you for your listening ear, support, and help for the last two years and especially during this stressful time. Finally, I need to thank Kayla Boortz for her support and friendship. Graduate school and the O'Brien lab would not have been the same without her there to listen to me complain, answer my questions, and try to keep me calm. I have truly missed her this last year, but am grateful for her continued friendship from afar.

I also need to thank the cores and collaborators at Vanderbilt that contributed to this work, specifically the Vanderbilt Hormone Assay and Analytical Services Core, Cell Imaging Shared Resource Electron Microscopy Core, and the Islet Procurement and Analysis Core. Our collaborations with the laboratories of Dr. Maureen Gannon, Dr. David Jacobson, Dr. Owen McGuinness, Dr. Dave Piston, Dr. Alvin Powers, and Dr. Masa Shiota were essential to the completion of this dissertation. I thank the members of these labs for their contributions to the experiments and for their expertise.

I would also like to thank the members of my thesis committee. The time, critiques and advice you generously offered over the past 4 years pushed me to become a better scientist and to think more critically about my work and my words.

Thank you to the MPB department students, staff, and faculty. Being a member of this collaborative and social department has made these last 4 years truly enjoyable. I will miss the happy hours, holiday parties, field days, and coffee hours. A special thank you to Colette Bosley for providing

support and a much-needed friendly smile to brighten my day. Thank you to both Colette and Karen Gieg for your help throughout this process, making scheduling, planning and paperwork so much easier.

Finally, at Vanderbilt, I need to thank Richard, without whom none of this would be possible. I cannot begin to express my gratitude for the endless hours and effort that Richard dedicated to my project. I am a better scientist, speaker, and writer because of the time that he took to let me learn under his guidance. He has attempted to make me a relentless optimist, taught me the importance of work-life balance, and taught me that a sense of humor truly is the best medicine. Thank you for creating a challenging environment in which to learn, but always giving me the encouragement and confidence I needed to succeed.

Lastly, I want to express my immense appreciation to my friends and family for their support and encouragement. Thank you to my friends that have supported me for the past 5 years. Although not all of them knew exactly what I was talking about, I always had someone to listen and to lean on during stressful times. I am so grateful for the dear friends that I met while here. I am especially grateful that I sat with Shilpy Dixit and Christi Gurniak that first week of IGP. These two make me a better scientist and a better person. I am so fortunate to have made lifelong friends during this time.

I am beyond grateful to my family. To my parents, Mary and Kevin, and my siblings, Colleen, Brian, Megan, Kaitlyn, Jessica, and Matt, thank you for your support over the course of this 5-year experience. Knowing that I have your unwavering support has made this process much easier. I cannot even begin to express what your love and support has meant to me. Thank you for allowing me to go after my goals at every stage of life. Although this process has not always been easy, my family has made the highs higher and the hard times a little easier. They have comforted me during the stressful points and helped me celebrate the victories. Thank you for never giving up on me even when I may have doubted myself.

ACKNOWLEDGMENT OF SUPPORT

Funding for this research has been provided to Dr. O'Brien through the National Institute of Health (grant number DK92589). I have been supported by the Molecular Endocrinology Training Grant (NIH 5T32 DK07563). Research from collaborating laboratories were supported by the following grants: O.P.M.: DK043748 and DK078188 and D.W.P.: DK085064. The Vanderbilt Hormone Assay and Analytical Services Core, Islet Procurement and Analysis Core and Cell Imaging Shared Resource are all supported by the NIH Grant P60 DK20593 (to the Vanderbilt Diabetes Research Training Center) and the NIH Grant DK59637 (to the Vanderbilt Mouse Metabolic Phenotyping Center).

TABLE OF CONTENTS

Page

ABBREVIATIONS

ABHD6	α/β-hydrolase domain-containing 6
ADP	Adenosine diphosphate
AMPK	Adenosine monophosphate -activated protein kinase
ATF6	Activating Transcription Factor 6
ATP	Adenosine triphosphate
BCS	Beta cell-specific
cAMP	Cyclic adenosine monophosphate
CHOP	C/EBP homologous protein
CICR	Calcium-induced calcium release
CLEC16 A	C-type lectin domain family 16 member A
CRE^{ERT2}	Cre recombinase fused to the modified estrogen receptor
CTLA4	Cytotoxic T-lymphocyte-associated protein 4
DB/DB	Leptin receptor deficient mouse model
DDP4	Dipeptidyl peptidase 4
DKA	Diabetic ketoacidosis
DM	Diabetes mellitus
EPAC2	Exchange protein activated by cAMP2
ER	Endoplasmic reticulum
ERAD	ER-associated protein degradation
ERK	Extracellular signal-regulated kinase
FBG	Fasting blood glucose
FPI	Fasting plasma insulin
G6P	Glucose-6-phosphate

G6Pase	Glucose-6-phosphatase
GAD 65	Glutamic acid decarboxylase
GCK	Glucokinase
GDM	Gestational diabetes mellitus
GIP	Glucose-independent insulintropic polypeptide
GLP-1	Glucagon-like peptide 1
GSIS	Glucose-stimulated insulin secretion
GWAS	Genome-wide association study
HbA1c	Hemoglobin A1c
HET	Heterozygous
HFD	High-fat diet
HGP	Hepatic glucose production
HLA	Human leukocyte antigen
HNF1A	Hepatic nuclear factor 1A
HNF1B	Hepatic nuclear factor 1B
HNF4A	Hepatic nuclear factor 4A
IBMX	3-isobutyl-1-methylxanthine
ICA	Islet cell autoantibody
IGRP	Islet-specific glucose-6-phosphatase catalytic subunit-related protein
IL-1β	Interleukin 1β
IL-6	Interleukin 6
IL2Rα	Interleukin 2 receptor α
IPGTT	Intraperitoneal glucose tolerance test
IR	Insulin receptor

IRE1	Inositol-requiring kinase-1
IRS1	Insulin receptor substrate 1
IRS2	Insulin receptor substrate 2
ITT	Insulin tolerance test
JNK	c-Jun N-terminal kinase
KO	Knockout
KOMP	Knockout Mouse Project
MAG	Monoacylglycerol
MAPK	Mitogen-activated protein kinase
MODY	Maturity onset diabetes of the young
mTOR	Mammalian target of rapamycin
NADPH	Nicotinamide adenine dinucleotide phosphate
NDM	Neonatal diabetes mellitus
Neo	Neomycin
NOD	Non-obese diabetic
NPY	Neuropeptide Y
OB/OB	Leptin deficient mouse model
OGTT	Oral glucose tolerance test
ORF	Open reading frame
PEPCK	Phosphoenol pyruvate carboxykinase
PERK	PKR-like ER kinase
PI3K	Phosphatidyl inositol 3’-kinase
PKA	Protein kinase A
PKC	Protein kinase C
PNDM	Permanent neonatal diabetes mellitus

POMC	Pro-opiomelanocortinergic
PPARγ	Peroxisome proliferator-activated receptor gamma
PPRE	PPARγ response elements
PTPN2	Protein tyrosine phosphatase nonreceptor type 2
PTPN22	Protein tyrosine phosphatase nonreceptor type 22
RIDD	Regulated IRE1-dependent decay
RIP	Rat Insulin promoter
ROS	Reactive oxygen species
RRP	Readily releasable pool
rtTA	Reverse tetracycline-dependent transactivator
RyR	Ryanodine receptor
S6K1	S6 kinase-1
SERCA	Sarco/endoplasmic reticulum calcium-ATPase
SGLT2	Sodium-glucose co-transporter 2
SH2B3	SH2B adaptor protein 3
SNP	Single nucleotide polymorphism
SOD	Super oxide dismutase
STZ	Streptozotocin
T1D	Type 1 diabetes mellitus
T2D	Type 2 diabetes mellitus
TCA	Tricarboxylic acid cycle
TK	Thymidine kinase
TNDM	Transient neonatal diabetes mellitus
TNFα	Tumor necrosis factor-α
TZD	Thiazolidinediones

UBASH3A	Ubiquitin associated and the SH3 domain containing A
UCP2	Uncoupling protein
WT	Wild type
ZIP	Zinc Influx Transporters
ZnT	Zinc Transporter
ZnT8	Zinc Transporter 8
ZnT8BKO	Zinc Transporter beta cell-specific knockout

LIST OF TABLES

LIST OF FIGURES

CHAPTER I

INTRODUCTION

Islet Structure and Function

The pancreas is comprised of endocrine and exocrine tissue. The exocrine tissue, which accounts for about 98% of the pancreas, is mainly responsible for release of digestive enzymes into the small intestines [9]. The endocrine tissue, the remaining 2%, is organized into islet of Langerhans structures. Within these islets, there are several endocrine cell types: beta, alpha, delta, epsilon and gamma cells, formerly known as PP cells. In humans, beta cells represent approximately 70% of the islet, alpha cells comprise 20%, delta cells are less than 10%, epsilon less than 1% and gamma cells less than 5% [10]. Each cell type produces a specific hormone that is released in response to secretagogues in the blood [10]. Beta cells produce and secrete insulin under high blood glucose conditions, stimulating blood glucose uptake and inhibiting hepatic glucose production (HGP) [10]. Beta cell function and insulin will be discussed further in the following sections. Alpha cells secrete glucagon when blood glucose is low resulting in increased HGP through activation of glycogenolysis and gluconeogenesis. Delta cells produce somatostatin, which inhibits both glucagon and insulin secretion via a paracrine mechanism. Epsilon cells secrete ghrelin, which promotes a state of hunger in the body, acting on the hypothalamus to increase feeding. Finally, gamma cells release pancreatic polypeptide in response to high protein consumption and hypoglycemia. Ultimately, pancreatic polypeptide has effects opposite to that of ghrelin to promote satiety. Figure 1.1 illustrates the structure of the human islet. Together, the regulation of all the islet cell types and the secreted hormones aids in the maintenance of glucose homeostasis. The focus of this dissertation will be the insulin-producing beta cells.

Beta Cell Function and T2D

Insulin Structure

The *INS1* gene encodes the insulin precursor, preproinsulin, which is processed into three peptides: A, B, and C shown in Figure 1.2 [11, 12]. Following translation of the protein, the N-terminal signal

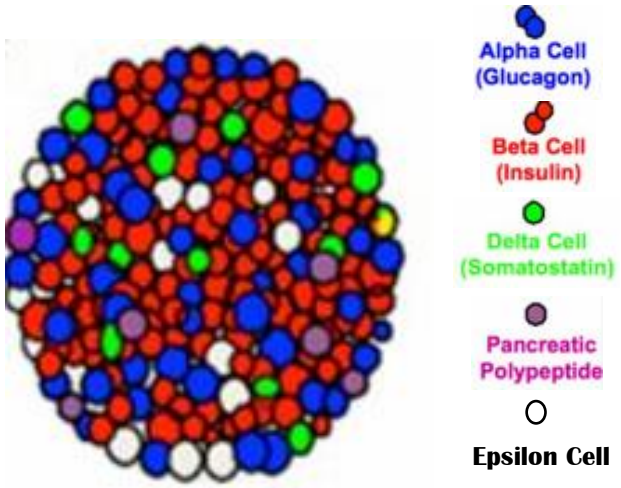

Figure 1.1 Model of human islet of Langerhans structure. Model of human pancreatic islet structure and cell type distribution. Adapted from [4].

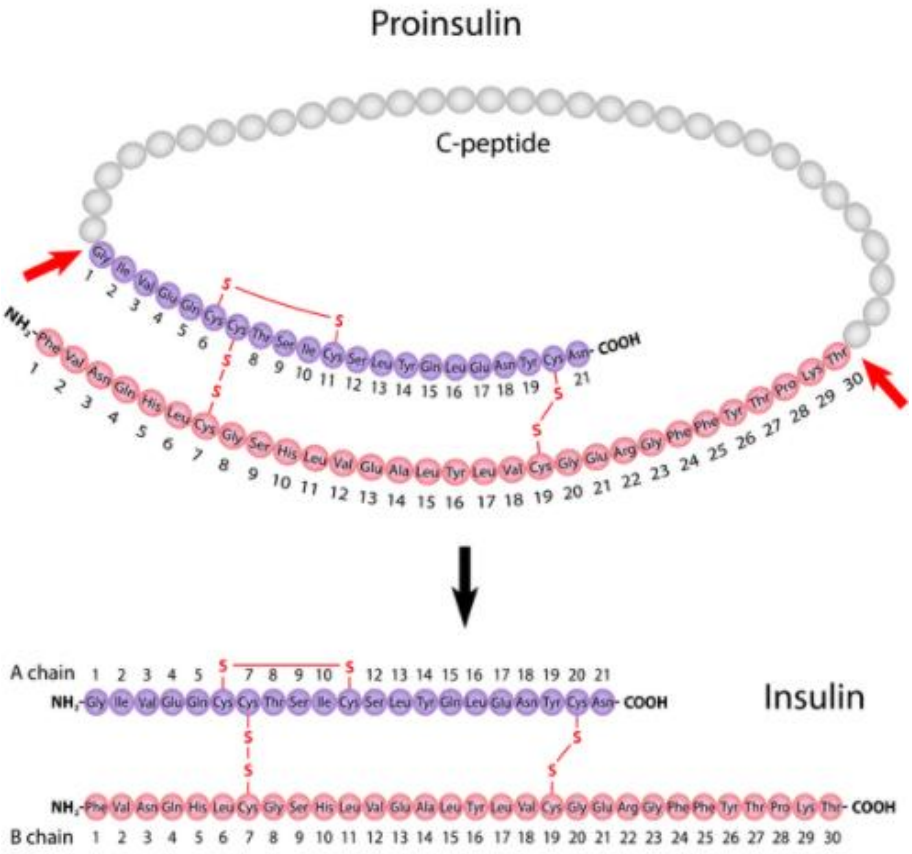

Figure 1.2 Model of proinsulin molecule. Diagram representing proinsulin and insulin molecule. The amino acid residues in the A chain are in purple, B chain in pink, and C peptide in gray. Red arrows indicate cleavage sites. Disulfide bonds link the A chain and B chain to form mature insulin molecule. Adapted from the NIH website.

peptide on the precursor allows translocation into the endoplasmic reticulum (ER) lumen [11]. After which, the signal peptide is cleaved generating proinsulin. Proinsulin is folded into a 3D structure with two disulfide bonds between the A and B peptides. Proinsulin is transported into the Golgi apparatus and finally insulin secretory vesicles where the C peptide is cleaved, resulting in a mature insulin molecule and a C peptide molecule. Insulin begins to aggregate into dimers as the concentration within the vesicle increases.

Glucose-Stimulated Insulin Secretion (GSIS)

Insulin is released from the beta cells in a glucose-dependent manner. The canonical pathway of glucose-stimulated insulin secretion (GSIS) is shown in Figure 1.3 [13]. Glucose enters the beta cell from the blood through the GLUT2 glucose transporter in rodents, GLUT1 in humans. In the cytoplasm, glucose is converted to glucose-6-phosphate (G6P) by glucokinase (GCK), which also consumes adenosine triphosphate [14]. G6P is subsequently metabolized by the mitochondria resulting in a net increase in the ATP:adenosine diphosphate (ATP:ADP) ratio. The increase in this ratio promotes the binding of ATP to the ATP-sensitive potassium channel on the plasma membrane. Binding of ATP closes the channel leading to depolarization of the plasma membrane. The change in membrane potential opens voltage-gated calcium channels. Influx of calcium through these channels and the resulting calcium-induced calcium release (CICR) from the ER leads to fusion of the insulin secretory vesicle with the plasma membrane and release of insulin into the bloodstream. Calcium promotes vesicle fusion with the plasma membrane by binding to the calcium-sensor SNARE protein, synaptotagmin. Synaptotagmin isoform III has been detected in primary islets, localizing to the insulin granules [15], [16].

Other secretagogues can also modulate insulin release, including incretins, amino acids and acetylcholine. Cyclic adenosine monophosphate (cAMP) amplifies GSIS independent of ATP-sensitive potassium channel closure. cAMP activation of protein kinase A (PKA) enhances GSIS through the phosphorylation of proteins associated with secretory mechanisms as well as enhancing CICR [17]. cAMP

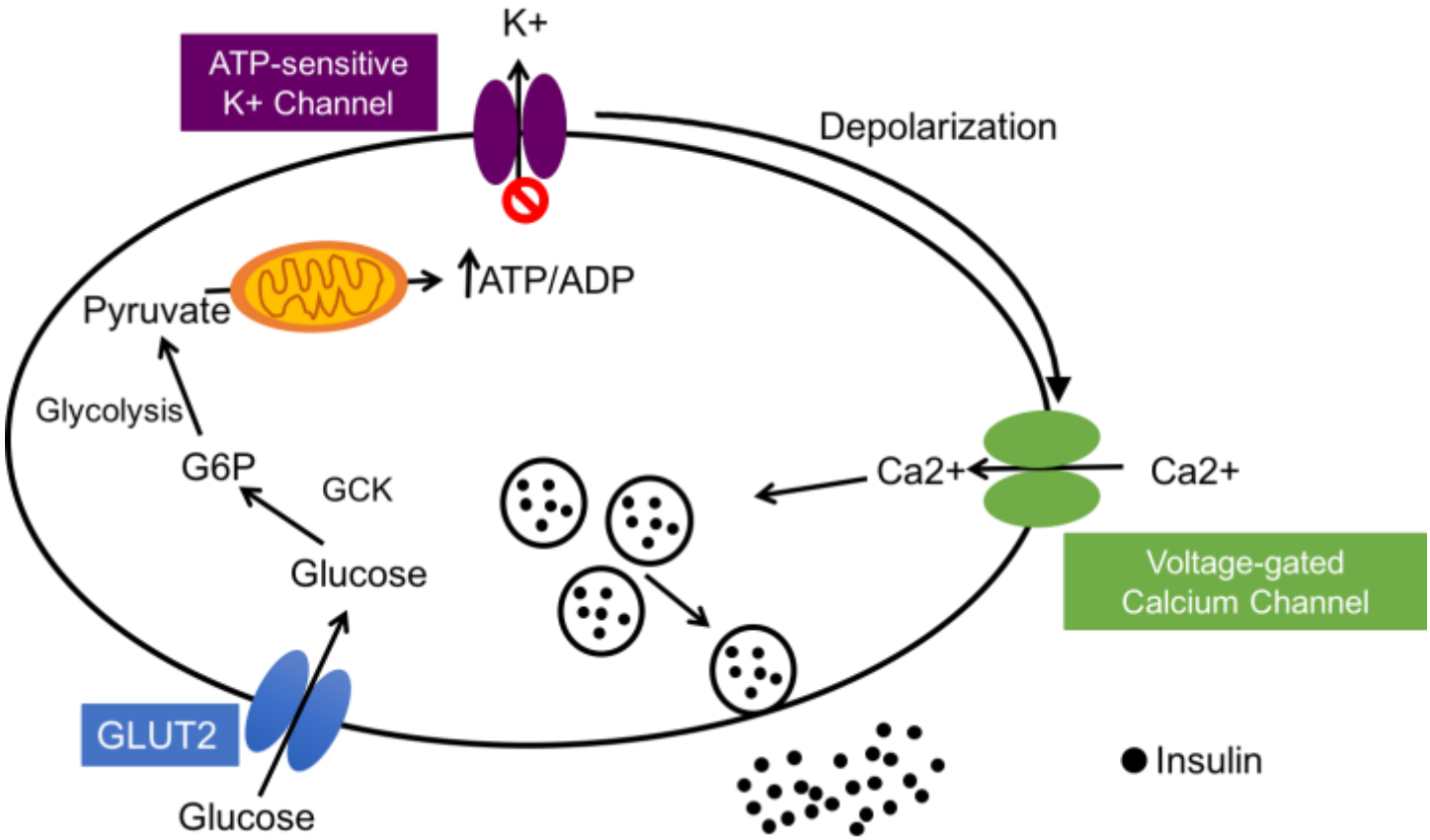

Figure 1.3 Diagram of canonical pathway of glucose-stimulated insulin secretion. Glucose enters the cell through the GLUT2 glucose transporter where once in the cell it is converted to glucose-6-phosphate (G6P) by glucokinase (GCK). G6P is then metabolized via the glycolytic pathway and TCA cycle. This increases the ATP:ADP ratio, resulting in an opening of the ATP sensitive potassium (K^+) channel, depolarization of the cell membrane, opening of the voltage-gated calcium channel, an influx of calcium (Ca^{2+}) into the cytoplasm and ultimately insulin secretion. Adapted from [2].

also enhances insulin secretion by binding with exchange protein activated by cAMP2 (EPAC2), which has been reported to stimulate CICR [18]. Additionally, EPAC2 activates Rap1, which mediates PKA-independent insulin exocytosis potentially through increasing the insulin granule pool near the plasma membrane [18]. Furthermore, EPAC2 inhibits the ATP-sensitive potassium channel (kang).

Lipolysis also plays a role in GSIS by producing an unknown signaling molecule, reviewed by Zhao *et al.* [19]. GSIS elevates monoacylglycerol (MAG) in beta cells. Inhibition or RNAi silencing of α/β-Hydrolase Domain-6-Accessible (ABHD6), a MAG lipase, increased GSIS in a beta cell-derived cell line. Increased concentrations of MAG can bind Munc13-1, a synaptic protein that regulates SNARE complex assembly, leading to Munc 13-1 translocation to the plasma membrane, and ultimately insulin granule exocytosis.

Regardless of the mechanism of release, insulin plays a major role in the maintenance of euglycemia. Therefore, dysfunction in the GSIS pathway has the potential to lead to hyperglycemia or hypoglycemia, and ultimately the development of diabetes mellitus (DM).

Insulin Signaling

Insulin is released from the beta cell into the portal bloodstream where it first encounters the liver where approximately 60% of the insulin is cleared [20]. After passage by the liver, insulin is delivered to the rest of the peripheral tissue including the metabolically important insulin-sensitive tissues, namely the brain, muscle, and adipose tissue. Insulin binds to the α subunit of its receptor, and stimulates the intrinsic tyrosine kinase activity of the β subunit of the insulin receptor (IR) resulting in autophosphorylation of multiple tyrosine residues. Autophosphorylation facilitates the recruitment of several scaffolding proteins and substrates, which are then phosphorylated, initiating the insulin signaling cascade. The two main insulin-stimulated pathways involve the activation of mitogen-activated protein kinase (MAPK) and phosphatidyl inositol 3'-kinase (PI3K) [7]. The former appears to be mainly involved in mediating effects of insulin on gene expression, cell proliferation and growth, while the latter is critical for mediating the metabolic actions of insulin, including the stimulation of glucose uptake into adipose tissue and muscle

and the suppression of HGP. A diagram showing key insulin signaling pathways can be seen in Figure 1.4. Insulin signaling at the liver, brain, muscle, and adipose tissue leads to glycolysis and protein synthesis. In the liver and muscle specifically, PI3K activation by insulin is also important for the stimulation of glycogen synthesis and decreases that rate of fatty acid oxidation [21]. It increases the rate of glucose transport across the membrane in muscle and adipose tissue [21, 22]. Insulin signaling also leads to a decreased rate of lipolysis exclusively in the adipose tissue [22]. Within the brain, specifically the hypothalamus, insulin is a satiety factor interacting with neuropeptide Y (NPY) and pro-opiomelanocortinergic (POMC) neurons [23, 24]. As explained in the next sections, defects in GSIS and insulin signaling are key aspects of type 2 diabetes (T2D).

Diabetes Mellitus

DM is a chronic disease characterized by hyperglycemia due to the inability of the pancreatic beta cells to produce and secrete sufficient insulin. Approximately 415 million people, according to the International Diabetes Federation, currently have a DM diagnosis and this figure is anticipated to reach over 640 million by 2040. 5 million deaths were associated with DM in 2015, leading to the World Health Organization prediction that DM will be the 7th leading cause of death by 2030. Complications from DM can lead to blindness, kidney failure, cardiovascular disease, and amputation [25], resulting in over $630 billion in healthcare costs. As the prevalence and cost of DM continues to rise, it is necessary to focus efforts on new treatments and new prevention methods. DM consists of a heterogeneous collection of disorders, mainly: type 1 diabetes (T1D), T2D, maturity onset diabetes of the young [26], neonatal diabetes (NDM) and gestational diabetes (GDM).

Type 1 Diabetes

T1D, previously designated juvenile diabetes or insulin-dependent diabetes, is caused by an autoimmune destruction of the insulin-producing beta cells. T1D, which develops due to genetic susceptibility in combination with unknown environmental factors, accounts for approximately 5-10% of the total DM cases in the United States [25]. The incidence of T1D cases has been increasing for

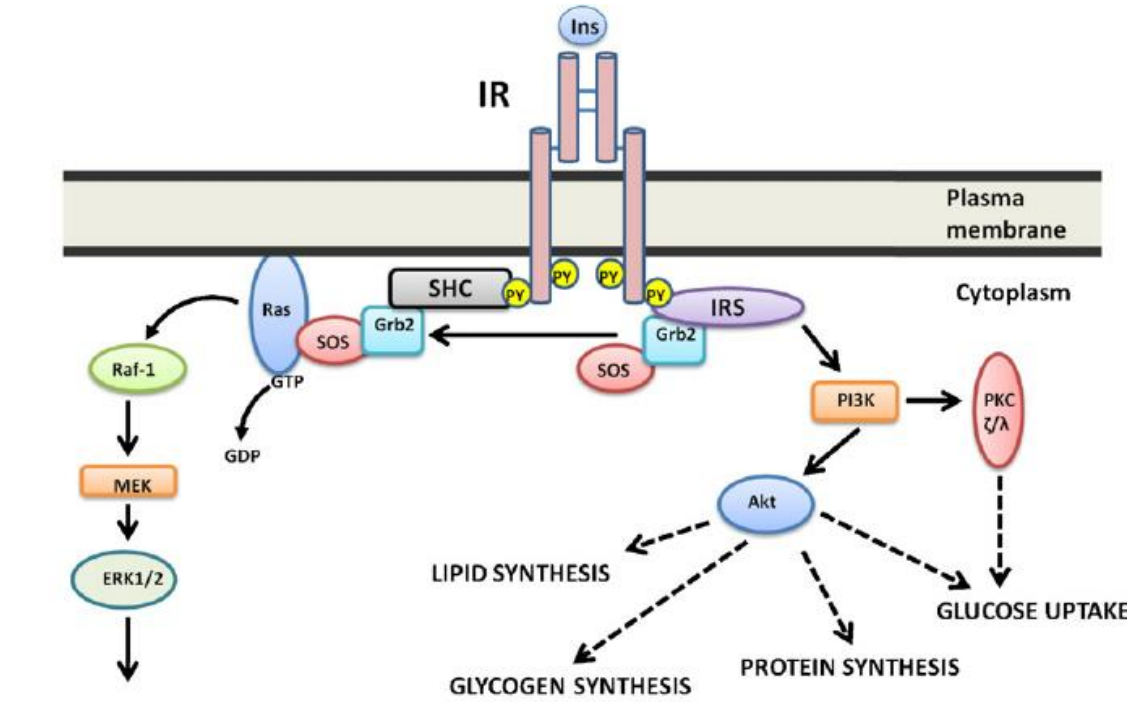

Figure 1.4 Diagram of insulin signaling pathways. Insulin binds to the α subunit of the insulin receptor (IR), stimulates the tyrosine kinase activity of the β subunit resulting in autophosphorylation of multiple tyrosine residues and the recruitment of several scaffolding proteins and substrates, which are then phosphorylated, initiating the insulin signaling cascade. The two main insulin-stimulated pathways involve the activation of mitogen-activated protein kinase (MAPK)/extracellular signal-regulated kinase (ERK) and phosphatidyl inositol 3'-kinase (PI3K) leading to cell proliferation, growth, gene expression, and metabolic actions of insulin. Adapted from [7].

several decades with approximately a 3% increase in the cases of T1D in children and teens [27]. The main symptoms of the disease are increased thirst, excessive urination, exhaustion, and hunger leading tochronic hyperglycemia. A distinguishing feature of a recent onset T1D case is the presence of autoantibodies. Autoantibodies specific to beta cell autoantigens appear in the blood and serve as markers of the disease to diagnose new patients [27]. The process of autoimmunity, once initiated, continues over months or years. Islet cell autoantibodies (ICAs) were the first identified group of autoantibodies and are targeted to multiple antigens in the islet cells [28]. More directed autoantibodies have since been discovered including those targeted to insulin, glutamic acid decarboxylase (GAD 65), islet-specific glucose-6-phosphatase catalytic subunit-related protein (IGRP) and insulinoma-associated antigen-2 [28, 29]. Most recently, autoantibodies to zinc transporter 8 (ZnT8) have been detected in newly diagnosed patients [30]. Interestingly, a non-synonymous single nucleotide polymorphism (SNP) associated with increased risk of T2D localizes to the *SLC30A8* gene encoding ZnT8. The amino acid encoded by this T2D-associated SNP, rs13266634, in the *SLC30A8* locus is a key determinant of the epitope of the ZnT8 protein targeted by the T1D-associated autoantibody [31]. This SNP is also associated with altered incidence of T1D diagnosis in children under 5 years old [30]. Overall, cytotoxic $CD8^+$ T cells and helper $CD4^+$ T cells are the principal mediators of the destruction of beta cells [32]. A role as antigen-presenting cells has been proposed for B cells during beta cell destruction. In studies of B cell depletion, the risk of diabetes is reduced [32, 33].

Although the environmental factors that lead to the development of T1D are not well understood, it is thought that after an undefined triggering event, the autoimmune destruction of the beta cells begins. When approximately 10% of the beta cell population remains, clinical symptoms manifest. The latent period in T1D progression is marked by beta cell stress and destruction and insulitis, but it is clinically silent [34]. Another distinct feature of T1D is diabetic ketoacidosis (DKA) [35]. DKA occurs under conditions of extremely high blood glucose. High glucose in combination with low insulin [35], increased autonomic tone due to glucose excretion [36] [37], and/or elevated glucagon [38] levels result in the

breakdown of fats as an alternate energy source. Fat breakdown leads to the accumulation of ketones in the blood and urine increasing the acidity to dangerous, life-threatening levels. Currently, insulin administration via injections or an exogenous pump is the only treatment for the disease.

Although there is no cure for or method to prevent the development of the disease, the genetic susceptibility for T1D has been well studied. T1D is a complex genetic trait in that multiple loci contribute to susceptibility in addition to the environmental factors that also play a role in development. Through candidate gene analysis, genome-wide linkage analysis and genome-wide association studies (GWAS), over 40 loci have been identified that are associated with altered risk of T1D development. The human leukocyte antigen (HLA) has the highest genetic association with altered risk of T1D development [39, 40]. The HLA peptide complex plays a role in directing the immune response and has been associated with over 100 autoimmune diseases. Although the effects are modest compared to those caused by variants in the HLA locus, SNPs in other loci have been linked to T1D risk. SNPs in the promoter region of the *insulin gene, protein tyrosine phosphatase nonreceptor type 22 (PTPN22), interleukin 2 receptor alpha (IL2RA), SH2B adaptor protein 3 (SH2B3), protein tyrosine phosphatase nonreceptor type 2 (PTPN2), C-type lectin domain family 16 member A (CLEC16 A), ubiquitin associated and the SH3 domain containing A (UBASH3A), and cytotoxic T-lymphocyte-associated protein 4 (CTLA4*) have all been associated with altered risk of T1D development [34, 40].

Type 2 Diabetes

T2D, previously referred to as non-insulin-dependent diabetes, is a chronic metabolic disorder associated primarily with lifestyle factors and genetic susceptibility [41]. Obesity is the primary risk factor for T2D [42]. Factors such as physical inactivity, high-fat diet (HFD), and aging also increase the risk of T2D development presumably through effects on body weight. Additionally, although cigarette smoking is associated with overall decreased body weight, it increases central obesity and stimulates inflammation and oxidative stress leading to an increased risk of T2D development [43]. The increased prevalence of obesity in children is correlated with an increase in T2D in the youth [41]. T2D is characterized by

hyperglycemia resulting from insulin resistance and beta cell failure or insufficient functional beta cell mass. Insulin resistance is a metabolic abnormality in which the ability of insulin to stimulate glucose uptake and suppress glucose production or lipolysis is blunted [44]. Therefore, there is an increased demand on the beta cells for insulin production. During a state of obesity, the body compensates for the increased demand with an increase in beta cell mass and therefore increased insulin production, but this increased insulin secretion cannot be sustained because of insufficient increase in beta cell mass and/or impaired function of the beta cells [45]. Ultimately, beta cell death and/or dedifferentiation occurs. Insulin resistance and beta cell failure are discussed further in the next sections: **Mechanisms of Insulin Resistance** and **Mechanisms of Beta Cell Failure.**

Despite a high contribution of life style factors to altered T2D development risk, several genes have been identified that are associated with disease risk such as, *TCF7L2*, *PPARG*, *FTO*, *KCNJ11*, *NOTCH2*, *WFS1*, *CDKAL1*, *IGF2BP2*, *SLC30A8*, *JAZF1*, and *HHEX* [46], [47]. The substantial monetary investment in investigating the genes associated with T2D has not yet resulted in significant progress in the treatment of T2D. The identification of and studies conducted on the identified loci will be discussed further in the **Genetic Contributions to T2D** section.

Mechanisms of Insulin Resistance

Multiple mechanisms explaining the development of insulin resistance have been proposed. First, during obesity, it is thought that the storage capacity of adipocytes is reached and lipids must be redistributed to other tissues and organs such as the skeletal muscle, heart, and liver [48]. Chronic exposure of muscle to increased intracellular lipids results in increased expression of genes in the fatty acid oxidation pathway, without a concurrent upregulation of the downstream pathway, the tricarboxylic acid cycle (TCA) cycle, resulting in incomplete fatty acid oxidation and accumulation of mitochondrially-derived lipid by-products. In the liver, increased exposure to intracellular lipids results in impairment in fatty acid oxidation and redirection towards biosynthetic pathways and production of triglycerides, leading to accumulation of lipids within the liver.

In both liver and muscle, lipid accumulation can lead to activation of stress-induced serine kinases, atypical protein kinase C (PKC) and c-Jun N-terminal kinases (JNKs) [48]. These kinases can impair insulin signaling by phosphorylating the insulin receptor and/or its substrates, insulin receptor substrate 1 (IRS1) and 2 (IRS2), on serine residues, thereby interfering with downstream insulin signaling. The role of these stress induced kinases in the development of insulin resistance has been validated using mouse models. Silencing ER PKCε in the liver prevented insulin resistance during short-term HFD in mice [49]. Similarly, PKCθ KO mice are protected from lipid-induced insulin signaling defects, such as IRS serine phosphorylation, and impaired glucose transport in the muscle [50]. JNKs are activated by the ER stress response pathway, which is activated during obesity [48].

The ER is the cellular component responsible for synthesis and folding of membrane bound and secreted proteins. Within the beta cell, the ER is critical for the biosynthesis and maturation of insulin. During states of obesity or insulin resistance, the demands on the ER are increased and associated with ER stress [51]. Changes in blood glucose concentration can lead to changes in demand for insulin production. In fact, increased glucose can lead to a 20-fold increase in insulin synthesis [52]. The high demand on the beta cells under high glucose conditions results in increased misfolded or unfolded proteins within the ER, resulting in ER stress [53]. ER stress can activate three transmembrane sensors: Inositol Requiring 1 (IRE1), PKR-like ER kinase (PERK), and Activating Transcription Factor 6 (ATF6), which, in turn, stimulate the unfolded protein response (UPR). Overall, this pathway leads to upregulation of chaperone proteins to increase proper folding, decreased demand on the ER by mRNA degradation and decreased translation, and increased ER-associated protein degradation [54] to clear unwanted, unfolded proteins [53]. The different braches of the UPR were recently reviewed by Wang *et al* [55]. During steady state conditions, the ER lumen domains of the three transmembrane sensors are bound by BIP, but increased concentrations of unfolded or misfolded proteins interact with BIP disrupting its interactions. Unbound IRE1 forms oligomers, which leading to autophosphorylation, activating its kinase and endoribonuclease domains. Activated IRE1 cleaves the transcription factor *Xpb-1*, leading to translocation

to the nucleus and regulation of genes involved in protein folding and ERAD. During chronic ER stress, IRE1 cleaves multiple mRNAs in a process called regulated IRE1-dependent decay (RIDD) and activates JNK, both leading to apoptosis. PERK regulates the second branch of the UPR. Release of PERK from BIP leads to formation of homodimers and autophosphorylation, activating PERK. PERK then phosphorylates eIF2α, attenuating mRNA translation initiation. Despite decreasing global translation, PERK activation is associated with increased translation of ATF4 and ATF5. ATF4 stimulates expression of genes involved in the antioxidant response and amino acid biosynthesis and transport. ATF4 also leads to expression of C/EBP homologous protein (CHOP), which is required for ER stress-mediated apoptosis. The final branch of the UPR is the ATF6 pathway. During UPR activation, ATF6 translocates to the Golgi apparatus where it is processed by proteases, resulting in an active transcription factor. ATF6 increases transcription of *Xpb-1* and genes that increase ER capacity.

In mice lacking IRE1, an ER stress sensor, chemical activation of ER stress failed to activate JNK. Furthermore, overexpression of Xbp1, a transcription factor modulator of the ER stress response pathway, activation of JNK is impaired in liver cells treated with ER-inducing agents.

The development of liver insulin resistance specifically involves increases in ceramide, a sphingolipid [56]. In rodents, obesity-induced insulin resistance was reduced with global inhibition of ceramide synthesis [57]. Whereas, overexpression of acid ceramidase, an enzyme that initiates the breakdown of ceramides, increased insulin sensitivity in the liver and adipose tissue and reduced liver lipid accumulation [56]. Ceramides regulate lipid accumulation through altered atypical PKC activation. Atypical PKC activation inhibits insulin signaling as explained above, but also leads to a feed forward mechanism in which increased hepatic liver exposure leads to increased ceramide levels, activating atypical PKC and potentially leading to altered lipid uptake activity [56, 58]. In the muscles, although increased levels of ceramides and other lipid signaling molecules are detected, ceramides may not play a key role in the development of muscle insulin resistance as it does in the liver [48]. Alternatively, the accumulation of mitochondrially-derived lipid by-products from incomplete fatty acid oxidation such as

several long- and medium-chain acylcarnitines observed in the muscle of obese rats may play a role in muscle insulin resistance [59].

An additional mechanism whereby adipose tissue affects insulin sensitivity is through the release of peptide hormones from the adipocytes, which allow for inter-organ communication [48]. These peptide hormones include leptin, adiponectin, retinol-binding protein-4 and resistin. Specifically, adiponectin and leptin have the capacity to decrease triglyceride synthesis and enhance insulin action in skeletal muscle and liver [60, 61].

Sub-acute chronic inflammation also appears to play a key role in insulin resistance: overnutrition leads to infiltration of immune cells into the adipose tissue, liver, and muscle and to the activation of transcription factor NF-κB in these cells [48]. This stimulates secretion of pro-inflammatory cytokines such as interleukin 6 (IL-6), IL-1β, and tumor necrosis factor-α (TNFα). These cytokines stimulate signaling pathways that can act to inhibit insulin signaling.

Another factor contributing to the development of insulin resistance is the increased exposure to amino acids. Increased plasma amino acids are detected in obese, insulin resistant patients [62]. Amino acids overload leads to a negative feedback loop in which amino acids activate the class 3 PI3K hVps34, leading to activation of mammalian target of rapamycin (mTOR) and downstream activation of ribosomal protein S6 kinase-1 (S6K1) [63]. S6K1 then phosphorylates IRS1, impeding insulin signaling. Overall, the combined effects of impairments in insulin signaling in separate tissues through multiple pathways appears to lead to the development of insulin resistance.

Mechanisms of Beta Cell Failure

Ultimately, beta cell failure, defined as an inability to produce sufficient insulin so as to control blood glucose levels, explains the progression from an insulin resistant state to T2D. It is currently thought that beta cell failure arises due to a combination of insufficient beta cell mass and a decline in beta cell function. Total beta cell mass is determined by the number, size, insulin secretory capacity of an individual's beta cells [64]. Beta cell neogenesis, proliferation, and hypertrophy increase beta cell mass,

whereas de-differentiation, apoptosis, and atrophy decrease beta cell mass. Although it was originally thought that the beta cells an individual was born with were the total beta cells the individual would have for life, it is now accepted that generation of beta cells can occur throughout life [64]. In addition to increased beta cell mass due to normal growth conditions, pregnancy and obesity promote a compensatory increase in maternal beta cell mass due to the increased demand for insulin so as to overcome insulin resistance. While proliferation, the main mechanism by which beta cell mass increases after birth, primarily increases beta cell mass by augmenting cell number, obesity and insulin resistance may increase beta cell mass by increasing insulin content within the cells. Maternal obesity also leads to defects in the beta cell development and function in the offspring. As reviewed by Alfaradhi *et al.*, maternal obesity leads to an increase in pancreas area and pancreatic insulin content in young offspring in mice [65]. Similarly, in sheep, obesity leads to an increase in fetal insulin-positive cells. However, in the offspring of both obese mice and sheep, there is an age-related decline in the number of beta cells and beta cell function, predisposing the offspring to glucose intolerance later in life. This may explain, in part, why the offspring of obese humans are at a greater risk of T2D. Inversely, poor maternal nutrition can lead to a decrease in beta cell mass at birth in rats (reviewed in [64]). Furthermore, in sheep, those born with a lower number of beta cells are at a much higher risk of glucose intolerance and T2D in adult life [65]. So, despite the ability to increase beta cell mass by increasing the number of beta cells, individuals with fewer beta cells at birth may not be able to produce as many new beta cells as individuals born with more beta cells, increasing their risk of T2D development. Therefore, although beta cell mass is relatively dynamic in the face of increased insulin demand, an inability of the organism to meet the demands leads to T2D.

The second factor leading to beta cell failure is a decline in beta cell function. The molecular mechanisms that lead to decreased beta cell function are not completely understood; however, metabolic overload, in the form of glucolipotoxicity, the combination of chronic hyperglycemia and chronic dyslipidemia, is thought to be key (reviewed in [48]). Metabolic overload of both glucose and lipids leads to oxidative and ER stress which contribute to decreased insulin gene expression, down regulation of key

beta cell transcription factors including Pdx1, down regulation of IRS1/2 signaling, up regulation of uncoupling protein 2 (UCP2) and decreased glucose-stimulated ATP production.

Type 2 Diabetes Treatments

As was previously mentioned, the prevalence of both T1D and T2D continues to increase worldwide, but T2D accounts for about 90% of the total cases of diagnosed DM [66]. Current treatments include metformin, thiazolidinediones (TZDs), sulfonlyureas, drugs that target the incretin signaling pathway, Sodium-glucose co-transporter 2 (SGLT2) inhibitors, and insulin. T2D patients are encouraged to maintain their blood glucose initially with diet and exercise lifestyle adjustments; however, these interventions are commonly not sufficient, and so additional therapies are prescribed.

Metformin, a member of the biguanide family, is a potent antihyperglycemic agent and is the most widely used anti-diabetic drug [67]. The main function of metformin is to decrease HGP through inhibition of mitochondrial respiratory-chain complex 1 resulting in the activation of AMP-activated protein kinase (AMPK) and inhibition of the gluconeogenic pathway. Additionally, metformin improves insulin sensitivity potentially through increased IR expression and tyrosine kinase activity. Recently, studies have shown that metformin administration increases plasma glucagon-like peptide 1 (GLP-1) levels and GLP-1 receptor expression on the islet, amplifying insulin secretion from the beta cell.

TZDs improve glycemic control by improving insulin sensitivity [68]. TZDs have a high-affinity for peroxisome proliferator-activated receptor gamma (PPARγ), which forms a heterodimer with retinoid X receptor. Upon TZD binding, the heterodimer undergoes a conformational change resulting in interaction with PPARγ response elements (PPREs) in target genes and transcription activation. Specifically, genes involved in lipid metabolism and energy balance are activated. The improvement in insulin sensitivity is mainly attributed to the effects in adipose tissue, but PPARγ is also expressed at lower levels in muscle. *In vivo*, administration of TZDs in animal models results in decreased free fatty acids and triglycerides, which may contribute to the reported improvement on glucose homeostasis. TZDs also

prevent beta cell apoptosis, promote beta cell proliferation, and stimulate insulin synthesis and secretion [69].

Sulfonylurea was formerly the most widely used antidiabetic drug for treatment of T2D [70]. It has two main mechanisms of action: targeting stimulation of insulin secretion from the beta cell and decreased hepatic insulin clearance. Pancreatic beta cells must still be intact for sulfonylurea treatment to be effective. Within the beta cells, sulfonylureas bind to the specific receptor, SUR1, inhibiting the ATP-sensitive potassium channel and depolarizing the membrane. The depolarization results in an influx of calcium and release of insulin. Because the mechanism of sulfonylurea action is glucose-independent, hypoglycemia is a significant concern for patients taking this therapy. Effects on insulin receptor sensitivity and quantity have also been reported. However, within years of starting sulfonylurea treatment, beta cell function begins to fail and patients must begin insulin injections to maintain blood glucose levels [71].

Another category of therapeutics for T2D, which was reviewed by Kim *et al.*, targets the incretin signaling pathway: GLP-1 receptor agonists and dipeptidyl peptidase 4 (DDP4) inhibitors [72]. Incretins are gut hormones released from the L cells in the small intestine after a meal. These incretin hormones, specifically GLP-1 and glucose-independent insulintropic polypeptide (GIP), enhance the utilization of glucose throughout the body. GLP-1 receptor expression has been detected in multiple tissues including pancreatic islet cells and ducts, kidney, heart, and the peripheral and central nervous system. GLP-1 binds to the GLP-1 receptor, activating adenylyl cyclase and increasing cAMP production. Increases in cAMP concentration leads to activation of PKA and EPAC2. In the beta cells, this ultimately results in influx of intracellular calcium and insulin secretion. Primarily, incretins modulate the insulin secretory response of the beta cells. Their action accounts for ~50% of the total insulin secreted after a meal. Infusion of GLP-1 receptor agonists has resulted in improved fasting and post-prandial glucose levels. Overall, endogenous GLP-1 and GLP-1 agonists stimulate insulin secretion, insulin biosynthesis, insulin sensitivity, and beta cell survival, and suppress glucagon secretion and the rate of gastric emptying. Although the incretin effect

is maintained in recent onset cases of T2D, implying that an impairment in incretin signaling is not a pathogenic factor in the development of T2D, an altered incretin effect is a long-term consequence of the disease. Targeting this system has shown to be effective in the treatment of T2D for most patients.

A second target within the incretin signaling pathway is DDP4, the enzyme that degrades both GLP-1 and GIP in the blood [72]. In clinical trials, DPP4 inhibitors effectively lowered hemoglobin A1c (HbA1c) in patients with T2D with uncontrolled glucose. A limitation of this therapy is that administration of the DPP4 inhibitor leads to a decrease in GLP-1 release over time; therefore, reducing the overall efficacy of inhibition of endogenous GLP-1 degradation.

SGLT2 inhibitors are also used for treatment of T2D. SGLT2 inhibitors are anti-hyperglycemia agents, which prevent the kidney from reabsorbing glucose into the blood stream [73]. Therefore, excess glucose can be excreted from the body through the urine. SGLT2 is responsible for about 90% of the reabsorption of glucose from the kidneys. These inhibitors lead to increased urinary glucose and decreased HbA1c and FBG. There is an improvement in blood pressure, body weight, and kidney function, and decreased cardiovascular events in patients. The beneficial effects of SGLT2 inhibitors are well-established, but there is an increased risk of genital mycotic and urinary tract infections, DKA, and bone fractures [74].

Finally, although T2D was previously considered non-insulin dependent diabetes, according to the CDC, 14% of T2D patients use insulin alone and an additional 13% of patients use insulin in combination with an oral medication. Over the duration of the disease, the increased demand on the beta cells results in beta cell destruction and/or dedifferentiation. When beta cells fail, T2D patients must supplement medications with insulin injections.

Maturity Onset Diabetes of the Young

Unlike T1D and T2D, which are polygenic diseases and are influenced by environmental factors, MODY is a monogenic form of DM and accounts for approximately 1 to 5% of the total diagnoses [41]. According to the NIH, individuals with MODY begin to present mild symptoms in childhood or

adolescence, but it is often not detected until adulthood. Without proper genetic testing, MODY diagnosed in adulthood is commonly misdiagnosed as T1D or T2D, a misdiagnosis that occurs in approximately 80% of cases [75]. MODY is inherited in an autosomal dominant fashion and arises from mutations in genes that are required for development, maturation, or function of the beta cell. It is thought that mutations are deleterious mainly due to effects in the beta cell, but these genes are expressed in other cell types, and therefore, the beta cell-specific etiology is not certain. Mutations in the genes encoding GCK, hepatic nuclear factor 1A (HNF1A), hepatic nuclear factor 4A (HNF1A), and hepatic nuclear factor 1B (HNF1B) are the most common causes of MODY. Mutations in other genes have been associated with MODY, but account for a much lower percentage of cases. Table 1.1 outlines the full set of the MODY genes identified thus far. Although obesity used to be rare in cases of MODY, because of the rise in obesity throughout the population, the absence of obesity is no longer a distinguishing feature between MODY and T2D.

Treatment of patients with MODY is dependent on the molecular basis of the disease according to the NIDDK. For example, MODY caused by mutations in the *GCK* gene is not treated with therapeutics because the resulting hyperglycemia is mild and no further complications occur. Sulfonylureas and GLP-1 agonists are an effective treatment for patients with mutations in the gene encoding HNF1A. Eventually, sulfonylurea treatment for HNF1A-MODY and HNF4A-MODY results in desensitization to the therapeutic and the patients become insulin dependent. HNF1B-MODY patients do not respond to sulfonylureas and so are commonly treated with insulin.

Neonatal DM

Similar to MODY, NDM is a monogenic form of DM, which occurs within the first 6 months of life. It is estimated that half of the cases are transient (TNDM) in that the disease is no longer present after 24 months of age, but can reappear later in life [76]. The other 50% of cases, the disease is permanent (PNDM). NDM is rare and only occurs in 1 in 100,000 to 500,000 live births. Patients present with high glucose levels in the blood or urine, and in severe cases, ketoacidosis. Fetuses do not grow well during development and this continues after birth without proper treatment such as sulfonylureas or insulin. Loci

Table 1.1 MODY-Associated Loci.

Type of Diabetes	Gene	Affected Protein	Type of Inheritance or Mutation
MODY 1	*HNF4A*	Hepatic nuclear factor 4α	Autosomal dominant
MODY 2	*GCK*	Glucokinase	Autosomal dominant
MODY 3	*TCF1*	Hepatic nuclear factor 1α	Autosomal dominant
MODY 4	*IPF1 (PDX1)*	Insulin promoter factor 1	Autosomal dominant
MODY 5	*TCF2*	Hepatic nuclear factor 1β	Autosomal dominant
MODY 6	*NeuroD1*	Neurogenic differentiation factor 1	Autosomal dominant
MODY 7	*KLF11*	Kruppel-like factor 11	Autosomal dominant
MODY 8	*CEL*	Carboxyl-ester lipase	Autosomal dominant
MODY 9	*PAX4*	Paired box 4	Autosomal dominant
MODY 10	*INS*	Insulin	Autosomal dominant
MODY 11	*BLK*	B-lymphocyte kinase	Autosomal dominant
MODY 13	*KCNJ11*	Potassium voltage-gated channel subfamily J member 11	Autosomal dominant
MODY 14	*APPL1*	Adapter protein, phosphotyrosine interacting with PH domain and leucine zipper 1	Autosomal dominant

Adapted from NIH NIDDK website.

that have been associated with NDM are listed in Table 1.2. In particular, heterozygous activating mutations in the *KCNJ11* gene, which encodes the Kir6.2 subunit of the ATP-sensitive potassium channel, account for 30-58% of PNDM cases diagnosed before 6 months of age [77]. Mutations in the Kir6.2 subunit cause the channels to remain open even in the presence of high glucose, reducing insulin secretion. Originally, patients with Kir6.2 mutations which affect ATP sensitivity were treated with insulin injections, but in 2006 oral sulfonylurea treatment was determined to be effective in most cases such that insulin injections could be discontinued. Interestingly, some patients are resistant to taking this medication having established a strong association with their image as an individual with DM.

Gestational DM

The final type of DM discussed in this thesis is GDM. As the name suggests, GDM occurs during pregnancy and is associated with risks to the mother and fetus [78]. The mother is at greater risk of caesarian delivery, pre-eclampsia, and developing T2D later in life, while the fetus has an increased risk of macrosomia, neonatal hyperglycemia, obesity and T2D in young adulthood. Currently, treatment includes metformin and insulin administration. Under normal conditions, during pregnancy, the mother becomes insulin resistant due to weight gain, which is combatted with increased beta cell mass and insulin production. These adaptations ensure normoglycemia and proper nutrition for the fetus. A 30% increase in maternal basal HGP aids in glucose delivery to the fetus. Although the mechanisms are not fully understood, development of GDM is due to the inability of the body to adapt to the increased insulin resistance and increased demand for insulin secretion. Risk factors include low insulin sensitivity, advanced maternal age, ethnicity, polycystic ovary syndrome, familial history of T2D, and a previous pregnancy with GDM [78, 79]. A meta-analysis of two GWAS associated *CDKAL1* and *MTNR1B* with altered risk of GDM [79]. An additional GWAS identified polymorphisms in the prolactin receptor gene which are associated with GDM [80].

Table 1.2 NDM-Associated Loci.

Type of Diabetes	Gene	Affected Protein	Type of Inheritance or Mutation
TNDM	*ZAC/HYMAI*	*ZAC:* Pleomorphic adenoma gene-like1 *HYMAI:* hydatiform mole-associated and imprinted transcript	Autosomal dominant/ spontaneous
TNDM	*ABCC8*	Sulfonylurea receptor 1	Autosomal dominant/ spontaneous
TNDM	*KCNJ11*	Kir6.2	Autosomal dominant/ spontaneous
TNDM	*TCF2*	Hepatic nuclear factor 1β	Autosomal dominant
PNDM	*KCNJ11*	Kir6.2	Autosomal dominant/ spontaneous
PNDM	*ABCC8*	Sulfonylurea receptor 1	Autosomal dominant/ spontaneous
PNDM	*GCK*	Glucokinase	Autosomal recessive
PNDM	*IPF1 (PDX1)*	Insulin promoter factor 1	Autosomal recessive
PNDM	*PTF1A*	Pancreas transcription factor 1A	Autosomal recessive
PNDM	*FOXP3*	Forkhead box P3	X-linked
PNDM	*EIF2AK3*	Eukaryotic translation initiation factor 2α kinase 3	Autosomal recessive

Adapted from NIH NIDDK website.

Genetic Contribution to T2D

Genetic Tools

As discussed in the previous section, several loci have been linked to altered risk of T2D development. In this section, the methods used to identify those loci and the data concerning each locus will be addressed. The three methods discussed here are candidate gene analysis, linkage analysis, and GWAS. To date, over 60 loci have been identified as being associated with altered risk of T2D development. Several will be highlighted in the following section.

Candidate Gene Analysis

The first attempts to identify a genetic association with T2D was completed by studying candidate genes, chosen based on their known physiological function. Because of the incomplete knowledge of T2D pathophysiology and the complex pathways that might be involved, this approach proved insufficient. Numerous candidate gene analysis studies to identify genes linked with T2D risk have been conducted, but the association with T2D has been consistently replicated at only a few loci. Those loci will be highlighted here. The *PPARγ* locus encodes the PPARγ nuclear hormone receptor transcription factor, which activates transcription of genes involved in lipid metabolism and energy balance. Whole body deletion of *Pparγ* in mice is lethal, but mice with deletion of *Pparγ* specifically from adipose tissue exhibit decreased fat accumulation and decreased insulin resistance [81]. GWAS have consistently shown an increased risk of T2D when the codon of amino acid 12 is changed from an alanine to a proline in the PPARγ protein sequence (rs1801282) [82]. Two other candidate genes investigated were those encoding the subunits of the ATP-sensitive potassium channel involved in glucose-stimulated insulin secretion (GSIS) from the beta cell: Kir6.2 and SUR1. Mice lacking Kir6.2 have mild glucose intolerance, and islets isolated from these mice have significantly reduced first phase insulin secretion and no second phase [83]. The relatively normal blood glucose levels in these mice may be due to increased insulin sensitivity in skeletal muscle. Mice lacking the SUR1 subunit are hyperglycemic during glucose challenge and hypoglycemic during fasted states [84]. Both subunits were originally analyzed in candidate gene studies

because of the essential role of the ATP-sensitive potassium channel in GSIS. This association was later confirmed in large-scale GWAS [85]. Specifically, the rs1799859 (AGG1273AGA) variant in the *ABCC8* locus, which encodes the SUR1 subunit, has been associated with increased risk of T2D development. This association has been confirmed in multiple studies [86-88], but is not significant in all the studies [89, 90]. Other variants have been identified, but are all in linkage disequilibrium, or nonrandom association between alleles, with each other and with the rs1799859 SNP [91]. Additionally, a SNP (rs5219) in the *KCNJ11* locus encoding the Kir6.2 subunit was identified and associated with altered risk of T2D development. A change at amino acid 23 from a glutamine to a lysine is associated with increased risk of T2D. Studies have demonstrated decreased insulin secretion with the lysine allele [92], but this is not seen throughout all studies [93]. The final candidate gene discussed here is *WFS1,* which encodes Wolframin, a protein originally identified for its role in Wolfram Syndrome [94]. A main hallmark of Wolfram Syndrome is the presence of juvenile diabetes. Wolframin is an ER transmembrane protein, which has been shown to translocate to the plasma membrane and interact with adenylate cyclase under high glucose conditions, increasing intracellular cAMP concentrations. *Wsf1* deficient mice have impaired glucose tolerance and insulin secretion and decreased beta cell mass [95]. The association of *WFS1* with T2D has been replicated in multiple GWAS [96-98]. Rs10010131 and rs6446482 are localized to the *WSF1* locus, both intronic, and are in linkage disequilbium with each other. Other candidate genes have been analyzed, but have resulted in inconsistent associations.

Linkage Analysis

Genome-wide linkage analysis studies have also been employed. In this technique, the cosegregation of markers, short tandem repeats spaced throughout the genome, and the phenotype of interest is assessed [99, 100]. The genetic markers that cosegrate with the disease phenotype are localized to specific chromosomal regions. Repeating the analysis using a concentrated map of markers within the region can lead to further localization of the locus of interest. After which, candidate genes are selected based on proximity to this locus of interest and physiological relevance. Using linkage analysis, 8 regions

of the genome have been consistently identified as regions of T2D susceptibilty: chromosomes 1q, 2q, 3q, 8p, 11q, 12, 18p and 20 [82]. Within the susceptibility region on chromosome 2q, three common intronic variants were identified in the *CAPN10* gene as being associated with increased risk of T2D. *CAPN10* encodes calpain-10 and belongs to the intracellular calcium-dependent cysteine protease family [82, 101, 102]. Several SNPs were identified in the *CAPN10* gene, but an association with T2D was not validated [102], [103]. SNPs in the *CAP10* gene were associated with altered insulin sensitivity [102], but this was a population-dependent association [103]. Within the 10q susceptibility region, the *TCF7L2* gene, which encodes transcription factor 7-like 2, also cosegregated with the T2D phenotype. There is an established role for TCF7L2 in the Wnt signaling pathway, regulating proglucagon gene expression in enteroendocrine cells, beta cell proliferation, GSIS, and incretin gene expression [104]. Multiple SNPs in the *TCF7L2* gene have been associated with T2D risk, and this has been replicated in multiple ethnic groups [94].

Genome-wide Association Studies

GWAS have most recently been utilized to further characterize the genetic contribution of T2D development. GWAS analyze SNPs throughout the genome for co-occurrence of variations and disease phenotypes in order to identify genetic variations that are more common in a population with the disease compared to healthy individuals [99, 100]. The first GWAS confirmed loci identified by candidate gene analysis or linkage analysis as well as identifying 2 new loci associated with T2D risk that had not been identified by other methods: *HHEX* and *SLC30A8* [46]. *HHEX* encodes hematopoietically expressed homeobox, a transcription factor involved in the Wnt signaling pathway [105]. *HHEX* is involved in the maintenance of somatostatin-expressing delta cells, thereby regulating beta cell activity in a paracrine manner [106]. Disruption of the *HHEX* expression leads to altered insulin secretion from the beta cell [106]. *SLC30A8,* which encodes ZnT8, is predominantly expressed in pancreatic islet beta cells. The genetics relating ZnT8 to T2D risk will be discussed in the section titled: **Human Genetic Studies on ZnT8**. These GWAS also identified the *CDKN2A/B, CDKAL1* and *IGF2BP2* loci as having an association

with T2D risk [25]. Furthermore, GWAS performed to identify loci linked with obesity identified the *FTO* gene as the strongest association [107, 108]. Although there is no direct association between *FTO* and T2D risk, obesity is a major contributor to T2D risk, and therefore, *FTO* may indirectly influence T2D development. However, only ~10% of the obese population develops T2D, highlighting the significance of beta cell failure in the development of the disease, according to Public Health England. Finally, meta-analyses were performed combining multiple GWAS to increase statistical significance. Using this approach, two loci, *NOTCH2,* neurogenic locus notch homolog protein 2, and *JAZF1,* which encodes a zinc finger transcription factor, were identified [109]. The mechanism by which SNPs in these loci affect the risk of T2D development has not yet been established.

Mouse Models of T2D

Diet-Induced Models of Obesity

The T2D research field has advanced because of the use of mouse models, and several of the most commonly used models will be discussed in this section. Models of obesity are frequently used to study T2D. Mice are placed on a diet of over-nutrition, specifically a HFD. Mice can be placed on these diets for various lengths of time, but an increase in beta cell proliferation has been recorded as early as 3 days in C57BL6/J mice on a 60% HFD [45]. This altered beta cell proliferation occurs before beta cell mass increases or peripheral insulin resistance was detected. Insulin resistance was not apparent until after at least 5 weeks on the HFD. The insulin tolerance of the control mice on a chow diet (11% fat) did not change over the course of the experiment. This progression of impaired beta cell function may mimic the natural progression in some humans who develop T2D.

Genetic Models of T2D

Several genetic HFD-independent models of T2D have been generated. Two such models developed by Jackson Laboratory are the NONcNZO10/LtJ and TALLYHO/JngJ mouse strains. The NONcNZO10/LtJ strain combines eight susceptibility loci from two different obesity and T2D prone mouse strains. By 6 months, 90-100% of the male mice present with hyperglycemia. The TALLYHO/JngJ

mouse strain is a polygenic T2D prone mouse strain in which both males and females develop obesity and the males present with hyperglycemia.

Monogenic models of obesity have also been used in T2D research. Two such models are the leptin deficient (ob/ob) and the leptin receptor deficient (db/db) mouse strains [110]. Leptin is a hormone synthesized and released by the adipocytes, which acts as a satiety factor [111]. Leptin signals at hypothalamic NPY and POMC neurons in the brain to alter food intake. The leptin receptor is expressed on both neuron populations, but leptin binding has divergent effects on NPY and POMC neurons [110]. Binding to receptors on POMC neurons stimulates neuronal activity whereas binding on NPY neurons inhibits activity, both ultimately leading to decreased food intake. The absence of leptin or the leptin receptor results in the hyperphagia and significant weight gain [112]. The ob/ob mouse model developed from a spontaneous mutation in the leptin gene, and this mouse strain presents with hyperglycemia by 4 weeks of age. The db/db mouse model was developed from autosomal recessive mutation in the leptin receptor. Hyperglycemia develops in these mice between 4 and 8 weeks of age. Ob/ob mice do not become diabetic due to intact beta cell compensation [113], but beta cell compensation fails in db/db mice leading to the development of diabetes [114] [115].

Chemically-Induced Models of T2D

Finally, chemically-induced models of pancreas injury have also been used to study beta cell function and regeneration (reviewed by [113]). In two related models, diphtheria toxin stimulates beta cell apoptosis. In the first model, a reverse tetracycline-dependent transactivator (rtTA) is expressed in beta cells and the diphtheria toxin expression is under the control of a rtTA responsive promoter. Upon administration of doxycycline, rtTA is activated, leading to expression of diphtheria toxin and apoptotic death of about 80% of the beta cells leading to overt DM. The second model utilizes the expression of diphtheria toxin receptor under the rat *insulin* promoter (*RIP*), which is not endogenously expressed in mouse cells. Diphtheria toxin is then administered resulting in the selective ablation, about 99%, of insulin producing cells. An additional model of chemical induction of T2D is the application of streptozotocin

(STZ). STZ, a naturally occurring beta cell toxin, administration results in hyperglycemia.

Transgenic and Knockout Models of T2D

To directly investigate the role of specific genes in the development of T2D, transgenic and knockout (KO) mouse models have been used extensively [113]. Additionally, tissue-specific expression or deletion of genes of interest has proven useful for studying the role of genes in specific cell types where global deletion is lethal (e.g. insulin receptor). Investigators have taken advantage of promoters driving genes traditionally thought to be exclusively expressed in the pancreas in order to generate pancreas-specific overexpression; however, expression of genes under several of these promoters, including the *RIP*, *Pdx-1*, and *Ngn3* promoters, has been detected in the hypothalamus as well [116]. Although interesting research has been conducted using these models, the fact that overexpression is not specific to the beta cells or pancreas is a major caveat.

A commonly used tool of genetic manipulation in mouse models is the application of Cre-recombinase. This recombinant technology allows genes of interest to be selectively deleted in a time and tissue-specific manner [117]. Briefly, 34 base pair *loxP* sites are introduced into the genome flanking a key region in the gene of interest. Cre recombinase binds to the *loxP* sites and excises the intervening DNA thereby inactivating the gene. If a mouse expressing its *loxP*-containing gene of interest is crossed with a mouse expressing *Cre recombinase* driven by a tissue-specific promoter, this will result in a tissue-specific deletion of the gene. An additional layer of temporal regulation is employed by the fusion of Cre recombinase to the modified estrogen receptor (CreERT2), which is then activated by tamoxifen. Similar to the caveat discussed above, *Cre recombinase* driven by tissue-specific promoters such as *RIP* or *Pdx1* can result in gene deletion in additional tissues. A relatively new model of beta cell-specific deletion utilizes the exclusive expression of the *Ins1* gene in the beta cell. Thorens and colleagues generated $Ins1^{Cre}$ and $Ins1^{CreERT2}$ mice in which *Cre recombinase* was knocked into the endogenous *Ins1* locus, which leads to selective expression of Cre recombinase in beta cells [118]. This model does not result in Cre recombinase expression in the hypothalamus, which has been an issue with previous models including

those strains using the *Ins2* promoter. Using this model there was no difference between Cre recombinase-expressing and control mice when body weight or glucose tolerance were assessed.

Role of Zinc in Insulin Biosynthesis and Insulin Signaling

Zinc and Insulin Biosynthesis and Processing

Interestingly, zinc, although a trace element in the human body, is detected at high concentrations within the pancreas, and specifically within the islet beta cells [119]. Zn is localized primarily in the insulin granule where it concentration exceeds 20 mM [120]. In contrast in the cytosol as well as in plasma zinc concentration are in the pM range [121]. The addition of zinc to commercial insulin preparations began in the 1930s [122]. Since the 1950s, it has been well-accepted that zinc plays an essential role in the stabilization of insulin through promotion of aggregation; 6 insulin molecules and 2 zinc ions interact to form stable crystalline structures [123]. The postulated functions of zinc within the beta cell have since expanded to include being important for insulin biosynthesis and processing. Zinc ions are found in excess within insulin secretory vesicles at 1.5 times the concentration necessary to bind and promote insulin crystallization [124]. Because of the essential role zinc plays in the processing of insulin as an enzymatic and structural cofactor, it would logically follow that the availability of zinc would be critical for the maintenance of insulin secretion and therefore glucose homeostasis. Localized on the insulin secretory vesicle, ZnT8 transports zinc into the vesicles, potentially increasing the aggregation and stability of insulin hexamers (Figure 1.5).

Guinea Pig Islet Zinc

As discussed, a well-established interaction between mouse and human insulin molecules and Zn ions exists, but this interaction is lost in Guinea pig insulin. The Guinea pig insulin molecule lacks the conserved histidine residue at the B10 position where Zn binds in other species [180]. The importance of Zn in islet beta cell biology and insulin stability has been recognized for decades, but the lack of Zn association with Guinea pig insulin calls this importance into question. Furthermore, Guinea pigs have decreased whole islet insulin content, which correlates with an absence of Zn bound to insulin, given that

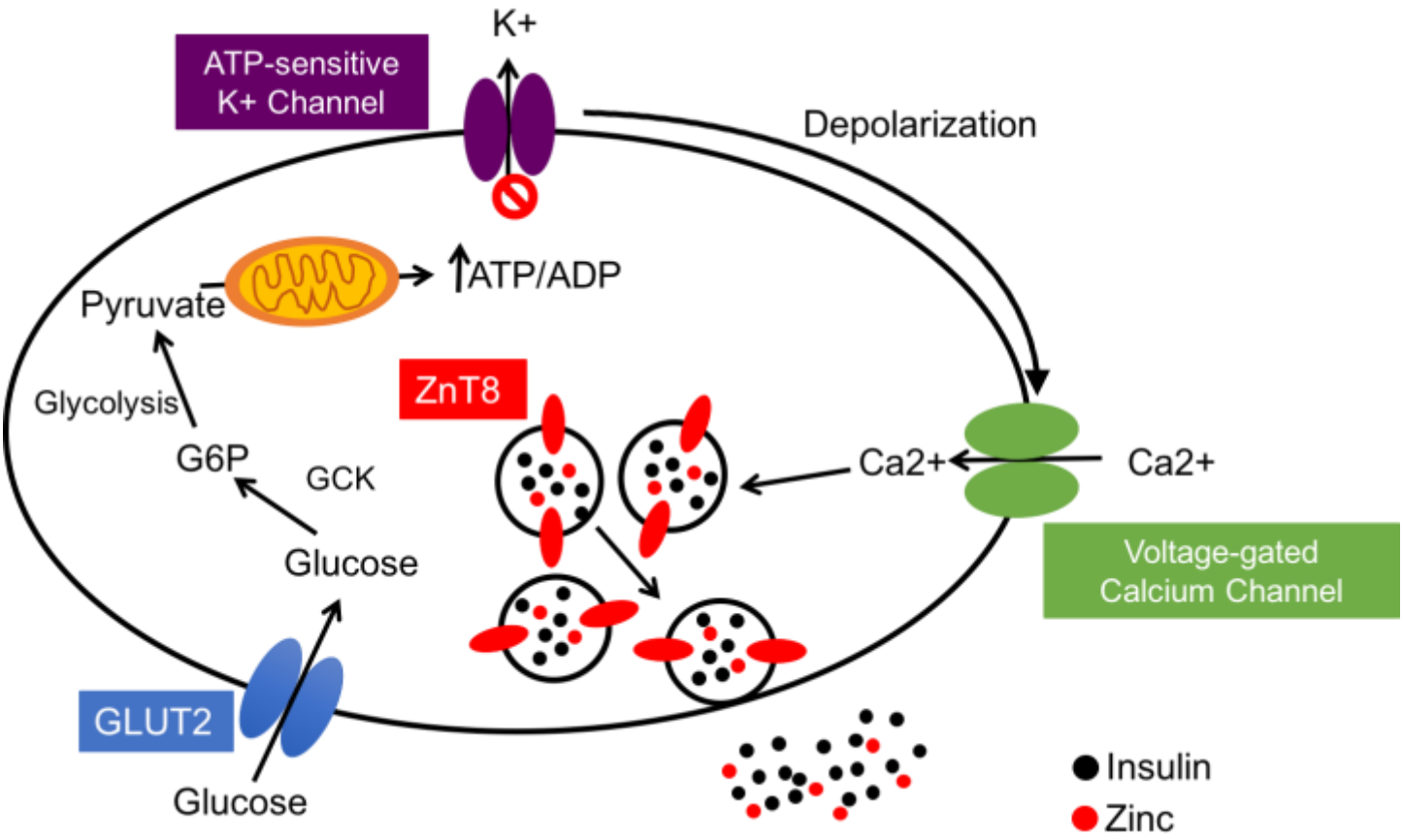

Figure 1.5 Diagram of the role of ZnT8 in canonical pathway of glucose-stimulated insulin secretion. Localization of ZnT8 on insulin secretory vesicles increases the zinc content within the vesicle, increasing insulin stability. During GSIS, zinc is co-secreted with insulin. Adapted from [2].

the high concentration of Zn in the pancreas is mostly due to the Zn within the insulin secretory vesicle [181].

The Role of Zinc in Insulin Signaling

Upon insulin and zinc secretion from the beta cell, the change from an acidic pH in the vesicles to the neutral pH in the bloodstream promotes the dissociation of the zinc ions and insulin molecules [125]. The dissociated zinc ions are postulated to affect the function of several islet cell types. First, zinc signals back to the beta cell to inhibit GSIS by acting as an autocrine inhibitory factor [126]. Zinc supplementation attenuated GSIS in pancreatic islets of the ob/ob mouse [127]. Experimental data show that the addition of zinc in pancreas perifusions decreases insulin release from the pancreas [128]. Furthermore, the addition of a zinc chelator to the media of wild type (WT) C57Bl6/J isolated islets increases insulin secretion in high glucose concentrations compared to WT islets without the chelator present [128]. In addition to the effects reported at the beta cell, high islet zinc levels have been reported to be important for paracrine signaling from beta to alpha cells [129], [130]. Zhou *et al.* showed that zinc is able to inhibit the release of glucagon from the alpha cell, amplifying the effect of insulin throughout the body [130]. However, the *in vitro* studies demonstrating this phenomenon used superphysiological concentrations of zinc [131].

There is also evidence for insulin-mimetic effects of zinc on the peripheral tissues. These include actions of zinc on glucose uptake, lipogenesis, tyrosine phosphorylation of the insulin receptor, inhibition of protein tyrosine phosphatases, transcription factor FOXO1a, phosphoenol pyruvate carboxykinase (PEPCK), and glucose-6-phosphatase (G6Pase), and activation of MAPKs [132, 133]. These effects of zinc on insulin signaling are presumably not related to beta cell zinc release because the zinc concentration would be diluted in the blood, but these insulin-mimetic effects in peripheral tissues may be due to dietary zinc intake. At the liver, zinc alone stimulates glycolysis and inhibits gluconeogenesis, but the effects of insulin and zinc are not additive [126]. In liver portal vein perfusion assays, zinc supplementation increases the passage of insulin through the liver, indicating that zinc inhibits insulin clearance [128]. However, once again, a caveat here is that the zinc concentrations used in this study exceed the portal vein

zinc concentration seen *in vivo* [131]. Similarly, in HepG2 cells, a liver cell line, Tamaki *et al.* demonstrated that increasing zinc concentrations in the media decreased insulin uptake again suggesting that zinc inhibits insulin clearance [128]. They also showed that insulin treatment decreased cell surface expression of IRs on HepG2 cells, but this internalization of the IR was inhibited by the addition of zinc.

The effects of zinc signaling at the peripheral tissue were reviewed by Ranasinghe *et* al [126]. At the muscle, zinc activates AMPKα phosphorylation and increases glucose transporter GLUT4 expression. Increased GLUT4 expression, also seen in adipose tissue, increases glucose uptake. In isolated adipocytes, incubation with zinc increased lipogenesis. In a separate study, incubation in zinc-supplemented media resulted in a decrease in free fatty acid (FFA) release from rat adipocytes. Additionally, exposure of zinc-deficient adipocytes to zinc increased insulin binding to the IR in a dose-dependent manner, and in cultured 3T3-Li adipocytes, zinc enhanced insulin signaling leading to increased Akt phosphorylation and GLUT4 expression and translocation to the membrane, thereby increasing glucose uptake.

Zinc and Oxidative Stress

Oxidative damage due to the production of reactive oxygen species (ROS) has been proposed as a hallmark of the development of T2D as well as long-term DM complications. A potential role for zinc in the protection of cells from oxidative damage has been indicated in multiple studies. Zinc deficiency in humans has been associated with increased oxidative stress and, consequently, increased oxidative damage to DNA, proteins, and lipids [134], [135]. *In vivo,* zinc supplementation in the elderly led to decreased oxidative stress biomarkers and inflammatory cytokines [135]. Multiple mechanisms explaining the connection between zinc and the regulation of oxidative stress have been described. For example, the nicotinamide adenine dinucleotide phosphate (NADPH) oxidases are plasma membrane-associated enzymes that catalyze the production of $\cdot O^{-}_{2}$ from oxygen, using NADPH as the electron donor (reviewed in [135]). Zinc inhibits NADPH oxidases leading to decreased ROS. Zn is also a co-factor for super oxide dismutase (SOD) isoforms 1 and 3, enzymes that catalyze the dismutation of $\cdot O^{-}_{2}$ to H_2O_2.

Zinc Defects in Humans and Mice with DM

Decreased zinc concentrations have been reported in individuals with DM. Given the extensive role that zinc plays in insulin biosynthesis, crystallization, and signaling [123], [132], [133], it is likely that these altered zinc concentrations in individuals with T2D contribute to disease pathophysiology. Post-mortem, investigators reported a 50% decrease in pancreatic zinc concentration compared to normal cadavers [136]. DM is associated with a decrease in plasma zinc and increased urinary zinc [137], [138]. In a systematic review and meta-analysis conducted by Jayawardena *et al.*, zinc supplementation on patients with DM resulted in improvements in fasting blood glucose (FBG) and HbA1c and reduced cholesterol and low-density lipoprotein [139]. Using mouse models, zinc supplementation was examined in obese db/db mice [140]. Mice fed a zinc-supplemented diet had increased pancreatic zinc and decreased blood glucose levels compared to zinc control and zinc-deficient mice. The investigators concluded that zinc supplementation attenuates hyperinsulinemia and hyperglycemia in db/db mice. Interestingly, when ob/ob mice were given zinc-supplemented diets, the hypersecretion of insulin in the ob/ob mice was attenuated, but, unlike db/db mice, there was no improvement in glucose tolerance [127]. In contrast to db/db mice, in this mouse model, zinc supplementation did not result in increased zinc in the pancreas. In a rat model of hyperlipidemia and STZ-induced T2D, zinc supplementation improved the T2D symptoms of dyslipidemia as well as reducing oxidative stress biomarkers [141].

Zinc Homeostasis

Previous sections have highlighted the essential roles that zinc plays within the cell as a signaling molecule and an enzymatic and structural cofactor, as well as an autocrine and paracrine signaling factor. Despite the major role that zinc plays throughout the body, it is a trace element, and cells are susceptible to zinc toxicity [142]. Zinc concentrations, therefore, must be maintained within a specific range. Maintenance of zinc cellular homeostasis through compartmentalization, availability, and transport are critical to ensure proper zinc concentration and signaling between and within cells [143]. The main players in this regulation are zinc transporters and metallothioneins. Metallothioneins are small, cysteine-rich

proteins that bind and sequester metals in order to protect the cell from metal toxicity [144]. Metallothioneins have the capacity to bind seven zinc ions with high affinity, acting as zinc chelators. The other main components of zinc cellular homeostasis are the zinc transporters. The two classes are the Zinc Influx Transporters (ZIP) family and the Zinc Transporters (ZnT) family. The ZIP family functions to increase cytoplasmic zinc concentrations, while the ZnT family decreases cytoplasmic zinc concentrations through efflux out of the cell or influx into intracellular organelles [5].

ZnT Family

The ZnT family of transporters are members of the broader cation diffusion facilitator family (reviewed in [5]). There were thought to be 10 members of the ZnT family, assigned ZnT1-10; however, ZnT9 was later found not to be a zinc transporter. The 9 bona fide zinc transporters have been detected in the islets. Eight out of the 9 of these ZnTs have a 6-transmembrane domain structure with the C- and N-terminals in the cytosol (Figure 1.6). Crystal structures have not been elucidated at this point, but a structure has been proposed based on the *Escherichia coli* Yiip Zn transporter. In this structure, there are histidine and aspartic acid residues in the second and fifth transmembrane domains that are postulated to bind zinc for transport across the membrane. Zinc is also thought to bind to a cytoplasmic domain, where it is believed to function as a zinc sensor acting by inducing orientation changes of the transmembrane domains. ZnTs form functional homodimers, but a heterodimer has been described between ZnT5 and ZnT6. Although there is a high degree of sequence variability between the ZnT family members, the cytoplasmic domain structure is highly conserved and sufficient for dimerization [5], [145]. The 9 ZnT members function as Zn^{2+}/H^{+} exchangers, using the proton gradient between the cytosol and vesicle lumen as the driving force to transport Zn against its concentration gradient.

The 9 ZnT family members are encoded by the *SLC30A* gene family. For example, *SLC30A1* encodes ZnT1. For ease of reading, the protein name, i.e. ZnT1, will be used to described both the gene and protein in this section. The ZnTs are expressed in a tissue-specific manner and localize differentially

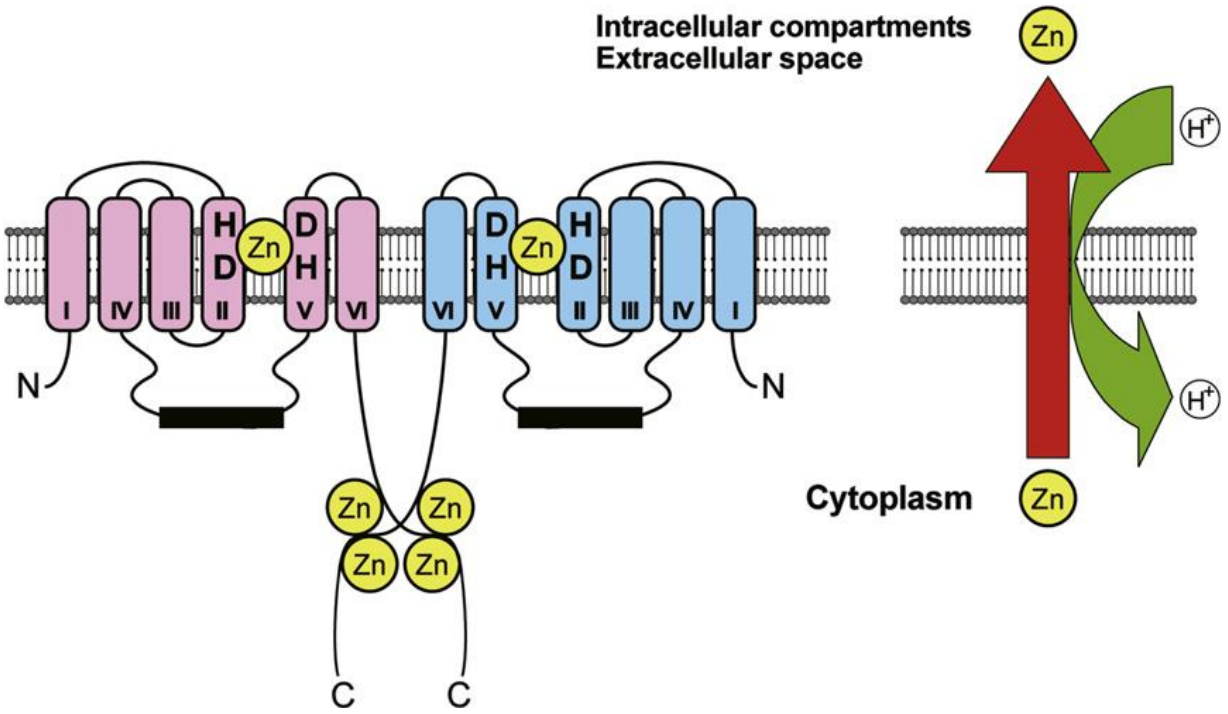

Figure 1.6 ZnT family predicted structure. The predicted ZnT structure is based on the X-ray structure of YiiP, the bacterial homologue. The ZnT homodimers have a predicted zinc-binding site at the 2 histidine (H) and 2 aspartic acid (D) residues within the transmembrane domains to transport zinc across the membrane. The thick black line represents a histidine-rich loop that may form an additional binding site. The C-terminal zinc binding site is thought to act as a zinc sensor and modify the orientation of the transmembrane domains, and therefore zinc transport. ZnT transporters function as zinc/H^+ exchangers. Adapted from [5].

within the cell. The function and localization of the ZnT family members were also reviewed in by Kambe [5]. Their specific intracellular localizations are shown in Figure 1.7. ZnT1 is ubiquitously expressed and localizes mainly to the plasma membrane. ZnT2 has also been detected in multiple tissue types and mostly localizes to secretory vesicles. ZnT3 is predominantly expressed in neurons where it localizes on synaptic vesicles. ZnT4, 5, 6, and 7 are localized to the Golgi apparatus and are ubiquitously expressed. ZnT5 is also located on cytoplasmic vesicles and has been detected on insulin secretory vesicles. ZnT8 is predominantly expressed in beta cells and localizes to insulin secretory vesicles in the pancreatic beta cells where it functions to increase the zinc concentrations within these vesicles. Finally, ZnT10 is predominantly expressed in vascular smooth muscle cells localizing to endosomes.

ZnT Family and Glucose Homeostasis

Mouse models have aided in the investigation into the potential functions of the 9 ZnT family members *in vivo*. *In vivo* data indicate that ZnT3, 5, 7, and 8 may play a role in glucose homeostasis and beta cell function.

ZnT3

Slc30a3 has been detected in beta cells and localizes to secretory vesicles, but is predominantly expression in neurons. Global *Slc30a3* deletion in mice results in deficits in learning and memory [146], without an apparent defect in glucose homeostasis or beta cell function. In order to uncover an abnormal phenotype specifically in glucose homeostasis in *Slc30a3* KO mice, the mice received STZ injections to induce beta cell stress. These mice have increased FBG levels compared to WT mice, but no change in glucose tolerance [147].

ZnT5

While *Slc30a5* is ubiquitously expressed, its expression is highest in the pancreas compared to its expression in other tissues, suggesting a potential role in beta cell function. However, upon global deletion of *Slc30a5*, greater than 60% of the male mice died suddenly due to bradyarrhythmias [148]. The glucose tolerance of *Slc30a5* KO mice has not been analyzed, but *Slc30a5* KO mice on a non-obese diabetic

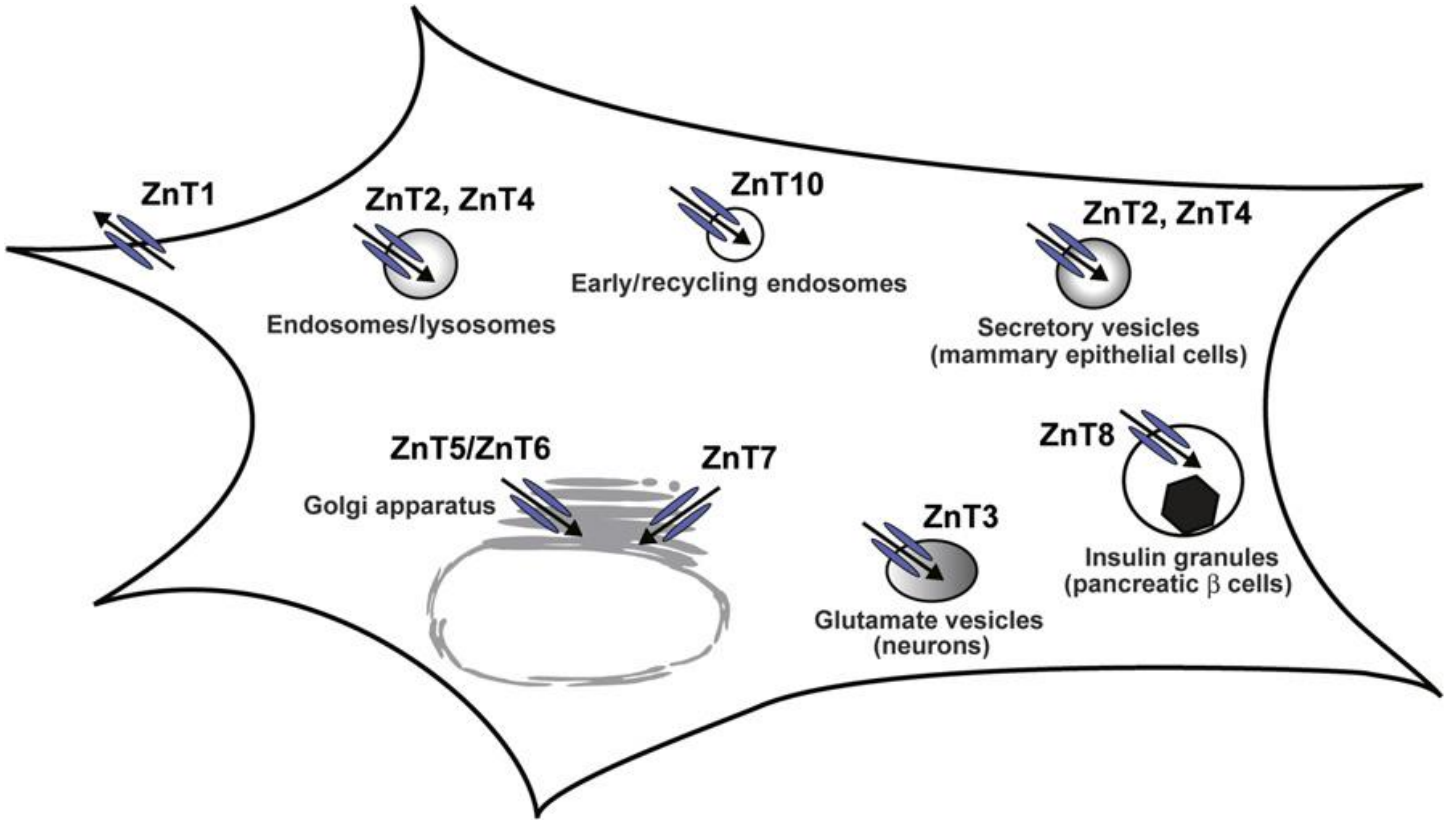

Figure 1.7 ZnT family subcellular localization. The localization of ZnT family members is depicted based on their known or predicted roles. ZnT8 is localized to insulin secretory vesicles. Adapted from [5].

(NOD) background have a decreased incidence of overt diabetes as assessed by non-fasting blood glucose [149].

ZnT7

Slc30a7 is ubiquitously expressed, including expression in the beta cells, with highest expression seen in the small intestines and the liver [150]. However, ZnT7 protein has not been detected in the liver [150]. While ZnT7 is localized mainly to Golgi apparatus, it is also found on cytoplasmic vesicles. *Slc30a7* global KO mice have decreased zinc absorption from the small intestines but no other detectable defects associated with general zinc deficiency [151]. When fed a chow diet, these mice also show a trend towards impaired glucose tolerance and increased plasma insulin levels during an oral glucose tolerance test (OGTT). Interestingly, when fed a HFD *Slc30a7* KO male mice on a HFD show impaired glucose tolerance and decreased plasma insulin levels during an OGTT as well as being insulin resistant relative to control mice [152]. In a rat pancreatic insulinoma cell line (RIN5mF), *Slc30a7* overexpression leads to an increase in cellular insulin content and increased basal insulin secretion, but no difference in GSIS [153].

ZnT8

SLC30A8 Expression

In humans and rodents the highest expression of *SLC30A8* is observed in the endocrine pancreas [8], [154], [155], [156] [157]. *SLC30A8* is not expressed in pancreatic exocrine tissue [156, 158, 159]. Within human islets, ZnT8 mRNA and protein levels are highly enriched in beta cells, but both are also present in alpha cells, albeit at significantly lower levels [157, 158, 160, 161]. This is also true in rodents [125, 127] but not in pigs, where *Slc30a8* appears to be restricted exclusively to beta cells [162]. In humans *SLC30A8* is also expressed in lymphocytes [132], retinal pigment epithelium [163], and several layers of the retina, where its loss may contribute to the pathology of ischemic retinopathy [164]. In both humans and rodents *SLC30A8* is expressed in adipocytes [165], [166] and several extra-pancreatic endocrine glands including the pituitary, adrenal, and thyroid [167, 168] (See GTEx database for human data).

Although not apparent on Northern blots [8], the Allen brain atlas shows that *SLC30A8* is expressed in specific regions of both human and mouse brain. Similarly, GTEx database analyses show that *SLC30A8* is expressed at low levels in several regions of the human brain, as well as multiple other tissues.

Its abundant expression in islet beta cells is driven, at least in part, by the beta cell-enriched transcription factor Pdx-1 [169]. Reporter gene analyses led to the identification of two intronic enhancers, designated enhancers A and B. Enhancer A is a beta cell-specific enhancer with two confirmed Pdx-1 binding sites, which upon mutation, leads to reduced fusion gene expression.

Slc30a8 KO Mouse Models

In an effort to understand the role that ZnT8 plays in glucose homeostasis and beta cell function, several *Slc30a8* KO mouse models have been examined. Although deletion of *Slc30a8* globally or in a beta cell-specific manner consistently results in a significant decrease in the abundance of free or loosely bound zinc in islets (Table 1.3), the effects of this deletion on glucose tolerance and GSIS are small and inconsistent. The effect of *Slc30a8* deletion on islet zinc content did not alter insulin granular density in our hands [159], but other investigators have reported changes in granular density [170-174]. A difference in protocols used to fix the pancreatic tissue can potentially explain these differences.

On a mixed C57BL/6J and 129SvEv genetic background, our group demonstrated that both male and female *Slc30a8* KO mice have decreased fasting plasma insulin (FPI) levels; however, there was no change in glucose disposal in male *Slc30a8* KO mice during an intraperitoneal glucose tolerance test (IPGTT) [156]. Unfortunately, insulin sensitivity was not assessed.

Interestingly, when *Slc30a8* is deleted from mice on a pure C57BL/6J background, our group reported a decrease in FPI levels in female mice with a similar trend in male mice [159]. However, there is no difference in insulin sensitivity in *Slc30a8* KO mice on a pure C57BL/6J background compared to WT mice. We hypothesize that these data indicate an improvement in insulin sensitivity in ZnT8 KO mice that results in decreased FPI but that the change is too small to be detected using insulin tolerance tests (ITTs). Male mice had a significant decrease in fasting proinsulin levels with a similar trend in female

Table 1.3. Data from *Slc30a8* KO mouse studies.

Authors	Deletion Location	Genetic B/G[1]	Body Weight[2]	Islet Insulin Content	Islet Zinc Content	Islet # Islet Size alpha/ beta	Islet EM	GSIS In Situ	ITT/ EH Clamp[3]	Fasting Glucose	Fasting Insulin	IPGTT 4-6 Weeks	IPGTT 12-22 Weeks	OGTT	GSIS In Vivo
Pound et al. BJ 2009	Global	Mixed	No change	No change	Down	No change	N.R.[4]	Down	N.R.	No change	Down	N.R.	No change	N.R.	N.R.
Pound et al. PLoS 2012	Global	C57BL /6J	No change	No change	Down	N.R.	No Change	No Change	No change	No change	No change	IGT	No change	No change	N.R.
Nicholson et al. Diabetes 2009[5]	Global	Mixed	No change	No change	Down	No change	Altered	Up[6]	No change	Up[7]	N.R.	IGT	No change[8]	N.R.	Down
Lemaire et al. PNAS 2009	Global	Mixed	No change	No change	Down	N.R.	Altered	No Change	No change	No change	N.R.	No change	No change	N.R.	N.R.
Wijesekara et al. Diabetol. 2010	Beta Cell	Mixed	No change	N.R.	Down	No change	Altered	Down	N.R.	No change	No change	N.R.	N.R.	IGT	No change
Tamaki et al. JCI 2013	Beta Cell	C57BL /6J	No change	No change	Down	No change	Altered	Up	No change	No change	No change	IGT	IGT	N.R.	Down

1. Designated mixed unless speed congenic backcrossing or at least 10 backcrosses onto a defined genetic background (B/G).
2. Body weight on a chow diet.
3. EH, euglycemic-hyperinsulinemic clamp
4. N.R., not reported.
5. Data are for the Toronto colony only.
6. GSIS was increased in islets from the Toronto colony mice at 12 weeks but unchanged in the London colony.
7. Fasting glucose was elevated at 6 weeks but normal by 12 weeks.
8. Glucose tolerance was normal in the Toronto colony at 12 weeks but impaired in the London colony.

Adapted from [6].

mice. A slight impairment in glucose tolerance was detected in these mice at 4 weeks of age, but this impairment was not observed in older mice. Similarly, Nicolson *et al.* reported a slight defect in glucose tolerance in 6-week-old *Slc30a8* KO mice relative to WT mice, but this difference from WT controls was absent when assessed in older animals [172]. Lemaire *et al.* also observed little change in glucose tolerance in *Slc30a8* KO mice at 6, 12, 25 and 52 weeks of age [170]. Islets isolated from *Slc30a8* KO mice on a mixed genetic background showed a significant decrease in insulin secretion following incubation in 11mM glucose, indicating an impairment in insulin secretion from the beta cells in response to glucose [156], but this effect was lost in islets isolated from *Slc30a8* KO mice on the pure C57BL/6J genetic background mice [159]. In perfusion studies, Lemaire *et al.* reported no difference in insulin secretion from islets isolated from mixed genetic background *Slc30a8* KO relative to WT mice in response to 15 mM glucose or 30 mM KCl [170].

Using the *RIP* to drive Cre recombinase expression as previously described, Wijesekara *et al.* generated a beta cell-specific *Slc30a8* KO (ZnT8BKO) mouse model [171]. These ZnT8BKO mice had a slight impairment in glucose tolerance as assessed by OGTTs at 6 weeks of age. Glucose tolerance was not examined in older mice, so it is unknown whether the effect was sustained or transient as was seen in the global *Slc30a8* KO animals. A slight decrease in the first phase of insulin secretion was observed in ZnT8BKO mouse islets compared to control mouse islets during perfusion studies. However, this did not translate into a difference in plasma insulin levels during OGTTs *in vivo.*

Studies by Tamaki *et al.* used the same *RIP-Cre* mouse line for generation of a beta cell-specific *Slc30a8* KO, but in contrast to Wijesekara *et al.,* Tamaki *et al.* failed to use the *RIP-Cre* mouse as the control [128, 171]. In IPGTTs Tamaki *et al.* reported an impairment in glucose tolerance and a corresponding decrease in plasma insulin levels in ZnT8BKO compared to their control mice [128]. However, these data are difficult to interpret given the effects that the presence of *RIP-Cre* alone can have on these measurements [175]. Indeed, Lee *et al.* described a nearly identical degree of beta cell dysfunction, specifically, impaired glucose tolerance and reduced plasma insulin levels in response to

glucose administration, in mice expressing just the *RIP-Cre* allele alone compared to WT C57BL/6J mice [175]. This strongly suggests that the presence of the *Cre recombinase* allele rather than the lack of ZnT8 explains the effects on glucose homeostasis reported by Tamaki *et al.*

Tamaki *et al.* also examined the effects of *Slc30a8* deletion on insulin clearance [128]. In pancreas perfusion studies, plasma insulin collected from the portal vein after perfusion with 16.7 mM glucose was significantly higher in ZnT8BKO mice compared to control mice. Interestingly, when 30 μM zinc was added to the perfusate, this increase in ZnT8BKO insulin secretion was lost. These data suggest that there is an increase in insulin secretion from ZnT8-deficient beta cells that is impaired by the presence of zinc. However, the 30μM concentration of zinc added to the perfusate in this study is superphysiological [131]. Combined pancreas-liver perfusion studies showed no difference in effluent insulin levels after passage through the liver, suggesting increased clearance of the higher insulin levels released from the ZnT8BKO pancreas [128]. These pancreas-liver perfusion data are at odds with Tamaki *et al.'*s *in vivo* data showing lower plasma insulin levels in *Slc30a8* KO mice in IPGTTs. Nevertheless, Tamaki *et al.* did see changes in C peptide levels in IPGTTs *in vivo*, again, suggesting changes in insulin clearance. We hypothesize that the failure to use the proper matching *RIP-Cre* control may also explain these apparent differences in insulin clearance.

The recently developed knock-in *Ins1Cre* strain can be used to delete the target genes specifically from the beta cell [118]. Using this model to delete *Slc30a8*, Mitchell *et al.* showed that glucose tolerance, insulin secretion stimulated by multiple stimuli, and beta cell mass were all unchanged compared to *Cre*-littermates [174].

Various factors may explain the inconsistent effects reported from *Slc30a8* KO mouse studies. First, small differences in technique and housing conditions may explain some of these inconsistencies. For example, blood collection from the retro-orbital plexus and after tail clipping results in differences in glucocorticoid release, which may affect blood glucose levels, specifically in some mouse strains [176]. Additionally, Nicolson *et al.* reported different results when *Slc30a8* KO mice from the same original

homologous recombination and breeding were maintained on chow diets, although the diets varied slightly, in different locations, namely London or Toronto [172]. While mice bred in London, which were backcrossed twice, were glucose intolerant at 12 weeks of age, those bred and examined in Toronto, which were backcrossed three times, were not. Further potential limitations in the comparison of different *Slc30a8* KO studies involve variations in the type and duration of anesthesia used, which have been shown to affect insulin secretion and glucose tolerance differently [177]. An additional potential variable between *Slc30a8* KO studies relates to the relationship between zinc concentrations and anesthesia. Changes in zinc levels in blood or tissues can affect the response of animals to anesthesia, and different anesthetics can alter the zinc concentration detected in serum and brain tissue [178, 179]. Therefore, the complicated interplay between anesthesia and zinc may contribute to the variations reported in the effect of *Slc30a8* deletion on glucose homeostasis.

Human Genetic Studies on ZnT8

Human genetic studies have examined the effect of common SNPs in *Slc30a8* and ZnT8 haploinsufficiency on the T2D risk. These will be discussed separately.

SLC30A8 Single Nucleotide Polymorphism rs13266634

GWAS identified a nonsynonymous SNP in *SLC30A8* that confers altered risk of T2D development [46]. This association has been verified in multiple studies and populations [47], [25], [182], [183]. This polymorphism determines whether amino acid 325 of ZnT8 is a tryptophan to an arginine residue (W325R) [46]. Individuals with the R325 allele of this SNP are at increased risk of T2D [47]. They have decreased proinsulin to insulin conversion [184], impaired glucose tolerance [185], and impaired insulin secretion [186] compared to those with the W325 allele, changes that may explain the association with T2D risk. Paradoxically, in Europeans, the rs13266634-C allele encoding the R325 high risk allele is more common than the rs13266634-T allele encoding the W325 low risk allele [31]. The reported genotype frequency in a European population is 52.3%CC, 44.1%CT and 3.6% TT.

Although amino acid 325 is near the dimerization domain, the alternate alleles of this amino acid do not alter the transporters' ability to dimerize [187]. However, the ZnT8 rs13266634 alleles have differential zinc transport activity. Rutter and colleagues originally reported that the R325 risk allele had reduced zinc transporter activity [172], which was difficult to reconcile with the reported protective effect of ZnT8 haploinsufficiency in humans (see below). However, in a recent study the opposite result was reported, specifically that the R325 risk allele increases transporter activity [188]. Additionally, in humans, carriers of the R325 have increased islet zinc content [189]. The reason why Rutter and colleagues originally found that the R325 allele confers reduced transporter activity is unclear. However, these new studies suggest that the R325 variant may confer T2D risk by increasing transporter activity leading to elevated islet zinc, which presumably is toxic.

The GWAS data that reported an association between the R325 ZnT8 allele with increased T2D risk involved comparisons of thousands of individuals with T2D versus healthy controls. In a significantly smaller study, Tamaki *et al.* examined 12 individuals with the R325 risk allele, and determined carriers of the risk allele have increased C peptide:insulin ratio suggesting increased insulin clearance in these carriers, although the ratio was highly variable among both groups [128]. While zinc can regulate insulin clearance, it is unclear how subtle changes in beta cell zinc release associated with the presence of alternate ZnT8 variants could affect insulin clearance given the dilution of islet-released zinc by the high blood flow in the portal vein in humans, as noted by Mitchell *et al.* [174].

ZnT8 Haploinsufficiency

A recent high-powered human genetic study involving 150,000 participants has shown that individuals who are haploinsufficient for ZnT8 have a 65% reduction in their risk for developing T2D [190]. In this study, Flannick *et al.* identified 12 protein-truncating mutations that lead to loss-of-function. In order to increase statistical power, data from these 12-identified loss-of-function mutations were combined. In this study population, 19 of the 30,433 individuals with T2D had a loss-of function mutation, while 326 of the 118,701 healthy controls had one of the 12 loss-of-function mutations. From the lower

prevalence of those mutations in individuals with T2D Flannick *et al.* calculated that those mutations confer a 65% reduced risk of developing T2D.

Summary

Overall when this project began, the data from the *Slc30a8* KO mouse models did not provide a clear role for ZnT8 in beta cell function or glucose homeostasis. Initially, the *Slc30a8* KO data appeared at odds with the human R325W genetic data. However, given the recent recognition that the transporter activity data reported by Rutter and colleagues were not correct, these differences can now be reconciled [172, 188]. The R325 risk allele of the rs13266634 SNP has increased zinc transporter function compared to the W325 allele, suggesting that the R325 allele is a gain-of-function variant, whereas the *Slc30a8* KO mouse studies examine loss-of-function mutations. This can therefore explain the difference between the mouse *Slc30a8* KO studies and the human genetic data on the rs13266634 SNP because separate models are being compared, one being loss-of-function and the other being gain-of-function. The *Slc30a8* KO mouse data still appear surprising in that the loss of *Slc30a8* appears to have no consistent effects on GSIS or glucose tolerance. In addition, the *Slc30a8* KO mouse data are still at odds with the human haploinsufficiency data in that deletion of *Slc30a8* has little effect on glucose metabolism rather than effects that might lead to protection from T2D.

This dissertation will show (1) that a role for ZnT8 in GSIS is uncovered when deletion of ZnT8 is combined with deletion of *Slc30a7*, suggesting a functional redundancy between ZnT7 and ZnT8; (2) that support for functional redundancy between ZnT8 and other ZnT isoforms comes from the discovery that ZnT8 is a pseudogene in Guinea pigs; and (3) that a beneficial effect of ZnT8 haploinsufficiency is uncovered in C57BL/6J mice in the context of a HFD.

CHAPTER II

MATERIALS AND METHODS

Generation of Mouse Models

Generation of the Slc30a7 Targeting Vector

Slc30a7 KO mice were generated by Lexicon Pharmaceuticals, Inc. (The Woodlands, TX) and then analyzed in collaboration with the O'Brien laboratory. A Slc30a7 targeting vector was derived using the Lambda KOS system [192]. The Lambda KOS phage library, arrayed into 96 superpools, was screened by PCR using exon 1- (Slc30a7-1 [5'- GCCGCCACCATACCGAGTC-3']) and exon 2-specific primers (Slc30a7-2 [5'-CAGTTGCTCCAGATGCCGTAGAGT-3']). The PCR-positive phage superpools were plated and screened by filter hybridization using the 444 bp amplicon derived from primers Slc30a7-1 and Slc30a7-2 as a probe. A pKOS genomic clone, pKOS-44, was isolated from the library screen and the presence of the Slc30a7 gene was confirmed by sequence and restriction analysis. Gene-specific arms (5'-CCCCCGCCTCCCGCTTTCCCGTCCCAGGACGCGTT-3') and (5'-CCCTCACCCTCTGCTTCCGCCCCAATCATCTTCCC-3') were appended by PCR to a yeast selection cassette containing the URA3 marker. The yeast selection cassette and pKOS-44 were cotransformed into yeast and clones that had undergone homologous recombination were isolated. DNA sequencing confirmed that recombination had replaced a 573 bp region, from bp 11 of exon 1 extending to the first 10 bp of the second intron, with the yeast selection cassette. This design removes the entire coding sequence of exons 1 and 2 while leaving the transcription start site intact. To complete the Slc30a7 targeting vector the yeast cassette was subsequently replaced with a selection cassette incorporating the LacZ gene, the herpes simplex virus thymidine kinase (TK) promoter and a neomycin (Neo) selectable marker. By removing the entire coding sequence of exons 1 and 2 while leaving the transcription start this design results in expression of LacZ mRNA being driven by the Slc30a7 promoter whereas expression of Neo mRNA is driven by the TK promoter with translation dependent on the endogenous Neo start codon.

Generation of Slc30a7 KO Mice

The Not I linearized targeting vector was electroporated into 129/SvEvBrd (Lex-2) ES cells. G418/FIAU resistant ES cell clones were isolated, and correctly targeted clones were identified and confirmed by Southern blot analysis using a 539 bp 5' internal probe (designated probe 19/20), generated by PCR using wild type Lex-2 ES cell genomic DNA as the template with primers (Slc30a7-19 [5'-GTTGCAGATAAACGCCACACGGATTACT-3']) and (Slc30a7-20 [5'-CAGTCTTTAAGTTGTGCAGCAGCGATGAAT-3']), and a 350 bp 3' external probe (designated probe 17/18), amplified by PCR using primers (Slc30a7-17 [5'-CATAAATCACTTCATGGAATACCTT-3']) and (Slc30a7-18 [5'-ATACAAATGACTGCAGCACGACAGA-3']). Southern blot analysis using probe 19/20 detected a 11.2 kbp wild type band and 7.2 kbp mutant band in Bst XI digested genomic DNA while probe 17/18 detected a 11.8 kbp wild type band and 5.2 kbp mutant band in Stu I digested genomic DNA. Correctly targeted clones were also confirmed by PCR using the following primer pairs:

Primer Slc30a7-1 (representing sequence in exon 1; 5'-GCCGCCACCATACCGAGTC-3')

Primer Slc30a7-2 (representing sequence in exon 2; 5'-CAGTTGCTCCAGATGCCGTAGAGT-3')

Primer Slc30a7-3 (representing Slc30a7 sequence in intron 2; 5'- GAGTTGCAGGAAATGAGAGTCC-3')

Primer Neo3A (representing sequence in the Neo gene; 5'- GCAGCGCATCGCCTTCTATC-3')

Cells from the correctly targeted ES cell clone were microinjected into C57BL/6 (albino) 4 blastocysts resulting in the generation of chimeric Slc30a7 heterozygous (HET) mice on a mixed 129/SvEvBrd X C57BL/6 genetic background.

Breeding Strategy for Slc30a7 KO and DKO Mice

F1 Slc30a7 chimeric (129SvEvBrd x C57BL/6J) mice were interbred to generate F2 wild type WT, HET and homozygous KO mice. The F2 Slc30a7 HET mice were then bred with F1 hybrid (C57BL/6J X 129SvEvBrd) WT mice. Male and female HET mice from this breeding, along with their offspring, were then interbred to generate a mouse colony at Lexicon Pharmaceuticals, Inc. Two male

mice from this colony were shipped to the O'Brien laboratory. One of these male mice was mated with female C57BL/6J WT. These C57BL/6J WT mice were generated through interbreeding of C57BL/6J Slc30a8 HET mice [159] rather than being purchased from an external vendor. The resulting mixed genetic background Slc30a7 HET mice were interbred to generate a colony of mixed genetic background WT, Slc30a7 HET and Slc30a7 KO mice. The other male mouse was mated with female C57BL/6J Slc30a8 KO mice. Again, additional rounds of backcrossing were not performed for the mice used in these studies. Instead the resulting mixed genetic background Slc30a7 HET X Slc30a8 HET mice were interbred to generate a colony of mixed genetic background Slc30a7 KO X Slc30a8 KO mice, designated as DKO mice.

Generation of Cre-inducible Slc30a8 KO mice

Generation of floxed ZnT8 mice was achieved by purchasing sperm containing a floxed ZnT8 allele from the Knockout Mouse Project (KOMP) Repository (Project #CSD30329). In the floxed allele, FRT sites surround the LacZ and Neo components of the targeting vector whereas LoxP sites surround ZnT8 exon 2, which encodes the first transmembrane domain [8]. The Vanderbilt Transgenic Mouse/Embryonic Stem Cell Shared Resource performed *in vitro* fertilization and generated live mice from the frozen sperm. Genotyping of these mice using primers that recognize the floxed but not WT ZnT8 allele identified mice containing the targeted allele. Female mice containing this allele were mated with male 129S4/SvJaeSor-Gt(ROSA)26Sor$^{tm1(FLP1)Dym}$/J mice from JAX (Stock #003946). These mice express the FLP1 recombinase gene driven by the *Gt(ROSA)26Sor* promoter. FLP1 was used to remove the LacZ and Neo components of the targeting vector in the floxed ZnT8 allele, thereby converting the allele from a non-expressive form to a conditional allele. Genotyping of the resulting offspring using primers that recognize the floxed ZnT8 allele minus the LacZ/Neo cassette indicated that the FLP1 recombinase had functioned to remove the LacZ/Neo cassette (data not shown).

To generate adult beta cell-specific (BCS) ZnT8 KO mice**,** the floxed ZnT8 mice were mated with *Ins1*^{CreERT2} knock in mice (JAX (Stock #026802)). These knock-in mice express the *CreERT2* recombinase

gene driven by the endogenous mouse *insulin1* promoter [118]. The use of these mice negates the valid concern regarding the use of the more common *Ins1*^{CreERT2} transgenic mice, which have aberrant growth hormone expression in beta cells [193]. These BCS ZnT8 KO mice were injected intraperitoneally with 3 200 mg doses of tamoxifen inducing recombination and removal of exon 2 from the floxed ZnT8 allele in beta cells in adult mice thereby inactivating the gene. Sequence analysis indicates that, were splicing of ZnT8 exon 1 to exon 3 to occur, an in-frame ZnT8 variant lacking only exon 2 encoded amino acids would not be generated.

Cloning of a Guinea Pig *SLC30A7* cDNA

cDNA was generated from Guinea pig pancreas RNA as described [194],[195] and then PCR was used to specifically isolate a Guinea pig *SLC30A7* cDNA in conjunction with the following primers (Hind III cloning sites underlined):

5'-CCCAAGCTT- ATGTTGCCCCTGTCCATCAAG-3'

5'-CCCAAGCTT- TCACTACATGGCGGCAAAGTC-3'

The sequence has been submitted to GenBank under Accession Number KY847522.

PCR Genotyping

The tail tips of mice were removed, the DNA isolated and genotyped using PCR in conjunction with primers that distinguished between the wild type and targeted alleles.

ZnT8 primers used to detect the WT Slc30a8 allele:

5'B (5'-TGCGGCTCATCTCTTAATTG-3')

3'B (5'- CCTCGATGACAACCACAAAG-3')

ZnT8 primers used to detect the targeted Slc30a8 allele:

KO L (5'-GGTGTTGGGTCGTTTGTTCG-3')

KO R (5'- TCCTGAGCAGCAGGCTTGTAG-3')

ZnT7 primers used to detect the WT Slc30a7 allele:

WT2a (5'-AATTCCCGGGTGTGTGTCTG-3')

WT2b (5’- TGGACAGGGGCAACATCTTC-3’)

ZnT7 primers used to detect the targeted Slc30a7 allele:

KO–a (5’-GCAGCGCATCGCCTTCTATC-3’)

KO–b (5’- GAGTTGCAGGAAATGAGAGTCC-3’)

Cre primers used to detect the Cre allele:

CreA (5’-AAACGTTGATGCCGGTGAACG-3’)

CreB (5’-CAGCCACCAGCTTGCATGAT-3’)

Ins1 primers used to detect the *Ins1* allele:

mIns1 GT F (5’-GGACCCACAAGTGGAACAAC-3’)

mIns1 GT R (5’-GCAGGAAGCAGAATTCCAGA-3’)

ZnT8 primers used to detect the modified allele:

CSDSlc30a8 F (5’-TCAAGATTCAGAATCAGTGTCATCTGG-3’)

CSDSlc30a8 ttR (5’-AGACACCTGATCATGCATTTGCACC-3’)

Tail DNA was isolated and purified by standard procedures [196]. The wild type and targeted allele fragments were amplified using 2.8 ng genomic DNA and the Bio-Rad iQ SYBR Green Supermix (Hercules, CA) under the following reaction conditions: 94ºC, 30 sec; 60ºC, 30 sec; 72ºC, 30 sec for 40 cycles. Standard curve analyses were performed for each set of samples to determine the efficiencies of the two PCR reactions, which were all greater than 95%.

Animal Care

The Vanderbilt University Medical Center Animal Care and Use Committee approved all protocols used. The animal housing and surgical facilities used for the mice in these studies meet the American Association for the Accreditation of Laboratory Animal Care standards. Mice were maintained on a standard rodent chow diet (LabDiet 5001; 23% protein and 4.5% fat; PMI Nutrition International) with food and water provided ad libitum. Where specified, mice were placed on a high fat (60% fat calories; Mouse diet F3282; BioServ) diet at 10 weeks of age and maintained on the diet for 15 weeks.

Male Hartley Guinea pigs were purchased from Charles River Laboratories (Wilmington, MA) and fed the 5025 Guinea pig diet (PMI Nutrition International, St Louis, MO). Food and water were provided *ad libitum*.

Measurement of Islet Zinc Content

Freshly isolated islets from WT, Slc30a8 HET and Slc30a8 KO mice were washed in Ca2+-free Hank's balanced salt solution and frozen down at −80°C in 20 islet aliquots. Islet pellets were lysed by re-suspension in 1 ml of lysis buffer [1% Triton X-100 in 10 mM Tris/HCl (pH 7.4). The Zn2+ concentration in the lysate was measured using the Zn2+-sensitive fluorescent dye FluoZin-3 (Invitrogen). In the presence of 1.181 μM FluoZin-3 the fluorescent signal at the emission peak (516 nm) was measured in the total sample lysateusing a fluorometer (PTI Instruments). The fluorescent signal was compared with a standard curve generated from serial dilutions of ZnSO4 in lysis buffer to obtain the lysate Zn2+ concentration and thus the Zn2+ content per islet. As a normalization factor, the protein content per islet was measured in the total sample lysate using the BCA (bicinchoninic acid) protein assay (Pierce). To minimize contaminating Zn2+, all solutions were made in double-distilled water (18.2 MΩ), avoiding the use of any glassware. Blank samples were also prepared during the islet isolation to quantify any additional Zn2+ contamination.

Phenotypic Analysis

Phenotypic analysis was performed on 6 h fasted mice at ~16 weeks of age. Mice were weighed after 5 h fasting and then allowed to recover for one hour prior to being anaesthetized using isoflurane for removal of blood from the retro-orbital venous plexus. Whole blood glucose concentrations were determined using an Accu-Check Advantage monitor (Roche). EDTA was added to blood samples prior to isolation of plasma by centrifugation. Cholesterol was assayed using the cholesterol reagent kit (Raichem), whereas triacylglycerol and glycerol were assayed using a serum triacylglycerol determination kit (Sigma). Insulin levels were quantified using radioimmunoassay (Millipore) by the Vanderbilt Diabetes Research and Training Center Hormone Assay Core. Proinsulin was measured using the

Rat/Mouse Proinsulin ELISA kit (Mercodia) according to manufacturer's instructions. The length of the mice was also measured.

Analysis of Gene Expression using RT-PCR

The methods used for isolation of RNA from mouse islets, the rat 832/13 islet-derived cell line, mouse and Guinea pig organs and the quantitation of gene expression using real time PCR were as previously described [195]. Briefly, Gene expression was quantitated after RNA isolation by using the Turbo DNA-free DNAse Treatment Kit (Ambion, Carlsbad, CA) to remove trace genomic DNA followed by cDNA generation using the iScript DNA Synthesis Kit (Bio-Rad, Hercules, CA) and then PCR using the dUTP-containing FastStart SYBR Green Master Mix in conjunction with Uracil-Glycosylase (Roche, Nutley, NJ). Gene expression was quantitated using the primer-probe TaqMan® approach from Life Technologies (Carlsbad, CA) as described [197]. Fold induction of gene expression was calculated using the 2(-ΔΔC(T)) method [198].

The following primer pairs were used:

Mouse *Gsy2* Forward	5'-CCACACTGCTTGGGCGTTAT-3'
Mouse *Gsy2* Reverse	5'-AGCATGTGCTCTGCCTCGAT-3'
Mouse *Slc30a7* Forward	5'-TTTGTGCTTCCCCCACAATC-3'
Mouse *Slc30a7* Reverse	5'-CCCGGTGACTACGCCAAATA-3'
Mouse *Slc30a8* Forward	5'-TTGCATCTGGGTGCTGACTG-3'
Mouse *Slc30a8* Reverse	5'-GCTCGGACACTGGCATTAGC-3'
Mouse *Ppia* Forward	5'-GGCCGATGACGAGCCC-3'
Mouse *Ppia* Reverse	5'-TGTCTTTGGAACTTTGTCTGCAA-3'
Rat *Slc30a7* Forward	5'-TCCTGGCTGGCTTTGTCAAT-3'
Rat *Slc30a7* Reverse	5'-CCAGAGCCGTGAGAATGTCC-3'
Rat *Slc30a8* Forward	5'-TTGCATCTGGGTGGTGACTG-3'
Rat *Slc30a8* Reverse	5'-TCGAACGCTGGCATTAGCTT-3'

Rat *Ppia* Forward	5’-AGCACTGGGGAGAAAGGATT-3’
Rat *Ppia* Reverse	5’-AGCCACTCAGTCTTGGCAGT-3’
Guinea pig *Slc30a7* Forward	5’-TTTCAAGCATGGAGGTCATGG-3’
Guinea pig *Slc30a7* Reverse	5’-GGGACCATCGTGAGAATGGA-3’
Guinea pig *Slc30a8* Forward	5’-CAGCTGGGACAGCCAGATTG-3’
Guinea pig *Slc30a8* Reverse	5’-TCATGATGTTGCCCATCGAA-3’
Guinea pig *Ppia* Forward	5’-GGTGAAGGAGGGCATGAACA-3’
Guinea pig *Ppia* Reverse	5’-GATGACAGGGCGTTTTGAGC-3’

Human islet gene expression was quantitated using the primer-probe TaqMan® approach using primers purchased from Life Technologies (Carlsbad, CA) as described [195].

Intraperitoneal glucose tolerance tests (IPGTTs) and oral glucose tolerance tests (OGTTs)

IPGTTs and OGTTs were performed on 6 hour fasted conscious mice. Age of mice are indicated in the respective chapters. Briefly, mice were fasted, weighed after 5 hours and then allowed to recover for 1 hour prior to injection or oral gavage with 2 g/kg body weight glucose in sterile PBS. Glycemia was assessed through the analysis of tail vein blood prior to glucose injection/gavage and thereafter at 15, 30, 60, 90 and 120 min using a Freestyle glucose meter (Abbott).

Insulin tolerance tests (ITTs)

ITTs were performed on 5 hour fasted conscious mice. Age of mice are indicated in the respective chapters. Briefly, mice were fasted for 4 hours, weighed, and then allowed to recover for 1 hour prior to injection with a 0.75 U/kg body weight dose of insulin. Glycemia was assessed through the analysis of tail vein blood prior to insulin injection and thereafter at 7.5, 15, 22.5, 30, 37.5, 45 and 60 min using a Freestyle glucose meter (Abbott).

Arginine Tolerance Tests

Arginine tolerance tests were performed on 6 hour fasted conscious mice as described previously [199]. Briefly, mice were fasted for 5 hours, weighed, and then allowed to recover for 1 hour. and basal

blood samples were isolated from the retro-orbital venous plexus. Mice were allowed to recover for 15 mins and glucose [200] was injected. 2 mins later mice were again anesthetized and blood samples were again isolated from the retro-orbital venous plexus. Glucose concentrations were measured in whole blood using an Accu-Check Advantage glucose meter (Roche, Indianapolis, IN). EDTA (5 ml; 0.5 M) was added to blood samples prior to isolation of plasma by centrifugation. Plasma samples were assayed form insulin and C-peptide using radioimmunoassay by the Vanderbilt Diabetes Research and Training Center Hormone Assay Core.

Analysis of Plasma Insulin Levels after Glucose Administration

Glucose-stimulated increases in plasma insulin *in vivo* during IPGTTs and OGTTs were measured as follows. Mice were fasted for 6 hours, anesthetized using isoflurane and basal blood samples were isolated from the retro-orbital venous plexus. Mice were allowed to recover for 15 mins and glucose (2 g/kg) was either injected IP or given via gavage. 15 mins later mice were again anesthetized using isoflurane and blood samples were again isolated from the retro-orbital venous plexus. Glucose concentrations were measured in whole blood using an Accu-Check Advantage glucose meter (Roche, Indianapolis, IN). EDTA (5 ml; 0.5 M) was added to blood samples prior to isolation of plasma by centrifugation. Plasma samples collected from the retro-orbital plexus were assayed for insulin using the MILLIPLEX Metabolic Hormone Multiplex Assay by the Vanderbilt Diabetes Research and Training Center Hormone Assay Core.

Measurement of Plasma C Peptide

Plasma samples collected from the retro-orbital plexus as described above were assayed for C peptide using the MILLIPLEX Metabolic Hormone Multiplex Assay by the Vanderbilt Diabetes Research and Training Center Hormone Assay Core.

Measurement of Plasma Proinsulin

Plasma samples collected from the retro-orbital plexus as described above were assayed for proinsulin using the Rat/Mouse Proinsulin ELISA kit (Mercodia) as previously described [159].

Measurement of Hepatic Glycogen Content

Hepatic glycogen content was determined as previously described [201]. Briefly, the frozen liver was extracted with boiling 5M KOH, the glycogen precipitated with 2 vol. of 95% (vol/vol) ethanol, and re-precipitated with ethanol. The residue was then dissolved in water [202]. Glycogen was hydrolyzed using amyloglucosidase [203]. Glucose was analyzed using UV-methods with hexokinase and glucose-6-phosphate dehydrogenase [204].

Mouse and Human Islet Isolation

Mouse islets were isolated by the Vanderbilt Islet Procurement and Analysis Core as previously described [156, 159]. Human islets were obtained by A.C.P. through the NIDDK-funded Integrated Islet Distribution Program (https://iidp.coh.org/). Human islets designated as 'Group A' based on islet perifusion analyses [205] were used for these studies. Briefly, isolated islets were rinsed and then incubated in RPMI-1640 medium containing 10% (v/v) FBS (fetal bovine serum), 100 units/ml penicillin, 100 µg/ml streptomycin and 11 mM glucose overnight at 37°C. The next day islets were transferred into medium with 5 mM glucose and allowed to equilibrate for 1 h at 37°C.

Analysis of Glucose-Stimulated Insulin Secretion *in vitro*

Islets were isolated from male mice as described above. After the equilibration period, 20-30 islets were incubated in 200 µl of medium with 5 or 16.7 mM glucose for 30 min at 37ºC. At the end of the static incubations, islets were collected, washed and extracted in 0.2 ml of acid alcohol for 48 h at 4ºC. The medium from the static incubations was centrifuged at 600g for 1 min at 4ºC. Islet extracts and static incubation media supernatants were stored at -80ºC until assayed for insulin using the MILLIPLEX Metabolic Hormone Multiplex Assay by the Vanderbilt Diabetes Research and Training Center Hormone Assay Core.

Measurement of Pancreatic Insulin Content

Mice were fasted for 6 hours and pancreas tissue was harvested and weighed. The tissue was homogenized in 5 mL acid alcohol (1 ml concentrated HCl; 110 ml 95% ethanol). The tissue homogenate

was incubated under mild agitation for 48 hours at 4°C. The homogenate was then centrifuged at 2500 rpm for 30 minutes at 4°C. The supernatant was collected and stored at -80°C. Insulin content was measured using using the MILLIPLEX Metabolic Hormone Multiplex Assay by the Vanderbilt Diabetes Research and Training Center Hormone Assay Core.

Analysis of Islet Size and Insulin Content

After collection of isolated islets as described above, islets were resuspended in 6 ml RPMI medium supplemented with 10% (vol/vol) fetal bovine serum, 0.05 mM βmercaptoethanol, 100 U/ml penicillin and 100 µg/ml streptomycin, and allowed to recover overnight at 37°C in small petri dishes. The islets were then transferred to 15 ml conical tubes and centrifuged at 1000 rpm for 2 minutes. The supernatant was removed and the islets were resuspended in 4000 µl RPMI medium with no glucose. Islets were transferred into eppendorf tubes (~ 50 islets/tube). The islets were then precipitated by centrifugation at 6000 rpm for 1 min. The supernatant was removed and the islets were resuspended in 100 µl PBS. 2 µl 5% Triton X-100 was added to each tube and incubated at room temperature for 10 minutes. The samples were then vortexed and 10 µl of the sample was added to 190 µl Hoechst buffer. These samples were placed at -80°C for DNA analysis. 50 µl of the remaining sample was added to 100 µl concentrated acid alcohol (75 ml ethanol:2 ml concentrated HCl:23 ml H2O). The sample was vortexed and incubated at 4°C for 48 hours. The tubes were then centrifuged at 13,000 rpm at 4°C for 5 minutes. The supernatant was transferred to a new tube and insulin content was assayed by the Vanderbilt Diabetes Research and Training Center Hormone Assay Core. DNA content was determined using 96 well plate reader: 50 µl sample was combined with 50 µl Hoechst buffer and 100 µl Hoechst reagent (2 ng/µl). Using a 350nm excitation wavelength and 450nm emission wavelength, the DNA content was measured and concentration calculated using a standard curve. Islet insulin content was measured relative to islet DNA content in each sample. The relative sizes of islets were compared by calculating the ratio of DNA content per islet.

Analysis of Islet Cellular Composition

Islet cellular composition was analyzed as previously described [206]. Briefly, pancreas tissue was harvested, fixed for 4 hours in 4% PFA in PBS at 4°C and embedded for paraffin sectioning. The pancreata were serial sectioned (5 µm sections) and sections 250 µm apart (10-13 slides per animal) were immunolabeled. Guinea pig anti-insulin (Dako Cat# A0564, RRID:AB_10013624; 1:200) and mouse anti-glucagon (Millipore Cat# AB932, RRID:AB_2107329;1:1000) were combined and detected with species-specific secondary antibodies conjugated to Cy 2 (Jackson ImmunoResearch Labs Cat# 706-545- 148, RRID:AB_2340472; 1:200) and Cy 3 (Jackson ImmunoResearch Labs Cat# 711-165-152, RRID:AB_2307443; 1:200), respectively. A ScanScope FL (Leico Biosystems) was used to obtain images. Using Webscope viewing software (Aperio, Vista, CA) and ImageJ (NIH), ~4000 total cells associated with glucagon or insulin were counted for each animal. Nuclei surrounded by red were counted as glucagon positive cells and nuclei surrounded by green were counted as insulin positive cells. The alpha:beta cell ratio was calculated as the number of glucagon positive cells divided by the number of insulin positive cells per animal.

Analysis of Beta Cell Size

Beta cell size was determined by dividing the total area of insulin+ cells (ImageJ, NIH) by the number of insulin+ nuclei (manually counted) as previously described [207].

Analysis of Beta Cell Mass

Beta cell mass was calculated as previously described [208]. Pancreata were harvested and fixed as described above. The pancreata were serial sectioned (5 µm sections) and sections 250 µm apart (10-13 slides per animal) were immunolabeled. Guinea pig anti-insulin (Dako Cat# A0564, RRID:AB_10013624; 1:1,000) with HRPconjugated donkey anti-guinea pig (Jackson ImmunoResearch Labs Cat# 706-035-148, RRID:AB_2340447; 1:400) were used to immunolabel the sections and the sections were counterstained with Eosin-Y (Fisher Healthcare, Houston, TX). The immunolabeling visualized with a DAB kit (Vector Laboratories, Burlingame, CA). A ScanScope CS slide scanner

(Aperio, Vista, CA) was used to obtain images at 20x magnification (resolution of 0.5 µm/pixel), which were then uploaded into a Spectrum digital slide interface (Aperio). The slides were analyzed for beta cell mass using Maulis Beta Cell Mass Classifier Macros [208]. The percentage of beta cell area on each slide section was calculated as the DAB stained area relative to total area and beta cell mass was then expressed relative to total pancreatic weight.

Electron Microscopy

Electron microscopy was performed as previously described [159], Briefly, pancreas tissue was harvested and fixed in 50 mL 2.5% glutaldehyde in 0.1M sodium cacodylate buffer with 1% calcium chloride, pH 7.4 as follows: The tissue was sliced into small sections and fixed for 1 hour at room temperature. The tissue was then cut into sections less than 1 mm, fixed at room temperature for an additional hour and then stored at 4°C overnight. Post fixation was performed with 1% osmium tetroxide, followed by a graded ethanol dehydration series and infiltration with epoxy resin. 500 nm thick sections of embedded tissue were cut and stained with 1% Toluidine Blue. The sections were reviewed for islet location and 70 nm thin sections were collected on grids. The sections were stained with 2% aqueous uranyl acetate and Reynolds lead citrate. These were examined by transmission electron microscopy using the FEI Tancai T-12 electron microscope operating at 100 keV by the VUMC Cell Imaging Shared Resource Core.

Assessment of ZnT7:ZnT8 Dimer Formation

A BLAST search of the NCBI nr database using the human SLC30A7 mRNA sequence as the query (NM_133496; Ref. (9)) identified an IMAGE clone (#30330665; accession number BC064692) containing the entire ZnT7 open reading frame (ORF) in the pBluescriptR vector. Similarly, a BLAST search of the NCBI nr database using the human SLC30A8 mRNA sequence as the query (NM_173851; Ref. (10)) identified an IMAGE clone (#8992162; accession number BC126446) containing the entire ZnT8 ORF in the pCR4-TOPO vector. The Human ZnT7 ORF was amplified using PCR from the IMAGE clone described above using the forward primer: 11 5'-CG GGATCC CCACC ATG

TACCCCTACGACGTGCCCGACTACGCC ATG TTGCCCCTGTCCATC -3'. and reverse primer (antisense sequence shown): 5'-CCC GTTTAAAC CTA CATGGCTGCAAAgTCAATCTGTAC-3'. The forward primer incorporates, in order, a BamHI site, an optimal Kozak sequence, a start codon, an HA tag, the ZnT7 start codon plus the next 5 codons of the ORF. The reverse primer incorporates, in order, a PmeI site, the ZnT7 stop codon plus the last 8 codons of the ORF. The lowercase nucleotide changes a mutation/SNP in the IMAGE clone back to the Slc30a7 sequence reported in NM_133496. The resulting PCR fragment was digested with BamHI and PmeI and ligated into the BamHI and PmeI digested pcDNA3.1D/V5-His TOPO vector (Invitrogen). The Human ZnT8 ORF was amplified from the IMAGE clone described above using the forward primer: 5'-CG GGATCC CCACC ATG GAGTTTCTTGAAAGA-3'. and reverse primer (antisense sequence shown): 5'-CCC GTTTAAAC TCA CGTAGAATCGAGACCGAGGAGAGGGTTAGGGATAGGCTTACCCTTGTCACAGGGGTCTTCA CA-3'. The forward primer incorporates, in order, a BamHI site, an optimal Kozak sequence, the ZnT8 start codon plus the next 5 codons of the ORF. The reverse primer incorporates, in order, a PmeI site, a stop codon, a V5 tag, a codon encoding lysine that replaces the ZnT8 stop codon plus the last 6 codons of the ORF. 12 The resulting PCR fragment was digested with BamHI and PmeI and ligated into the BamHI and PmeI digested pcDNA3.1D/V5-His TOPO vector (Invitrogen). DNA sequencing was used to confirm the absence of polymerase errors. Human cervical-derived HeLa cells were passaged as sub-confluent cultures in RPMI medium supplemented with 10% (vol/vol) fetal bovine serum, 0.05 mM βmercaptoethanol, 100 U/ml penicillin and 100 µg/ml streptomycin. After seeding into 10 cm plates, the cells were transiently transfected with expression plasmids (18 µg) encoding HA-tagged ZnT7 alone, V5-tagged ZnT8 alone, or HA-tagged ZnT7 in combination with V5-tagged ZnT8 using the Lipofectamine Reagent (Invitrogen, Carlsbad, CA) at a Lipofectamine (µl):DNA (µg) ratio of 5:1 according to manufacturer's instructions. The amount of DNA transfected was kept constant by adding the empty pcDNA3 plasmid vector. After an overnight incubation in RPMI serum-containing medium, the cells were washed with cold PBS. The cells were then harvested by addition of 1 ml of RIPA lysis buffer with added

protease inhibitors (10 ml RIPA lysis buffer with one cOmplete ULTRA Tablet, Mini, EDTA-free, EASYpack protease inhibitor cocktail; Roche, Basel, Switzerland) and transferred to pre-chilled ependorf tubes. The lysates were sonicated (~20 pulses), mixed by rotation for 30 minutes at 4°C, and then centrifigued at 12,000 rpm at 4°C for 10 minutes. 350 µl supernatant was transferred to new tubes and incubated with 1 µl primary antibody for 1 hr at 4°C with rotation: anti-HA-HRP (Roche Cat# 12013819001, RRID:AB_390917; 1:350) or anti-V5 (Santa Cruz Biotechnology Cat# sc-81594,RRID:AB_1131162; 1:350). Pierce protein AG magnetic beads (30 µl) were washed in RIPA buffer, resuspended in 24 µl RIPA buffer and then added to supernatant. The beads and supernatant were rotated overnight at 4°C. The beads were then washed three times in 1 ml RIPA buffer and resuspended in 20 µl RIPA buffer. 10 µl SDS-PAGE sample buffer was added to the beads and proteins separated by SDS-PAGE electrophoresis. 13 HA-tagged ZnT7 and V5-tagged ZnT8 were detected using Western blotting in conjunction with antiHA-HRP (Roche Cat# 12013819001, RRID:AB_390917; 1:1000 dilution) or anti-V5 (Santa Cruz Biotechnology Cat# sc-81594, RRID:AB_1131162; 1:1500 dilution). A secondary HRP-conjugated antimouse IgG antibody (Promega Cat# W4021, RRID:AB_430834; 1:10,000) was used to detected V5 antibody binding. HRP activity was assayed using the Western Lightning Plus-ECL reagent (PerkinElmer, Waltham, MA).

Analysis of Body Composition

Body composition was assessed using an mq10 NMR analyzer (Bruker Optics).

Cell Culture

The rat INS-1 derived 832/13 cell line, a generous gift from Dr. Chris Newgard, was cultured as described [209].

Statistical Analysis

Mouse data were analyzed using a one-way or two-way ANOVA assuming normal distribution and equal variance. A post hoc analysis was performed using the Bonferroni correction for multiple comparisons. The level of significance was as indicated. Other data including analysis of time zero basal

glucose and singular time point measurements were analyzed using Student's t-test: two sample assuming equal variance or one-way ANOVA's. The level of significance was as indicated (two-sided test). Gene expression data were analyzed using a Student's t-test: two sample assuming equal variance. The level of significance was as indicated. A P value less than 0.05 was considered significant.

CHAPTER III

Combined Deletion of *Slc30a7* and *Slc30a8* Unmasks a Critical Role for ZnT8 in Glucose-Stimulated Insulin Secretion

Introduction

In the introduction to this dissertation, the function of ZnT8 and *Slc30a8* KO mouse models were extensively discussed, and the association of rs13266634 SNP in the *SLC30A8* locus with T2D was emphasized. Previous studies describing a potential role of ZnT7 in beta cell function and glucose homeostasis were also discussed. Based upon these observations, we hypothesized that functional compensation by ZnT7 may be limiting the impact of *Slc30a8* deletion on islet function. We show here that deletion of *Slc30a7* alone has complex effects on glucose metabolism *in vivo* but no effect on GSIS in isolated islets, whereas combined deletion of *Slc30a7* and *Slc30a8* abolishes GSIS. These data demonstrate that the function of ZnT8 in islets can be unmasked by deletion of a second ZnT and imply that, because the absence of ZnT8 alone has limited effects on beta cell function, ZnT8 may affect T2D susceptibility through actions in other tissues.

Results

Combined Deletion of *Slc30a7* and *Slc30a8* has Mild Effects on Fasting Metabolic Parameters

A modified mouse *Slc30a7* allele, in which exons 1 and 2 [150] were replaced by a LacZ/Neo cassette, was generated by homologous recombination in ES cells (Fig. 3.1A). This design abolishes *Slc30a7* expression while leaving the transcription start site intact such that expression of LacZ mRNA is driven by the *Slc30a7* promoter. Correct gene targeting was confirmed by Southern blot (Fig. 3.1B) and PCR (data not shown) analyses prior to injection of ES cells into blastocysts and subsequent generation of *Slc30a7* HET mice on a mixed 129/SvEv^{Brd} X C57BL/6 genetic background. These mice were interbred to generate *Slc30a7* KO mice, designated as ZnT7 KO.

Using an assay that detects free or loosely bound zinc, Figure 3.1C shows that zinc content was markedly reduced in isolated ZnT7 KO mouse islets relative to those isolated from WT mice. ZnT7 KO

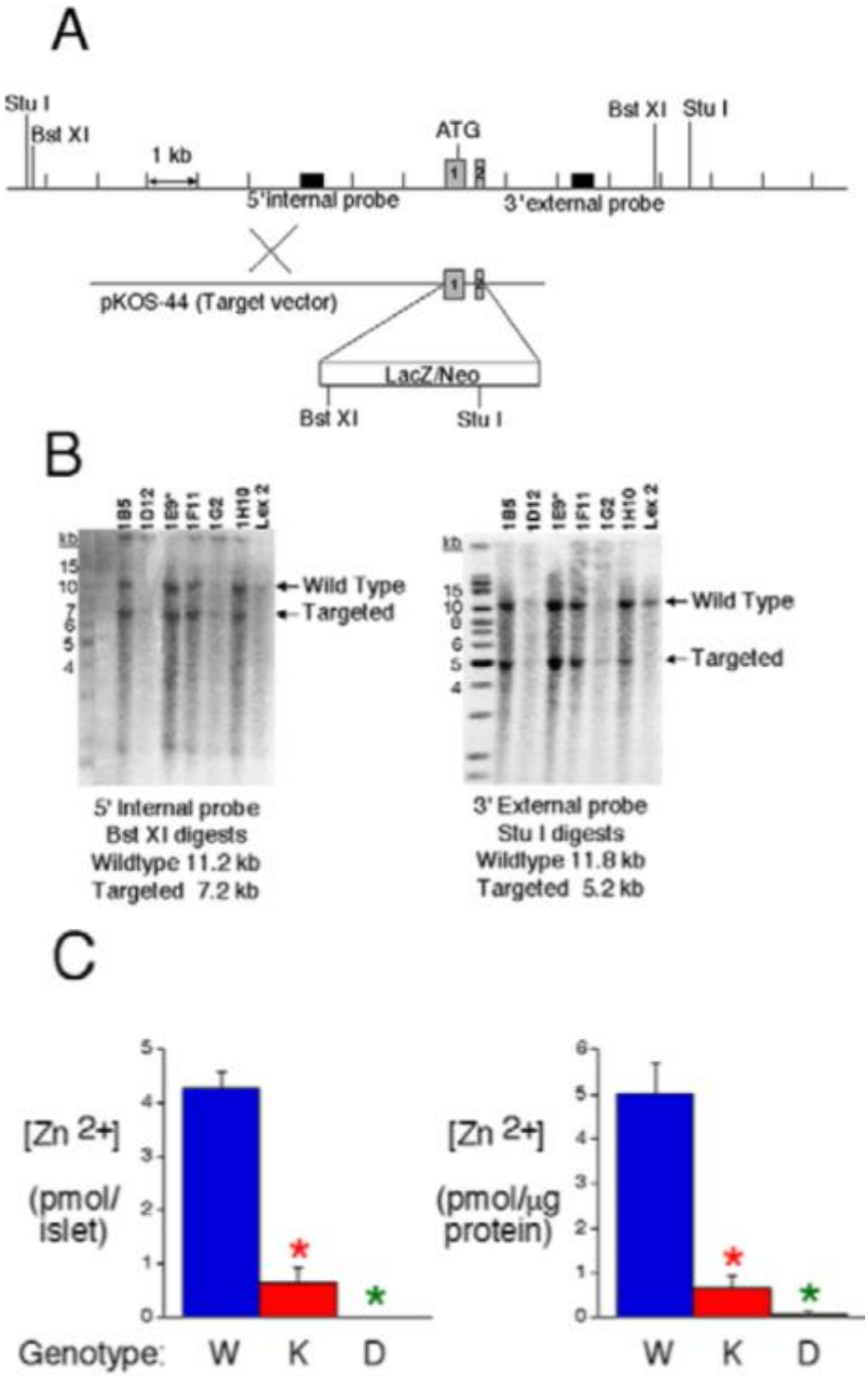

Figure 3.1 Generation and analysis of islet zinc content and fasting metabolic parameters in ZnT7 KO and DKO mice. A, Schematic representation of the WT murine Slc30a7 locus and the targeting construct used to generate ZnT7 KO mice by homologous recombination in ES cells. Exons 1 and 2 were replaced with a cassette containing the LacZ cDNA and a TK-neomycin selectable marker. B, Southern blot analysis of the Slc30a7 locus using genomic DNA extracted from the indicated targeted ES cell lines, or WT ES cell gDNA, designated Lex-2, as a control, using 5′ and 3′ diagnostic probes (A). The sizes of the WT locus, targeted allele, and DNA markers are indicated. Clone 1E9 was used to achieve germline transmission. C, Zinc content in isolated approximately 17-week-old ZnT7 KO and DKO male mouse islets. Results represent the mean ± SEM (n = 3–14); P < .0001, one-way ANOVA; *, differences with WT.

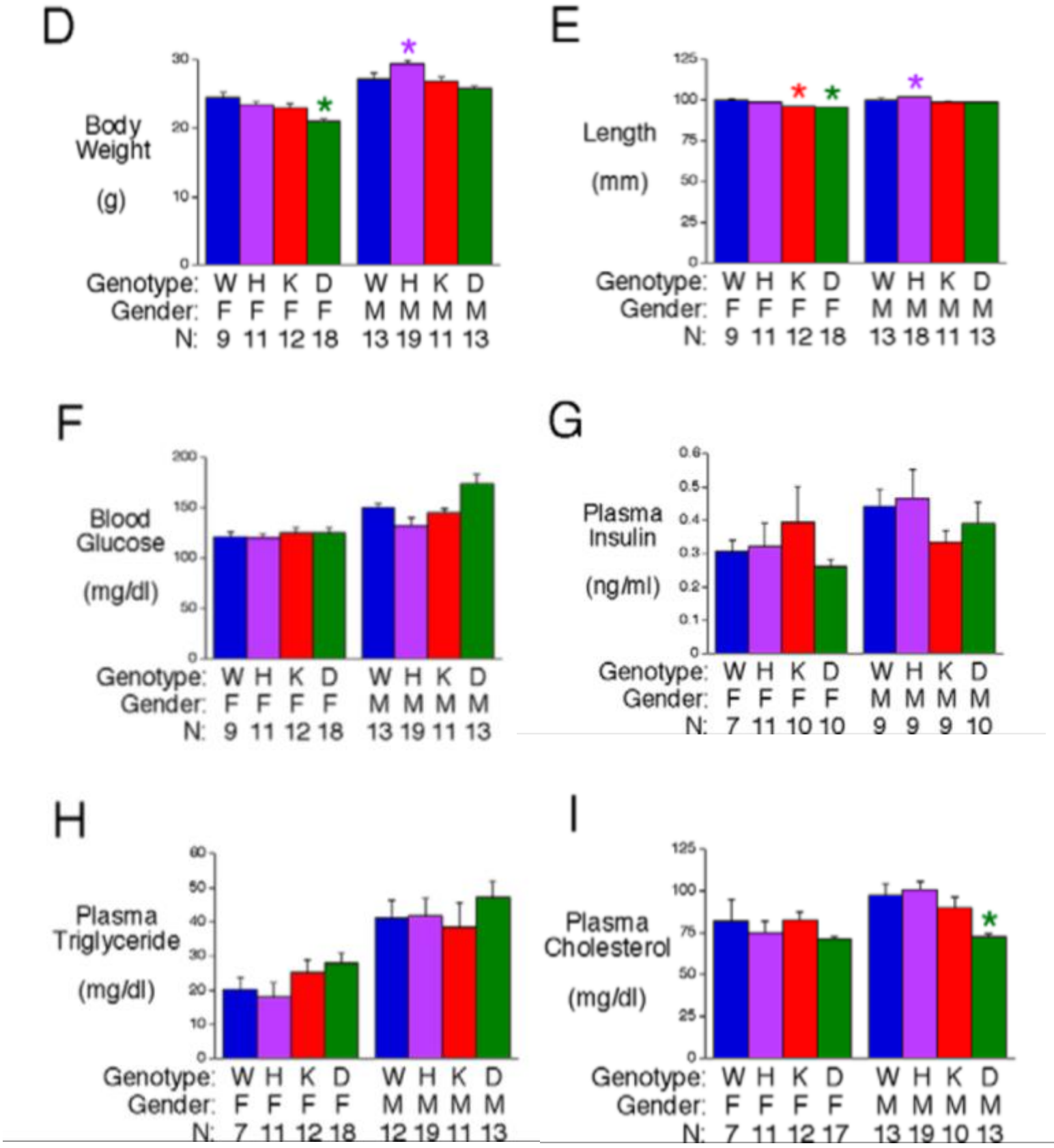

Figure 3.1 Generation and analysis of islet zinc content and fasting metabolic parameters in ZnT7 KO and DKO mice. D–I, Phenotypic parameters in 6-hour fasted 16-week-old ZnT7 KO and DKO mice. Results are the mean ± SEM of data with the genotype, gender, and number of animals indicated. W, WT; H, HET; K, KO; DKO; F, female; M, male. F, $P < .0001$ and M, $P = .001$ (D); F, $P < .0001$ and M, $P = .0002$ (E); M, $P = .0010$ (F); M, $P = .0007$ (I); one-way ANOVA; *, differences with matching WT are indicated.

mice were interbred with ZnT8 KO mice [159] to generate mice lacking both ZnT7 and ZnT8, designated as DKO mice. Figure 3.1C shows that, as expected, zinc content was markedly reduced in isolated DKO mouse islets.

Female, but not male, DKO mice showed a modest reduction in body weight (Fig. 3.1D) and length (Fig. 3.1E) whereas male ZnT7 HET mice showed a modest increase in body weight (Fig. 3.1D) and length (Fig. 3.1E) relative to WT mice. The explanation for these differences is unclear. Despite the marked reduction in islet zinc content, in 16-week-old mice following a 6 hour fast, deletion of ZnT7 alone or in combination with ZnT8 had no effect on fasting glucose (Fig. 3.1F), insulin (Fig. 3.1G) or triglycerides (Fig. 3.1H), though cholesterol was slightly reduced in male DKO mice (Fig. 3.1I). These results suggest that ZnT7 and ZnT8 both have a limited effect on whole body glucose metabolism under fasting conditions, at least in 16-week-old mice.

The Combined Absence of ZnT7 and ZnT8 Markedly Impairs Glucose Tolerance in Male Mice

Since some metabolic disturbances only become readily apparent under stimulatory rather than basal conditions we next investigated whether the absence of ZnT7 alone or in combination with ZnT8 affected the responses to the physiological challenges associated with injections of insulin or glucose. We observed a consistent elevation in blood glucose levels at t=0 in ZnT7 KO mice relative to WT mice following tailing prior to ITTs, OGTTs and IPGTTs (Fig. 3.2). This contrasts with no difference following retro-orbital bleeding (Figs. 3.1 & 3.2) and suggests that ZnT7 KO mice are sensitive to the rise in corticosterone that is associated with the stress of tail [210] but not retro-orbital bleeding [211].

The difference in blood glucose levels between WT, ZnT7 KO and DKO mice at t=0 makes the interpretation of the results of ITTs complex. When expressed relative to starting glucose values, insulin sensitivity appears impaired in both ZnT7 KO and DKO mice relative to WT mice (Fig. 3.2A). However, when expressed as a percentage of starting glucose values, insulin sensitivity appears unchanged between WT, ZnT7 KO and DKO mice (Fig. 3.2B).

In contrast, in ~20-week-old mice, OGTTs using 2 g/kg glucose showed a clear impairment in

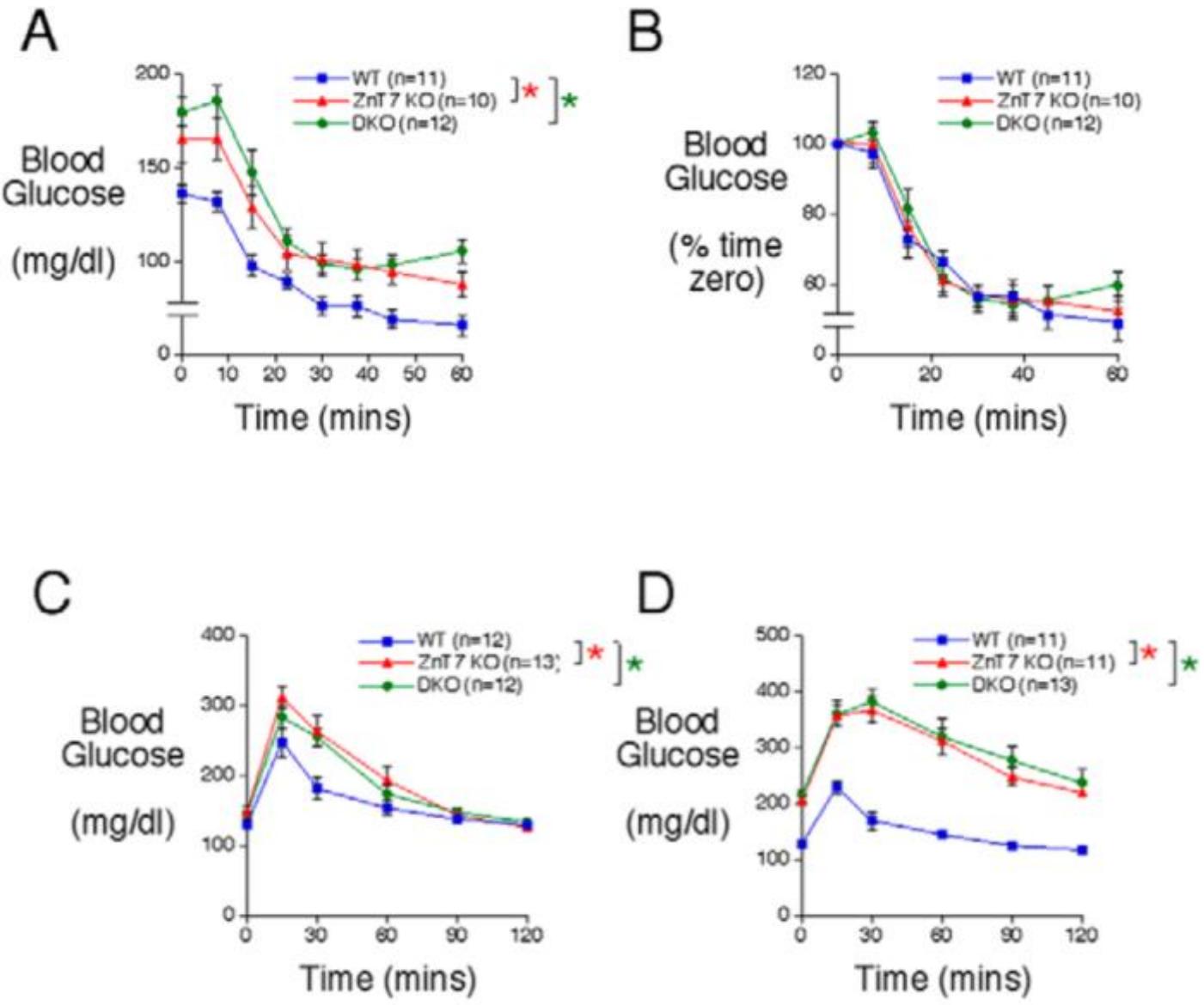

Figure 3.2 Analysis of insulin sensitivity, glucose tolerance, and plasma insulin in ZnT7 KO and DKO mice. A and B, ITTs were performed on 21- to 24-week-old 5-hour fasted conscious male mice. Results show the mean glucose concentrations ± SEM expressed as mg/dL (A) or as a percentage of blood glucose at t = 0 (B). A, P = .0141, two-way ANOVA. C and D, OGTTs were performed on 6-hour fasted 20-week-old female (C) and male (D) conscious mice. Results show the mean glucose concentrations in tail blood ± SEM. C and D, P < .0001, two-way ANOVA.

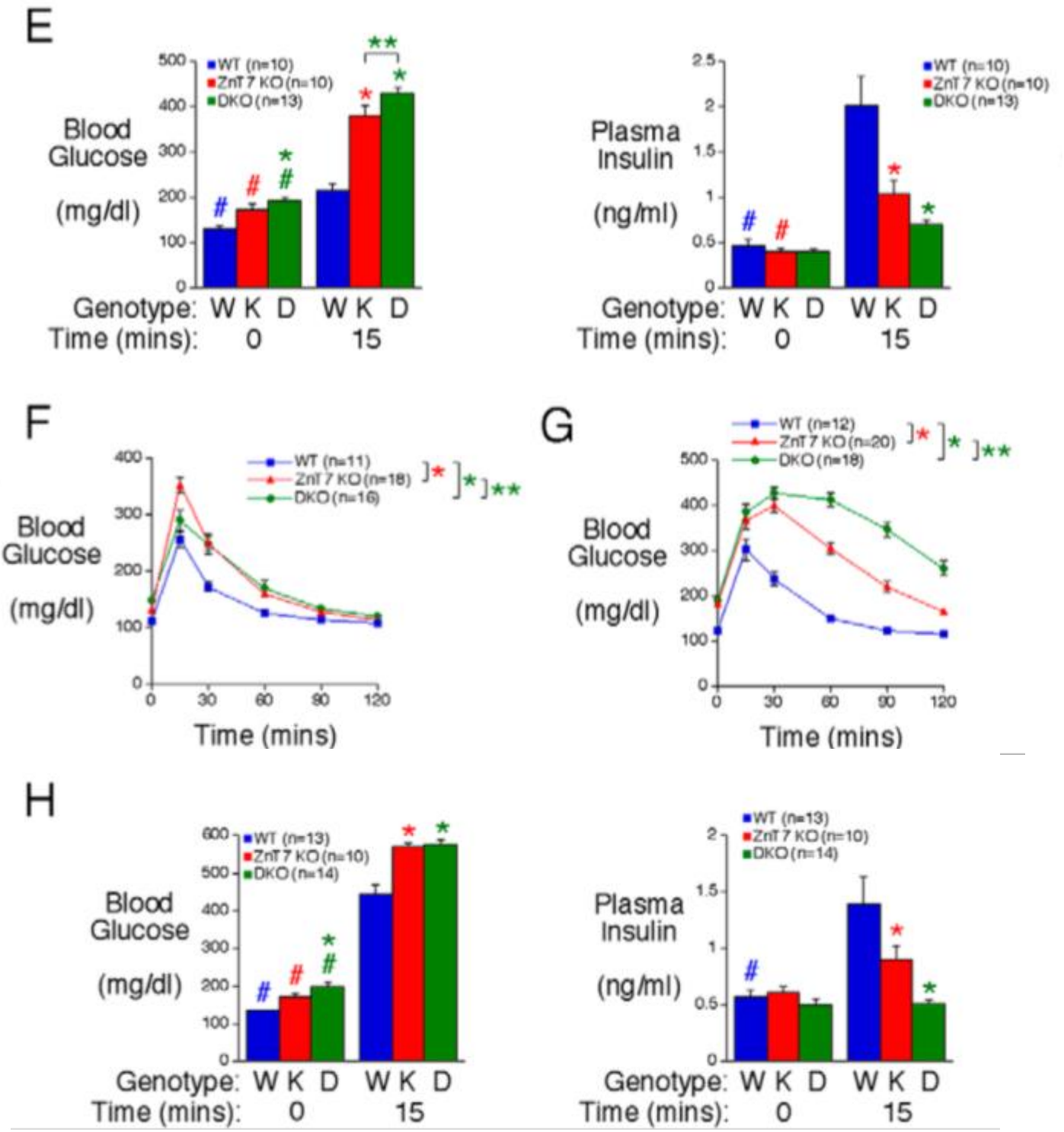

Figure 3.2 Analysis of insulin sensitivity, glucose tolerance, and plasma insulin in ZnT7 KO and DKO mice. E, OGTTs were performed on 6-hour fasted 29- to 30-week-old male conscious mice. Results show the mean glucose and insulin concentrations in blood isolated from the retro-orbital plexus ± SEM. Glucose and insulin data: $P < .0001$, two-way ANOVA; *, differences with WT; **, differences between ZnT7 KO and DKO; #, differences between t = 0 and t = 15. F and G, IPGTTs were performed on 6-hour fasted 10-week-old female (F) and male (G) conscious mice. Results show the mean glucose concentrations in tail blood ± SEM. F and G, $P < .0001$, two-way ANOVA; *, differences with WT; **, differences between ZnT7 KO and DKO. H, IPGTTs were performed on 6-hour fasted 22- to 25-week-old male conscious mice. Results show the mean glucose and insulin concentrations in blood isolated from the retro-orbital plexus ± SEM. Glucose data, $P < .0099$, two-way ANOVA. Insulin data: $P < .0017$, two-way ANOVA; *, differences with WT; #, differences between t = 0 and t = 15.

glucose clearance between female (Fig. 3.2C) and male (Fig. 3.2D) WT and ZnT7 KO mice. This impairment was not further enhanced in DKO mice (Figs. 3.2C & D). In slightly older ~30-week-old mice, OGTTs showed a marked reduction in glucose-stimulated plasma insulin levels in both male ZnT7 KO and DKO mice relative to WT mice (Fig. 3.2E). Huang et al. previously analyzed a ZnT7 KO mouse model generated by gene trap insertional mutagenesis [152], [151]. The insertion in intron 6 of the *Slc30a7* gene resulted in the generation of a ZnT7 protein truncated at amino acid residue 221 [151]. In contrast to our data, Huang et al. [152] reported a selective impairment in glucose tolerance in OGTTs in male mice but not females.

IPGTTs also showed an impairment in glucose tolerance between female (Fig. 3.2F) and male (Fig. 3.2G) WT and ZnT7 KO mice but, in contrast to OGTTs, this impairment was clearly enhanced in male (Fig. 3.2G), though not female (Fig. 3.2F) DKO mice. This impaired intraperitoneal glucose tolerance was associated with a marked reduction in glucose-stimulated plasma insulin levels in male ZnT7 KO mice relative to WT mice whereas in DKO mice the normal increase in plasma insulin levels in response to glucose injection was abolished (Fig. 3.2H). The difference in the response of male DKO mice to OGTTs (Figs. 3.2D & E) and IPGTTs (Figs. 3.2 G & H) suggests that incretin-stimulated insulin secretion remains at least partially intact, consistent with a trend towards increased plasma insulin in DKO mice 15 mins post glucose gavage (Fig. 3.2E).

The Combined Absence of ZnT7 and ZnT8 Affects Islet Morphology

We next investigated the basis for the impaired glucose-stimulated increase in plasma insulin in ZnT7 KO and DKO mice. We first considered the possibility that islet abundance or morphology had been affected. Figure 3.3A shows that pancreatic insulin content is reduced in both ZnT7 KO and DKO mice. This is associated with reduced beta cell mass (Fig. 3.3B) but not insulin (Fig. 3.3C) or DNA content (Fig. 3.3D) in isolated islets or with a change in beta cell size (Fig. 3.3E). These data suggest that islet size is unchanged in ZnT7 KO and DKO mice but pancreatic insulin content is reduced due to reduced beta cell mass. We also observed an increase in alpha:beta cell ratio (Fig. 3.3F). In ZnT7 KO mice we observed an

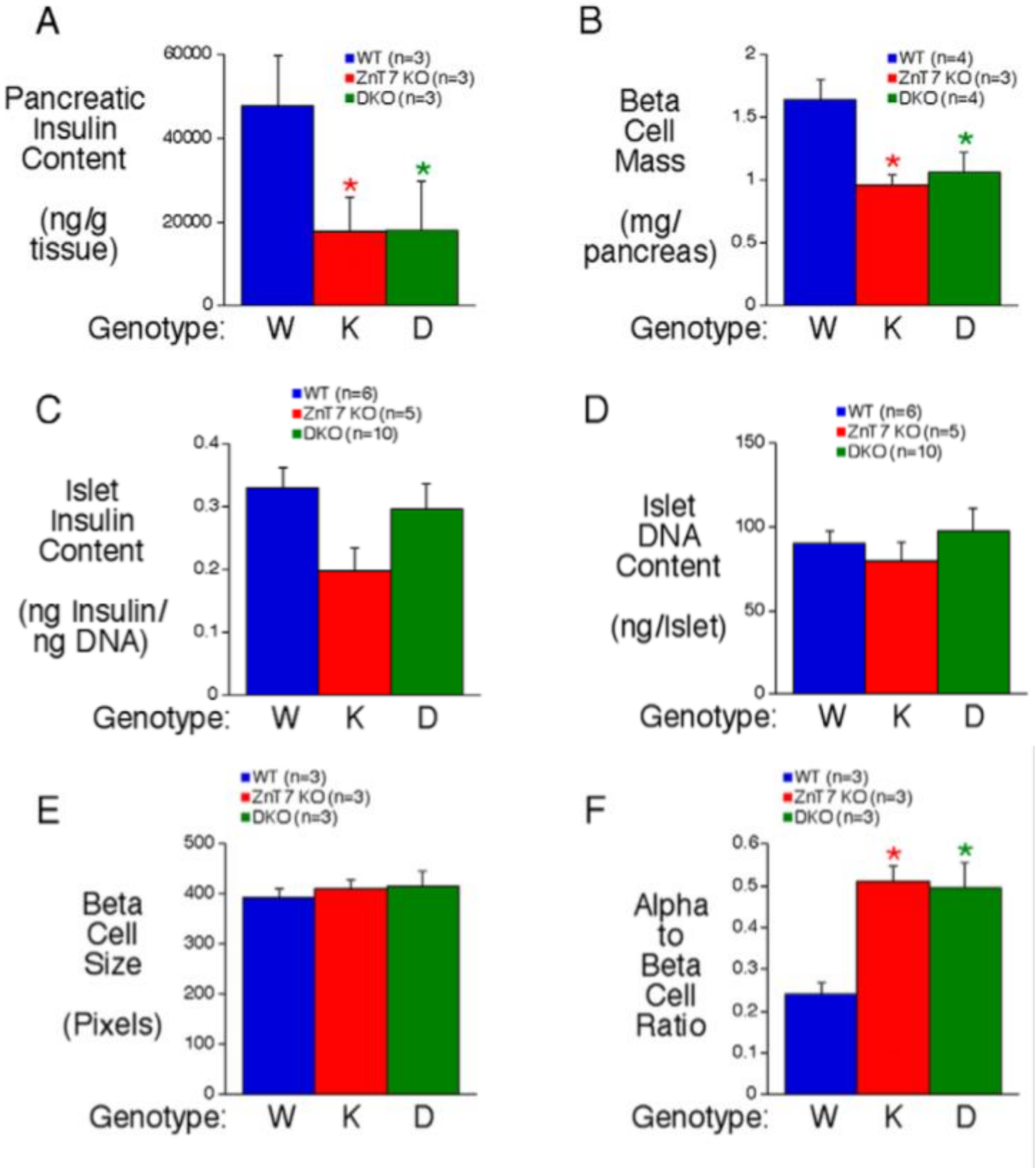

Figure 3.3 Analysis of pancreatic insulin content and islet structure in ZnT7 KO and DKO mice. A, Insulin content in whole pancreas from 20- to 24-week-old 6-hour fasted male mice. Results represent the mean ± SEM (n = 3); P = .0148, one-way ANOVA; *, differences with WT. B–D, β-Cell mass (B), isolated islet insulin content (C), isolated islet DNA content (D), β-cell size (E), and α- to β-cell ratio (F) in male mice. Pancreas and islet results represent the mean ± SEM; P = .0174, one-way ANOVA (B); P = .0029, one-way ANOVA (F); *, differences with WT.

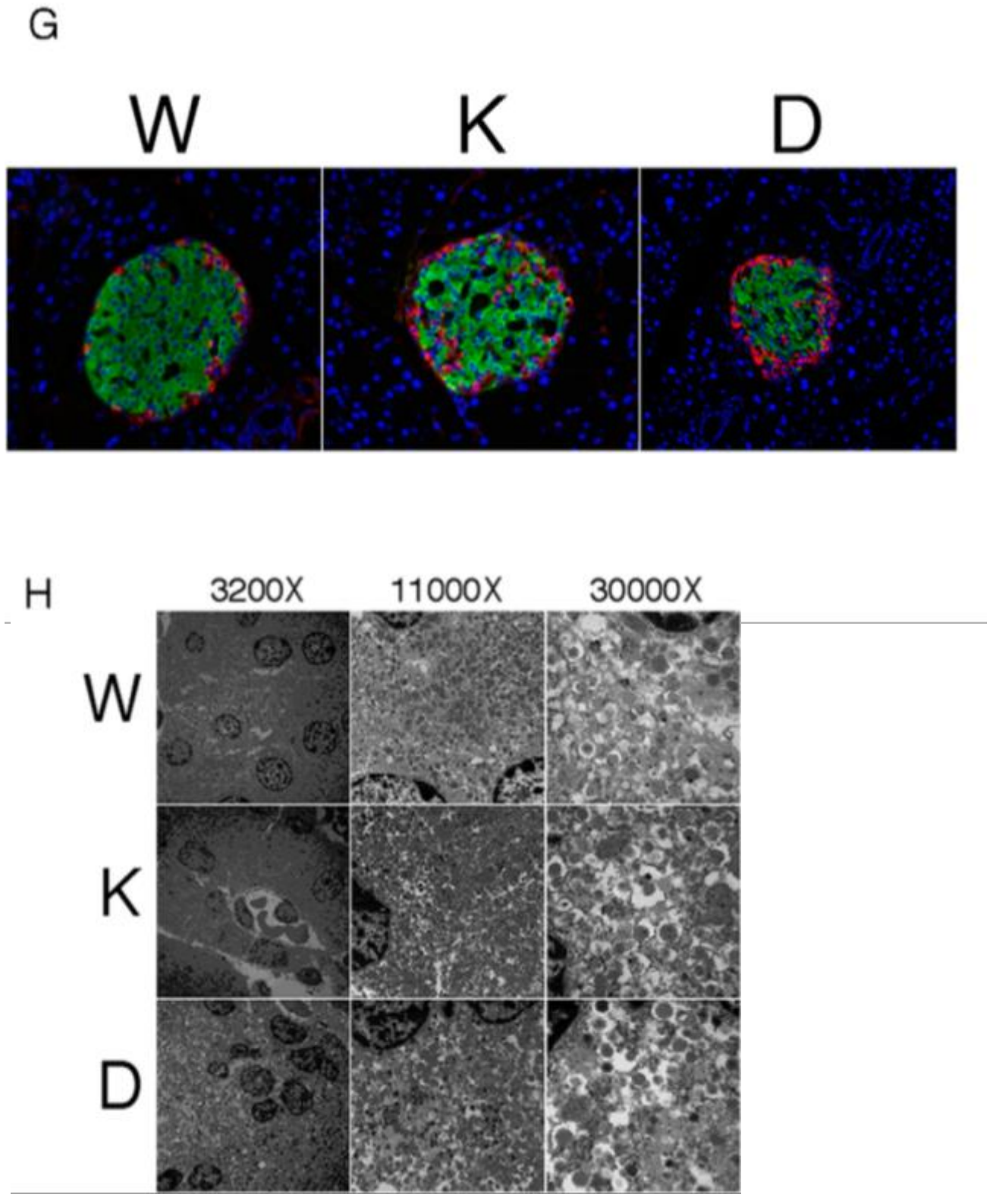

Figure 3.3 Analysis of pancreatic insulin content and islet structure in ZnT7 KO and DKO mice. G, Immunofluorescent staining of 18-month-old male mouse pancreata with antisera raised to insulin and glucagon. Representative pictures (×15 magnifications) are shown. H, Analysis of insulin secretory granule structure in 12-week-old male mice using EM. Representative micrographs are shown.

increase in alpha cells within the islet core whereas in DKO mice peripheral alpha cells appeared to be increased (Fig. 3.3G). Electron microscopy revealed no major structural differences in beta cells (Fig.3. 3H). Specifically, no changes in insulin granule density were identified.

GSIS is Abolished in Islets Lacking both ZnT7 and ZnT8

We next considered the possibility that the absence of ZnT7 alone or in combination with ZnT8 also directly affects islet cell function. Following overnight culture in 11 mM glucose followed by culture in 5 mM glucose for 1 hour GSIS was assessed after static islet incubations in either 5 mM or 16.7 mM glucose for 30 min. Strikingly, GSIS was unaffected in ZnT7 KO islets but was abolished in DKO islets (Fig. 3.4A). These results imply a key role for ZnT7 and ZnT8 in GSIS and demonstrate that deletion of ZnT7 unmasks the function of ZnT8.

The apparent difference between the marked impairment in glucose-stimulated plasma insulin levels in ZnT7 KO mice *in vivo* (Fig. 3.2E & I) compared to the lack of effect on GSIS in isolated ZnT7 KO mouse islets (Fig. 3.4A) presumably largely reflects a deficit in pancreatic insulin content (Fig. 3.3A). In isolated islet studies, the secreted insulin is calculated as a percent of the insulin content. Similarly, when we correct the plasma insulin levels after glucose stimulation in the IPGTT for pancreatic insulin content a difference is observed between WT and DKO but not ZnT7 KO mice consistent with the isolated islet data (Fig. 3.4B).

Because ZnT7 is expressed in multiple tissues other than islets including liver, kidney and brain [150] we investigated whether the absence of ZnT7 in other tissues affected other aspects of metabolism *in vivo*. In liver, both glycogen accumulation (Fig. 3.4C), and expression of *Gsy2* (Fig. 3.4D), which encodes glycogen synthase, are reduced in ZnT7 KO mice. In addition insulin clearance actually appears reduced in ZnT7 KO mice in both IPGTTs (Fig. 3.4E) and OGTTs (Fig. 3.4F), though the interpretation of these data is complex because ZnT7 expression in kidney may have affected clearance of C peptide [212]. Interestingly, in DKO mice hepatic glycogen accumulation was markedly increased (Fig. 3.4C),

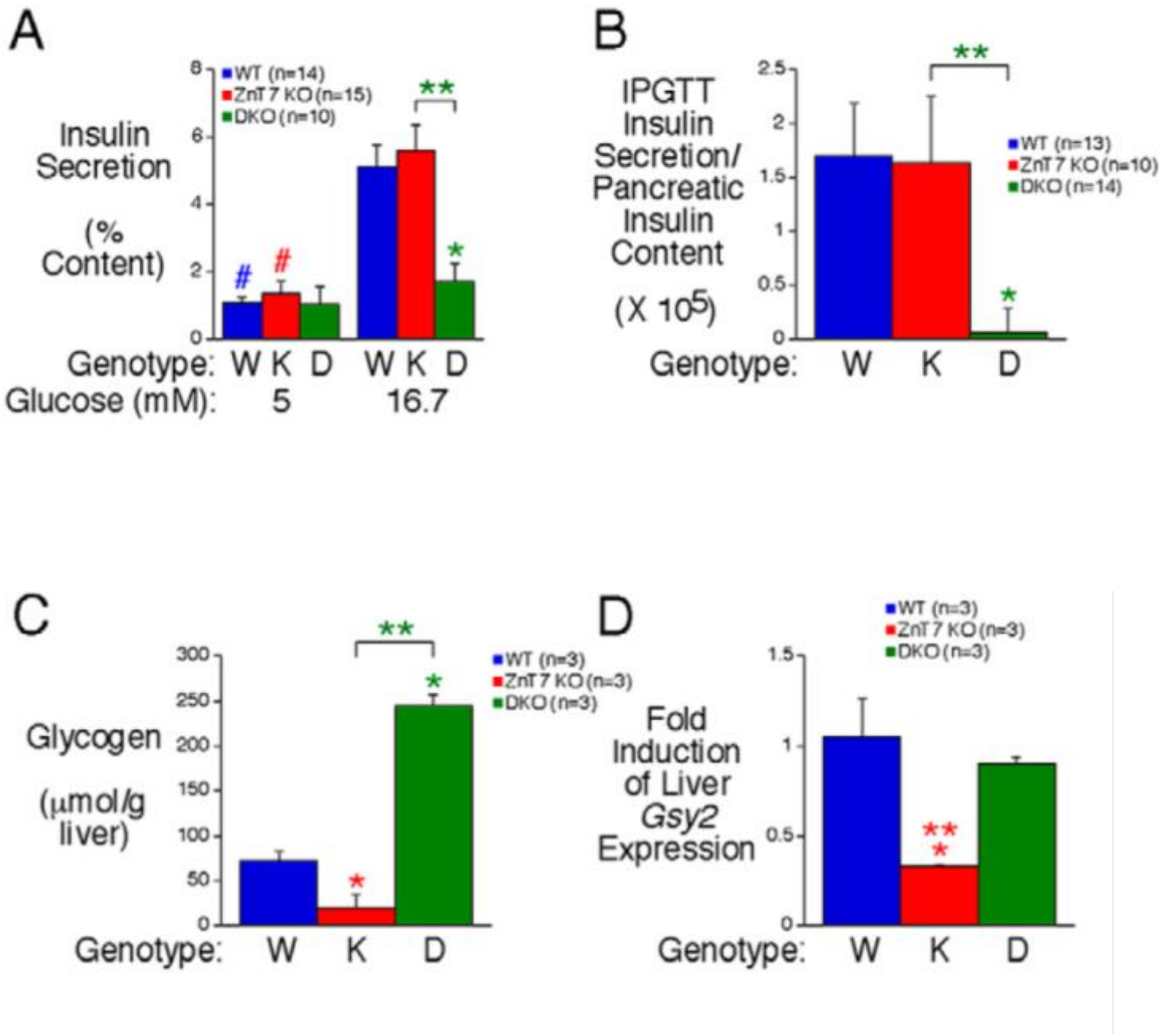

Figure 3.4 Analysis of insulin secretion in vitro in islets isolated from ZnT7 KO and DKO mice and the molecular basis for altered plasma insulin levels in vivo. A, GSIS in islets isolated from approximately 34-week-old male ZnT7 KO and DKO mice. Results show the mean data ± SEM from 5–10 islet preparations. P = .0046, two-way ANOVA; *, differences between WT and DKO; **, differences between ZnT7 KO and DKO; #, differences between 5mM and 16.7mM glucose. B, Ratio of plasma glucose-stimulated insulin at t = 15 during IPGTTs in 6-hour fasted 20- to 25-week-old male conscious mice relative to pancreatic insulin content. Results represent the mean ± SEM; P = .0125, one-way ANOVA; *, difference between WT and DKO; **, difference between ZnT7 KO and DKO. C and D, Hepatic glycogen content (C) and Gsy2 expression (D) in 6-hour fasted 28- to 36-week-old male mice. Results represent the mean ± SEM; P < .0001, one-way ANOVA (C); P = .0140, one-way ANOVA (D); *, differences with WT; **, differences between ZnT7 KO and DKO.

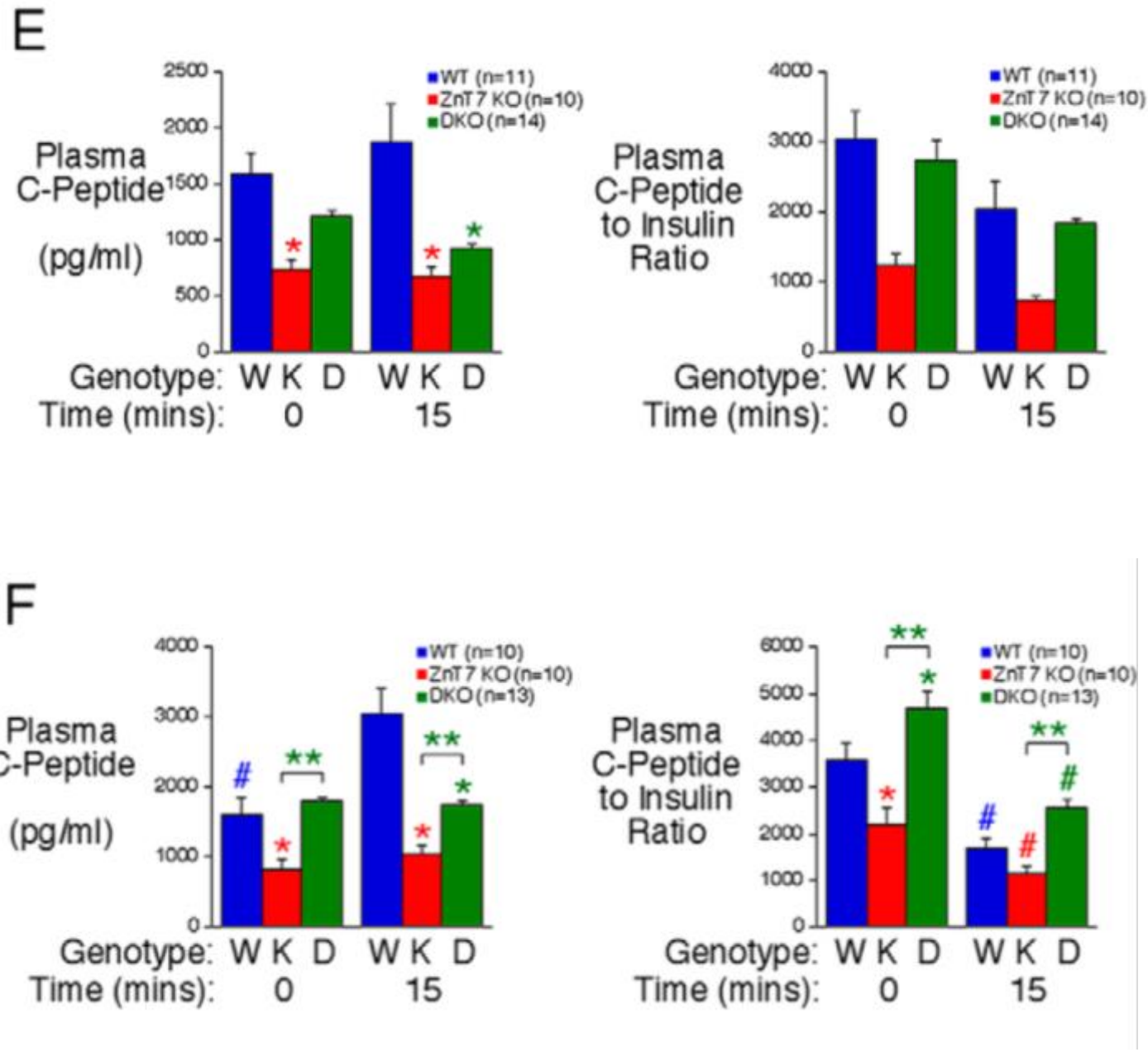

Figure 3.4 Analysis of insulin secretion in vitro in islets isolated from ZnT7 KO and DKO mice and the molecular basis for altered plasma insulin levels in vivo. E and F, IPGTTs (E) or OGTTs (F) were performed on 6-hour fasted 22- to 30-week-old conscious male mice. Results show the mean C peptide concentration in blood isolated from the retro-orbital plexus ± SEM. Matching insulin data are from Figure 2, E and H. C peptide data: P = .0362 (E); C peptide data: P < .0001 (F); C peptide:insulin data: P = .0105 (F), two-way ANOVA; *, differences with WT; **, differences between ZnT7 KO and DKO; #, differences between t = 0 and t = 15.

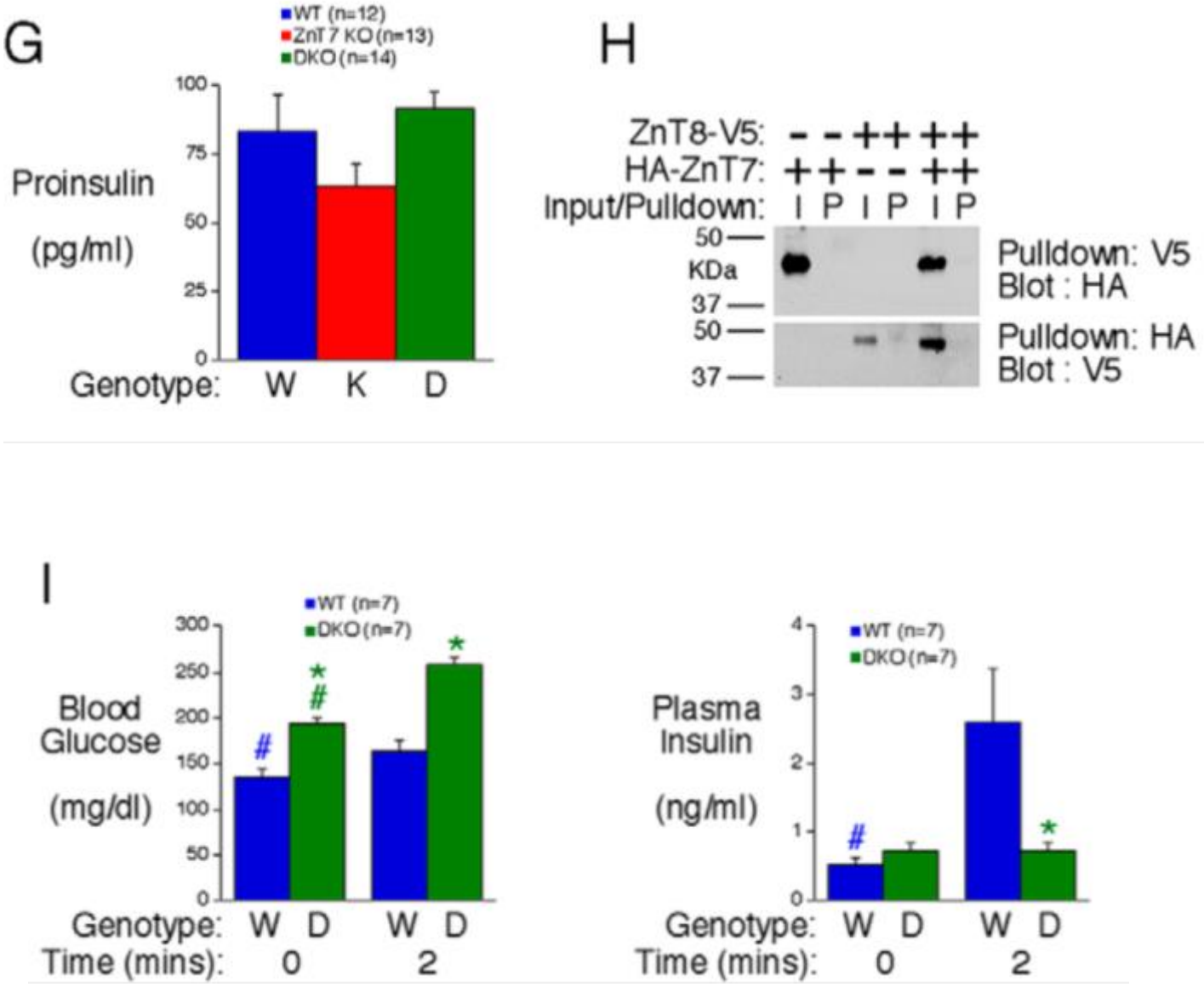

Figure 3.4 Analysis of insulin secretion in vitro in islets isolated from ZnT7 KO and DKO mice and the molecular basis for altered plasma insulin levels in vivo. G, Plasma proinsulin levels in 6-hour fasted 29- to 30-week-old conscious male mice. Results represent the mean ± SEM. H, Absence of ZnT7:ZnT8 dimer formation as assessed using pulldown assays. Representative blots are shown. I, Arginine tolerance tests were performed on 6-hour fasted 28- to 34-week-old conscious male mice. Results show the mean glucose and insulin concentrations in blood isolated from the retro-orbital plexus ± SEM. Glucose data: P = .0005; insulin data: P = .0161, two-way ANOVA; *, differences with WT; #, differences between t = 0 and t = 2.

though *Gsy2* expression (Fig. 3.4D) and insulin clearance in both IPGTTs (Fig. 3.4E) and OGTTs (Fig. 3.4F) were unaffected.

We next explored the mechanism for the impaired GSIS in isolated DKO islets *in situ* (Fig. 3.4A). Because zinc is important for proinsulin to insulin conversion [6] and, in humans, *SLC30A8* SNPs are associated with impaired proinsulin conversion [184], we hypothesized that insulin processing might be altered in DKO islets. However, no difference in plasma proinsulin was observed in ZnT7 KO or DKO mice (Fig. 3.4G), suggesting the absence of a defect in insulin processing, which is consistent with normal fasting insulin levels (Fig. 3.1G).

Although ZnT7 is predominantly located in the Golgi [150] and ZnT8 in secretory granules [129], because ZnTs form dimers [172], [6], we considered the possibility that ZnT7:ZnT8 dimers may be functionally important in beta cells. However, pull down assays showed no evidence for dimer formation (Fig. 3.4H). Finally, arginine-tolerance tests were performed to begin to determine the location of the defect in GSIS in DKO islets. While arginine enters beta cells it is not metabolized and causes depolarization [213]. Figure 3.4I demonstrates that intraperitoneal injection with 1 g/kg arginine stimulated an increase in plasma insulin in WT but not DKO mice suggesting that the defect in GSIS in DKO islets is distal to the activation of voltage-gated calcium channels.

Discussion

While the global absence of ZnT8 has little effect on glucose tolerance or GSIS [156], [159], [170], [172] the absence of ZnT7 markedly impairs glucose tolerance and the rise in plasma insulin in IPGTTs (Fig. 3.2). However, strikingly GSIS is not impaired in isolated ZnT7 KO islets (Fig. 3.4). In contrast, the rise in plasma insulin in IPGTTs in DKO mice *in vivo* (Fig. 3.2) and GSIS in isolated DKO islets *in situ* (Fig. 3.4) are both abolished. These observations appear to dissociate islet zinc levels and GSIS because a marked reduction in zinc is observed in both ZnT7 KO (Fig. 3.1) and *Slc30a8* KO [156], [159], [170], [172] islets with little or no effect on GSIS. Future studies will use this DKO mouse model to uncover the molecular mechanism whereby these ZnTs regulate GSIS (Fig. 3.4) and islet development (Fig. 3.3).

The observation that insulin clearance is not altered in DKO mice (Fig. 3.4) contrasts with a recent study using RIP-Cre mice to specifically remove ZnT8 from beta cells. This study suggested that the absence of ZnT8 increased hepatic insulin clearance thereby impairing insulin secretion *in vivo* and glucose tolerance [128]. However, this study used *Slc30a8* floxed mice rather than RIP-Cre mice as matching controls [128] and the reported impairments in insulin secretion *in vivo* and glucose tolerance were very similar to those associated with RIP-Cre alone [175]. Indeed, another study looking at beta cell-specific *Slc30a8* deletion using RIP-Cre mice as controls reported little effect of *Slc30a8* deletion on glucose tolerance or GSIS *in vivo* [171].

Flannick et al. [190] have strikingly shown that *SLC30A8* haploinsufficiency is protective against the development of T2D in obese humans. To reconcile the observations of Flannick et al. [190] with previous human GWAS data we suggested in a recent review [6] that the GWAS data should be re-interpreted in terms of the minor rs13266634 T allele being associated with protection against T2D, though other interpretations have been suggested [121]. We hypothesized that the protective mechanism might relate to regulating oxidative stress in beta cells [6] but the conclusion that ZnT7 can functionally compensate for ZnT8 in beta cells may indicate that this protective effect is mediated by altered ZnT8 action in other tissues, where it is expressed at much lower levels than islets.

Based on the results of these studies, we conclude that ZnT7 is functionally redundant with ZnT8; however, the basis for this redundancy is not due to heterodimer formation between these two isoforms (Figure 3.4H). Within the vesicle, the zinc concentration is 1.5 times that which is necessary for proper insulin crystallization [124], and the amount of zinc present in *Slc30a8* KO mouse models is sufficient for proper beta cell function [156] [159]. Potentially, the zinc concentration necessary for proper GSIS is transported into the Golgi apparatus by ZnT7 farther upstream in the insulin biosynthesis and secretory pathway than vesicular budding and zinc transport by ZnT8 into the mature vesicle. This would support our conclusion that ZnT8 is not essential for beta cell function, as the appropriate zinc content is already available within the vesicles.

Interestingly, ZnT7 KO mice appear to have a more dramatic phenotype compared to WT and DKO mice, specifically, a reduction in glycogen content, *glycogen synthase* expression, and insulin clearance (Figure 3.4C, D, E, F), but GSIS is abolished in DKO and not in ZnT7 KO mice (Figure 3.4A). This was unexpected. A potential explanation for this phenomenon is differential expression of *Slc30a7* and *Slc30a8* in different tissues. For example, deletion of *Slc30a7* from certain tissues may result in the observed defects, but the additional deletion of *Slc30a8* from a different set of tissues may attenuate the phenotype. The loss of *Slc30a7* and *Slc30a8* in tissue where they are co-expressed, i.e. the beta cells, would lead to severe defects, such as those seen in GSIS in isolated islets.

CHAPTER IV

The Diabetes Susceptibility Gene *SLC30A8* that Encodes the Zinc Transporter ZnT8 is a Pseudogene in Guinea Pigs Potentially Explaining Low Guinea Pig Islet Zinc Content

Introduction

As demonstrated in the previous chapter, combined deletion of *Slc30a7* and *Slc30a8* abolished GSIS [176], and these data demonstrate that the function of ZnT8 in islets can be unmasked by removal of ZnT7. The role of zinc in islet function was also highlighted in the introduction of this dissertation, which appears at odds with the observation that deletion of *Slc30a8* in mice markedly lowers islet zinc with little effect on glucose metabolism [6], [121]. In addition, Guinea pigs lack zinc-bound insulin and have low islet zinc content. Based on the observation that ZnT7 can compensate for the absence of ZnT8 in islets [176], we wondered whether Guinea pigs would still retain high islet expression of *SLC30A8* despite having low zinc levels. Such a result might suggest an important role of ZnT8 in Guinea pig islets despite the low zinc content. Surprisingly we report here that *SLC30A8*, but not *SLC30A7*, is a pseudogene in Guinea pigs. We also show that *SLC30A7* is expressed in human islets though the ratio of *SLC30A7* to *SLC30A8* expression varies considerably. These observations suggest that the inability of Guinea pig insulin to bind zinc and the absence of ZnT8 may both contribute to low islet zinc content. More importantly, these data suggest that ZnT7 may compensate for the absence of ZnT8 in both human and Guinea pig islets, which would imply that ZnT8 is not essential for islet function and support the hypothesis that *SLC30A8* haploinsufficiency is protective against the development of T2D, not due a reduction of ZnT8 in beta cells, but in other tissues where it is expressed at low levels.

Results

The *SLC30A8* Gene is a Pseudogene in Guinea Pigs

As a first step towards determining whether Guinea pig islets still maintain high *SLC30A8* expression, despite low zinc content, we attempted to isolate a Guinea pig *SLC30A8* cDNA. A BLAST search of the NCBI nr and refseq_rna databases using the human *SLC30A8* cDNA sequence (NM_173851)

as the query failed to identify any clones. We therefore searched for the Guinea pig *SLC30A8* gene by performing a BLAST search of the NCBI refseq_genomic database using the human *SLC30A8* cDNA sequence as the query. This identified a genomic scaffold that contains the entire Guinea pig *SLC30A8* gene as a contiguous sequence (NT_176419).

Potential exon/intron splice junctions in the putative Guinea pig *SLC30A8* gene were determined by comparison with the human *SLC30A8* [8] and mouse *Slc30a8* [156] genes and the consensus sequence for RNA splicing [3] (Table 4.1). As with the human *SLC30A8* [8] and mouse *Slc30a8* [156] genes, the Guinea pig *SLC30A8* gene appeared to contain 8 exons, 7/8 of which matched the sizes of the human and/or mouse exons (Table 4.1). However, closer inspection of the sequence while attempting to re-construct a putative Guinea pig *SLC30A8* cDNA revealed that the Guinea pig *SLC30A8* gene is a pseudogene (Fig. 4.1). Notable differences with the human *SLC30A8* open reading frame include a switch from a starting methionine to a valine, the presence of two in-frame stop codons and the deletion of 11 base pairs in exon 7 (Table 4.1) that would result in a frame-shift (Fig. 4.1). In addition, comparison with the splice junctions identified in the human *SLC30A8* [8] and mouse *Slc30a8* [156] genes reveals changes away from the consensus at three junctions that would be predicted to impair splicing (Table 4.1). Since 95.55% of the bases are assembled for the Guinea Pig genome, the possibility that the *SLC30A8* gene underwent duplication in Guinea Pigs and that we have failed to identify an intact *SLC30A8* variant appears remote.

The *SLC30A7* Gene is Intact and Expressed in Guinea Pigs

We next explored the possibility that ZnT7 may be able to compensate for the absence of ZnT8 in Guinea pigs as it can in mice. A BLAST search of the NCBI nr database using the human *SLC30A7* cDNA sequence (NM_133496) as the query identified a computer predicted Guinea pig *SLC30A7* cDNA (XM_003479176). The computer predicted sequence differs at 4 amino acids that are highly conserved in other species leading us to suspect that the computer prediction was incorrect. We therefore cloned a

Table 4.1 Comparison of the Exon/Intron Boundaries of the Human and Guinea Pig *SLC30A8*

Intron	Species	5′ Exon/Intron Junction	3′ Intron/Exon Junction	Exon	Exon Size (bp)
A	Human	CACTAGAAAG/gtaatagatg	tcatccatag/TGTGGAACTCCAA	1/2	71/200
	Mouse	CTCTAGACAG/gtaagaagat	tcctcaacag/AGAACTTCGA		71/197
	Guinea Pig	CCCTGGAGAG/gtaagagaca	tcatccacag/TATGGAACTC		71/197
B	Human	GAGGTCGTGG/gtgagtcttt	cattctctag/GTGGGCACAT	2/3	200/147
	Mouse	GAGGTGGTGG/gtgagtactg	catctcacag/GTGGACACGT		197/147
	Guinea Pig	GAAGTCGTGG/gtaagtacgg	acccctgtag/TTGGGCACAT		197/147
C	Human	CACCGAGCAG/gtacggttca	gaattcctag/AGATCCTTGG	3/4	147/154
	Mouse	TATCGAGCAG/gtaacattct	tgactcccag/AGATCCTCGG		147/154
	Guinea Pig	TACCAAGCAG/gtacagttct	gaattctcac/AGATTTTTGG		147/154
D	Human	CCAACATTGT/gtaagtcatc	tctctttcag/ACTAACTGTG	4/5	154/151
	Mouse	CCAACATTGT/gtaagtcata	tctctttcag/ACTAACTATG		154/151
	Guinea Pig	CCGACGTTGT/tgtgtaagta	tctttttcag/AATAAATGTG		154/151
E	Human	CTACTTTAAG/gtgagtttga	ttttttctag/CCAGAGTATA	5/6	151/106
	Mouse	CTACTTTAAG/gtgagtgtgt	tgttttccag/CCTGACTACA		151/106
	Guinea Pig	CTACTTTAAG/gtgaatgtga	tgttttccag/ACAGATTACA		151/106
F	Human	CTCATGGAAG/gtaggagtga	cttttgtcag/GTGTGCCAAA	6/7	106/135
	Mouse	CTCATGGAAG/gtaggactgc	cctttgtcag/GTGTTCCAAA		106/135
	Guinea Pig	CTCATGGAAG/ataggaggga	ccttcatcag/GTGTAGCCAA		106/124
G	Human	GTTGCTACAG/gtcagtgagt	ttatcaacag/CAGCCAGCCG	7/8	135/146
	Mouse	GTTGCTACAG/gtcagtgagt	ttatcaacag/CTGCCAGCCA		135/143
	Guinea Pig	GTCACTGCAG/gtcactgagc	ctaccatcag/TGGCCAGCTG		124/146
	Consensus	(A or T)G/gtaa	cag/G		

Exon and intron sequences are shown in uppercase and lowercase letters, respectively. The 5' and 3' consensus splice sequences are from Jackson et al. [3]. The sizes of exons 1 and 8 represent just the coding sequence within these exons and do not include untranslated regions. Differences between human and mouse are shown in red, differences between human and Guinea pig are shown in blue. Both mouse and Guinea pig exon 2 encode one less amino acid than human exon 2 but the changes occur in different locations.

```
Guinea Pig  1    VESLERTYLVTDKDIRMYDCTLESMELQRNTANKDRGPGKRSEQ-EPGGIYHCHSSSKAT  59
                 +E LERTYLV DK  +MY  TLES+ELQ+   NKD+ P +R E+ E GG+YHCHS SK T
Human       1    MEFLERTYLVNDKAAKMYAFTLESVELQQKPVNKDQCPRERPEELESGGMYHCHSGSKPT  60

Guinea Pig  60   ENRTKEQVGGRWKLGVAWAICLLLVIAEVVVGHIAGSLAIITGAAHLLVDLTNFLLCLFS  119
                 E    E    +WKL  A AIC + +IAEVV GHIAGSLA++T AAHLL+DLT+FLL LFS
Human       61   EKGANEYAYAKWKLCSASAICFIFMIAEVVGGHIAGSLAVVTDAAHLLIDLTSFLLSLFS  120

Guinea Pig  120  LWLSTRSSSKKLTFGWYQAEIFGALLSILCICVMTRLLMDLVSGHLLCPDWXIQAILLII  179
                 LWLS++  SK+LTFGW++AEI GALLSILCI V+T +L+ L    LL PD+ IQA ++II
Human       121  LWLSSKPPSKRLTFGWHRAEILGALLSILCIWVVTGVLVYLACERLLYPDYQIQATVMII  180

Guinea Pig  180  ISGCAVVADVVINVLLHQRCLGHNHKKVXVNASVRAAFMHTLGDVLDSISVLITSTLVTYF  239
                 +S CAV A++V+ V+LHQRCLGHNHK+V  NASVRAAF+H LGD+  SISVL S L+ YF
Human       181  VSSCAVAANIVLTVVLHQRCLGHNHKEVQANASVRAAFVHALGDLFQSISVLISALIIYF  240

Guinea Pig  240  KTDYRIADLICMFVFTILVLGSTITIVKNFTIVLMEGVAKGLSYSYVKTLILAINGVZZZ  299
                 K +Y+IAD IC F+F+ILVL STITI+K+F+I+LMEGV K L+YS VK LILA++GV
Human       241  KPEYKIADPICTFIFSILVLASTITILKDFSILLMEGVPKSLNYSGVKELILAVDGVLSV  300

Guinea Pig  300  KGLNLCSLTMNQVMLLVKVTAVASWDSQIVWRGVTRALSKSFTIYLLTIQMESLADQNPK  359
                   L++ SLTMNQV+L   V   AS DSQ+V R + +ALSKSFT++ LTIQMES  DQ+P
Human       301  HSLHIWSLTMNQVILSAHVATAASRDSQVVRREIARALSKSFTMHSLTIQMESPVDQDPD  360

Guinea Pig  360  CFLCEDPKD  368
                 C  CEDP D
Human       361  CLFCEDPCD  369
```

Figure 4.1 Alignment of the human and non-functional Guinea pig ZnT8 peptide sequences. The alignment of the peptide sequence of human ZnT8 (Accession Number NM_173851) with the non-functional Guinea pig ZnT8 is shown. Identities are indicated by matching letters and similarities by the '+' symbol. The two stop codons (X) in the Guinea pig peptide sequence are shown in red. An 11 bp deletion in the putative Guinea pig exon 7 deletes 3 amino acids (indicated by ZZZ in blue) and creates a frameshift mutation. If translated, the open reading frame would be maintained 3' of this frameshift as shown. Putative transmembrane domains predicted using TOPCONS web server [1] are shaded in gray. The locations of the 6 transmembrane domains are somewhat different to those previously predicted [8].

Guinea pig *SLC30A7* cDNA. An alignment of human and Guinea pig ZnT7 shows 96.5% amino acid identity, including conservation of all 4 ambiguous amino acids (Fig. 4.2).

Figure 4.3A shows expression of Guinea Pig *SLC30A7* in multiple tissues, namely brain, liver, pancreas and testis. Mouse *Slc30a7* is expressed in the same tissues (Fig. 4.3B) whereas mouse *Slc30a8* is predominantly expressed in pancreas (Fig. 4.3C). No signal was detected using primers to Guinea Pig *SLC30A8* as predicted (data not shown).

ZnT7 can compensate for the absence of ZnT8 in mouse islets [176] despite ~10 fold higher expression of *Slc30a8* than *Slc30a7* [172]. A similar ratio (mean 1:19.2 ± 4.9; n=8) of *SLC30A7* to *SLC30A8* expression was observed in human islets classified as 'Group A' on the basis of robust GSIS in islet perifusion analyses [205] suggesting that ZnT7 may also have the potential to compensate for the absence of ZnT8 in human islets. Interestingly, though *SLC30A8* expression in islets was consistently higher than *SLC30A7* (Fig. 4.3D), the ratio between individuals was variable (Fig. 4.3E).

In contrast to mice, changing *Slc30a8* expression in the islet-derived INS-1 cell line reproducibly affects GSIS [214]. However, compared to mouse islets, the ratio of *Slc30a7* to *Slc30a8* expression is higher (mean 1:32.8 ± 4.3; n=4) (Fig. 4.3F) and using the same assay that detects loosely bound zinc in islets [176], zinc was undetectable in INS-1 cells. These differences may explain why reducing *Slc30a8* expression selectively affects GSIS in INS-1 cells.

Discussion

To reconcile the observation by Flannick et al. [190] that *SLC30A8* haploinsufficiency reduces T2D risk with the observation that the major rs13266634-C allele increases T2D risk, we initially suggested that the GWAS data should be re-interpreted in terms of the minor rs13266634-T allele being associated with protection against T2D [6]. And we hypothesized that the protective mechanism might relate to the regulation of oxidative stress by cytoplasmic zinc in beta cells [6]. However, the observations that *SLC30A8* is a pseudogene in Guinea pigs (Fig. 4.1) and that ZnT7 can compensate for ZnT8 in mice [176], and perhaps

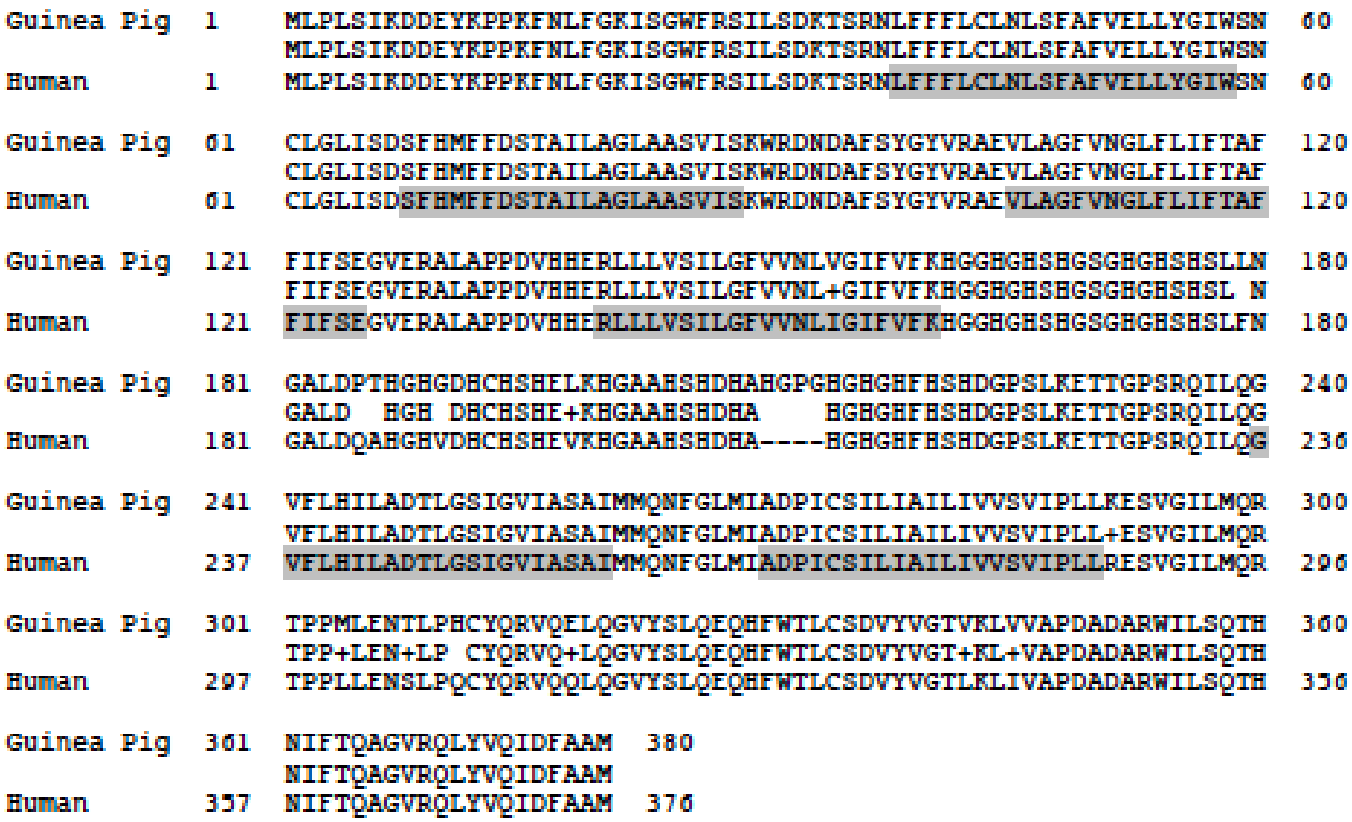

Figure 4.2 Alignment of the human and Guinea pig ZnT7 peptide sequences. The alignment of the peptide sequence of human ZnT7 (Accession Number NM_133496) and Guinea pig ZnT7 (Accession Number KY847522) is shown. Identities are indicated by matching letters and similarities by the '+' symbol. Putative transmembrane domains predicted using TOPCONS web server [1] are shaded in gray.

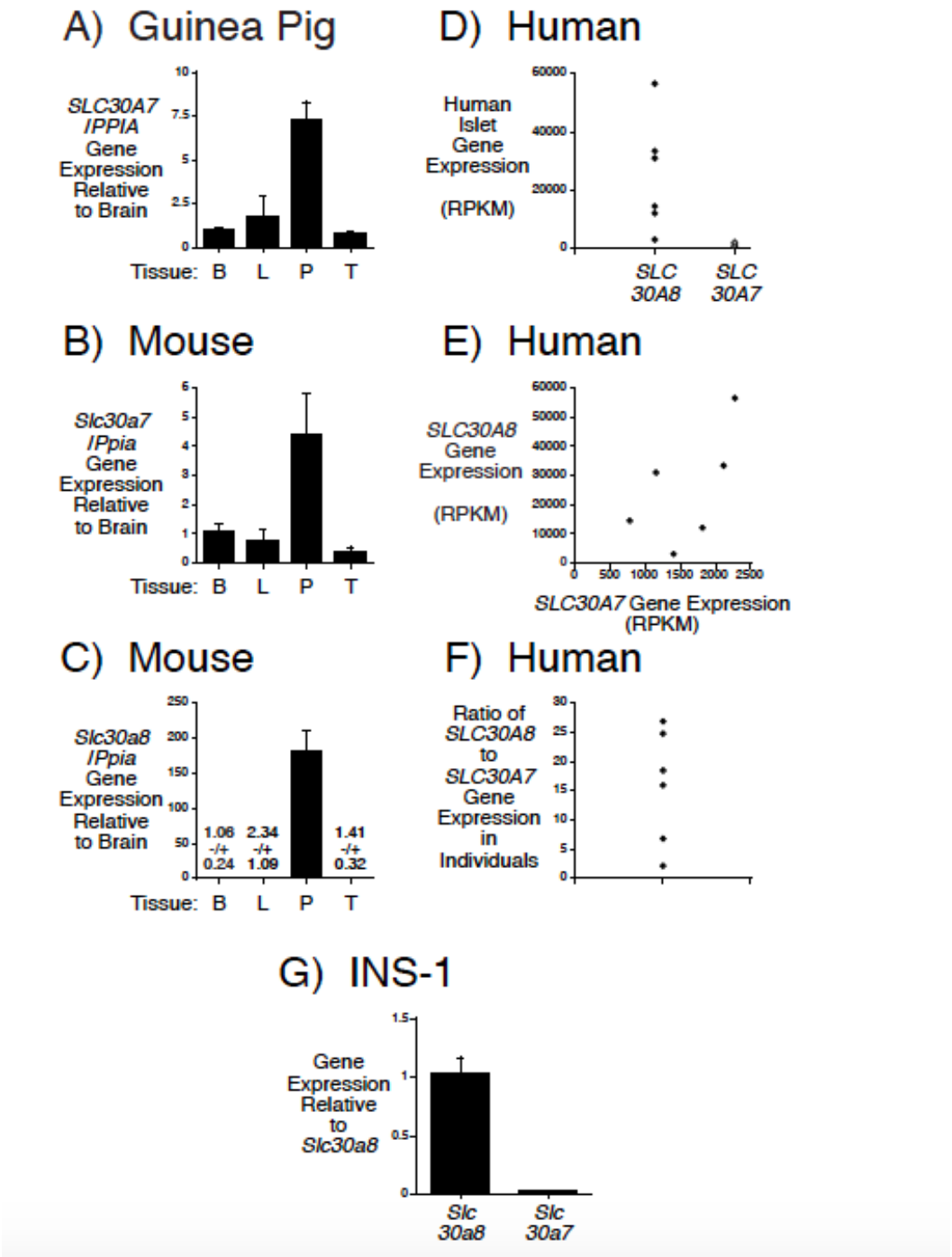

Figure 4.3 Comparison of *SLC30A7* and *SLC30A8* expression between different organs and species. Real time quantitative PCR was used to compare Guinea pig *SLC30A7* (Panel A), mouse *Slc30a7* (Panel B), and mouse *Slc30a8* (Panel C) gene expression in different organs. Results show the mean ± S.E.M. of 3 animals. Real time quantitative PCR data show that *SLC30A8* expression is higher than *SLC30A7* in human islets (Panel D), though the ratio of *SLC30A7* to *SLC30A8* expression between individuals is variable (Panel E). Results show the mean ± S.E.M. of 8 Group 1 islet analyses. Real time quantitative PCR was used to compare rat *Slc30a7* and *Slc30a8* gene expression in INS-1 cells (Panel F). Results show the mean ± S.E.M. of 4 experiments.

humans (Fig. 4.3) supports the alternate hypothesis that *SLC30A8* haploinsufficiency reduces T2D risk through an action in another tissue where it is expressed at low levels [167].

An equally interesting issue is the identification of the mechanism by which the rs13266634-C allele increases T2D risk. Results from both human studies [184], [185], [186] and a recent transgenic mouse study [215] suggest that the ZnT8 R325 variant impairs beta cell function and therefore represents a deleterious gain of function, in contrast to the absence of ZnT8 that has little effect on beta cell function. A recent study has shown increased transporter activity with the R325 variant [188] which leads to increased zinc content in humans with this variant [189], which is presumably toxic.

CHAPTER V

Heterozygous and Homozygous Deletion of *Slc30a8* Protects Against Diet-Induced Obesity

Introduction

Mouse models investigating the deletion of *Slc30a8* have shown modest and inconsistent effects of on glucose tolerance, insulin secretion, and proinsulin-to-insulin ratios. These data from *Slc30a8* KO mouse models did not demonstrate a key role for ZnT8 in glucose homeostasis or beta cell function and appeared at odds with the human rs13266634 SNP transporter activity data, which initially showed that the R325 risk allele had reduced zinc transport activity relative to the W325 variant [172]. However, recent studies reexamining the transporter activity of the SNP variants demonstrated that the risk R325 allele actually has an increased rate of zinc transport relative to the W325 variant [188], leading to elevated islet zinc content in humans [189]. This elevated zinc is hypothesized to be toxic to the cell, impairing beta cell function. These new data suggest that the risk allele is a gain-of-function variant, whereas *Slc30a8* KO mice represent loss-of-function models.

Flannick *et al.* examined over 150,000 individuals and identified 12 ZnT8 protein-truncating mutations that lead to loss-of-function [190]. Their data indicated that individuals who are haploinsufficient for *SLC30A8* have a 65% reduced risk of T2D development. In their study, Flannick *et al.* initially increased statistical power by sequencing exons in 352 young, lean individuals with T2D and 406 elderly, obese euglycemic controls. We predicted that there would be a protective effect of *Slc30a8* haploinsufficiency in mice, as in humans, but only in the context of a diabetogenic environment. In this study, we show that in mice on a high fat diet (HFD), the heterozygous or homozygous loss of ZnT8 protects against diet-induced obesity (DIO), leading to improved glucose tolerance and insulin sensitivity. These observations suggest that *SLC30A8* haploinsufficiency may be protective against the development of T2D by reducing body weight. Given the results of the studies on DKO mice, namely the functional redundancy between ZnT7 and ZnT8 and the conclusion that ZnT8 is not essential for beta cell function,

we hypothesize that this protective effect is due to *SLC30A8* haploinsufficiency in peripheral tissue where *Slc30a8* is expressed at low levels.

RESULTS

Heterozygous or Homozygous Global Germline Deletion of ZnT8 Does Not Affect Glucose Tolerance in Mice on a Chow Diet

We previously investigated the phenotype of *Slc30a8* KO mice, designated here as ZnT8 KO, on a pure C57BL/6J background, but these studies did not include *Slc30a8* heterozygous mice. In light of the publication by Flannick *et al.* [190], we repeated the phenotypic analysis of ZnT8 KO mice but now included *Slc30a8* heterozygous (HET) mice, designated as ZnT8 HET. As previously reported, free or loosely bound zinc was markedly reduced in isolated ZnT8 KO islets compared to WT islets (Figure 5.1A). As expected, an intermediate level of islet zinc was observed in isolated ZnT8 HET islets relative to ZnT8 WT and ZnT8 KO mouse islets (Figure 5.1A). Despite the significant decrease in islet zinc content, IPGTTs showed no difference in glucose tolerance between ZnT8 WT and ZnT8 HET male mice on a chow diet at 4 weeks of age (Figure 5.1B). A slight impairment in glucose tolerance between ZnT8 KO and ZnT8 WT mice was observed, which replicates our previously published IPGTT data in 4-week-old mice [159]. We previously showed that this difference was lost in older mice (~20 weeks) [159]. Similarly, there was no difference in FBG or FPI or blood glucose and insulin levels 15 minutes after IP administration of 2g/kg glucose between the genotypes at 10 weeks of age (Figure 5.1C-F). Additionally, there was no difference in C peptide levels (Figure 5.1G) or insulin to C peptide ratios, an indicator of insulin clearance, between the genotypes during the same IPGTT (Figure 5.1H). These data suggest that homozygous or heterozygous deletion of *Slc30a8* has little effect on glucose metabolism in mice on a chow diet on a C57BL/6J genetic background.

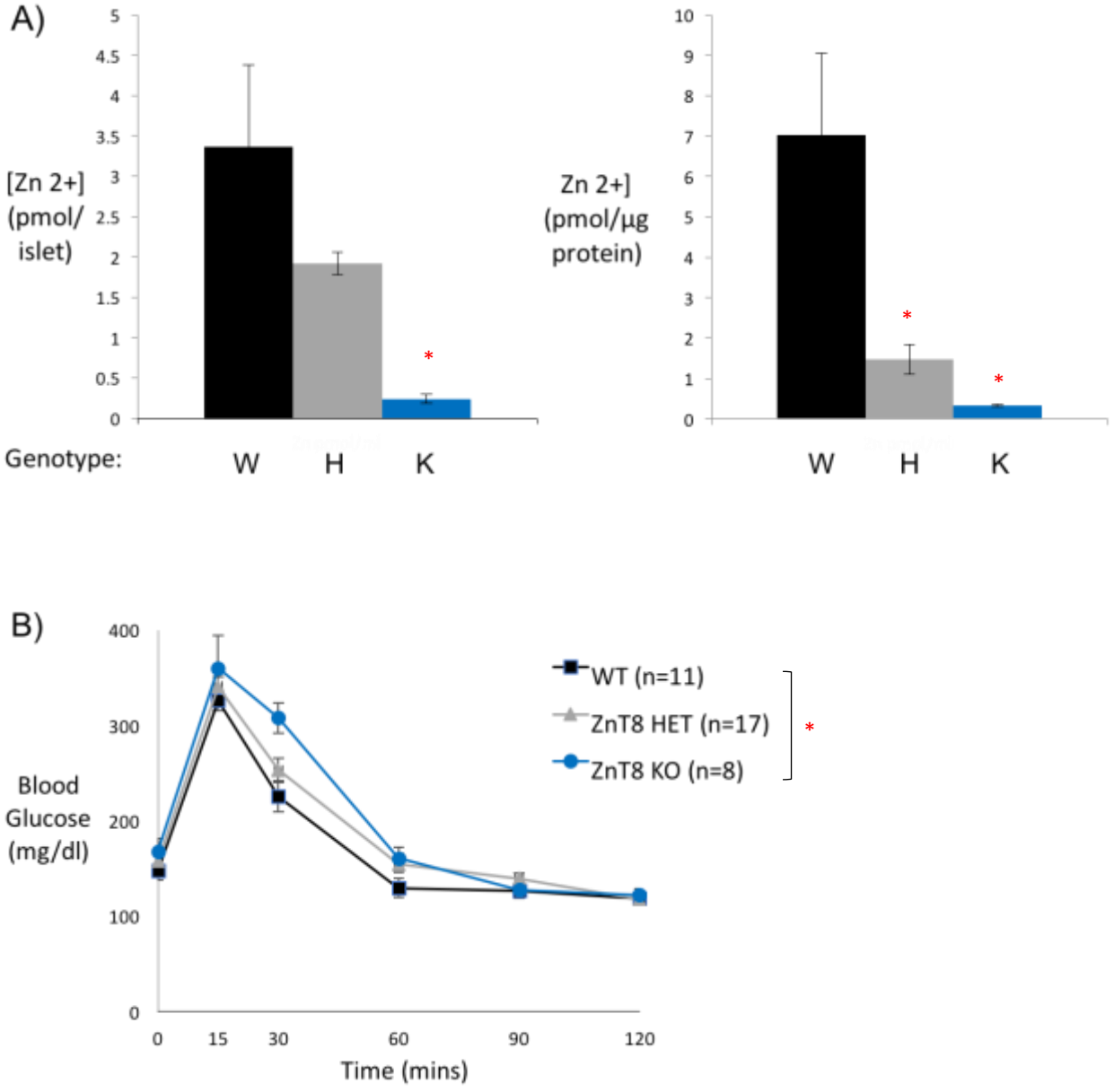

Figure 5.1 Analysis of zinc content, glucose tolerance, plasma insulin and C peptide in ZnT8 HET and KO mice. A, Zinc content in isolated approximately 22-week-old ZnT8 HET and KO male mouse islets. Results represent the mean ± SEM (n=3–4); P=.015, .0061, one-way ANOVA; *, differences with WT. B, IPGTTs were performed on 6-hour fasted 4-week-old male conscious mice. Results show the mean glucose concentrations in tail blood ± SEM; P = .0379, two-way ANOVA; *, differences with WT. W, WT; H, HET; K, KO.

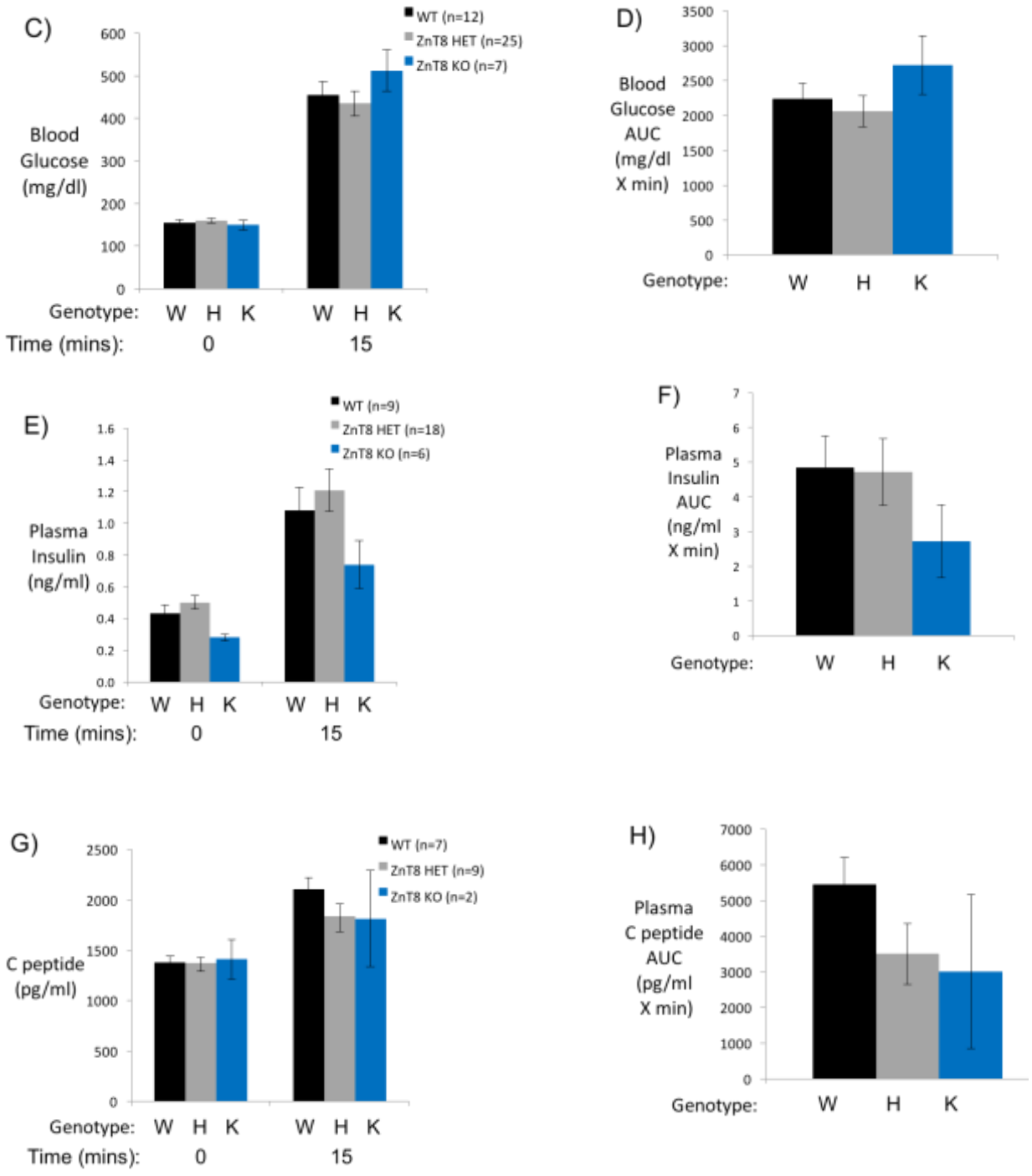

Figure 5.1 Analysis of zinc content, glucose tolerance, plasma insulin and C peptide in ZnT8 HET and KO mice. C-H, IPGTTs were performed on 6-hour fasted 10-week-old male conscious mice. Results show the mean (C) blood glucose, (E) plasma insulin and (G) plasma C peptide concentrations in blood isolated from the retro-orbital plexus or the area under the curve (AUC) (D, F, H) ± SEM. W, WT; H, HET; K, KO.

Heterozygous or Homozygous Deletion of ZnT8 in the Adult Beta Cell Does Not Affect Glucose Tolerance in Mice on a Chow Diet

Given the lack of a consistent phenotype reported in germline *Slc30a8* KO mouse models and the functional redundancy of ZnT7 and ZnT8 in the beta cell, we explored the possibility that developmental compensation may have obscured a phenotype in ZnT8 KO mice. Compensatory gene expression changes frequently occur during development when genes are deleted in the germline [216], [217-219]. The same concern applies to *Slc30a8* KO mouse models where ZnT8 has been deleted in the pancreas at embryonic day 13.5 by using the insulin promoter to drive expression of Cre recombinase [128, 171, 174]. To address this possibility, we generated an inducible beta cell-specific *Slc30a8* KO mouse model, in which the deletion of *Slc30a8* in adult mouse beta cells eliminates developmental compensation.

This model was generated using sperm containing a modified mouse *Slc30a8* allele purchased from the KO Mouse Project (KOMP) repository. This modified allele contains an intronic lacZ/neo cassette bordered by FRT sites with the second exon of the ZnT8 gene bordered by *loxP* sites (Figure 5.2A). The Vanderbilt Transgenic Mouse/Embryonic Stem Cell Shared Resource performed *in vitro* fertilization and generated live mice from the frozen sperm. Genotyping of these mice using primers that recognize the floxed but not WT *Slc30a8* allele identified mice containing the targeted allele. Female offspring with heterozygous expression of the modified *Slc30a8* allele, confirmed by RT-PCR (data not shown), were then bred with a male mouse expressing the FLP recombinase resulting in deletion of the lacZ/neo cassette. The female offspring of this breeding were then bred with a male C57BL/6J homozygous $Ins1^{CreERT2}$ mouse. In $Ins1^{CreERT2}$ mice, administration of tamoxifen induces Cre nuclear translocation. The $Ins1^{CreERT2}$ mouse line does not show any expression of Cre recombinase in the hypothalamus [116] and was not designed with the human growth hormone minigene [193], which have been issues with previous Cre recombinase-expressing mouse lines designated to confer gene deletion in beta cells. Mice heterozygous for the $Ins1^{CreERT2}$ allele and the floxed *Slc30a8* allele were interbred to generate mice homozygous for the $Ins1^{CreERT2}$ allele and heterozygous for the floxed *Slc30a8* allele.

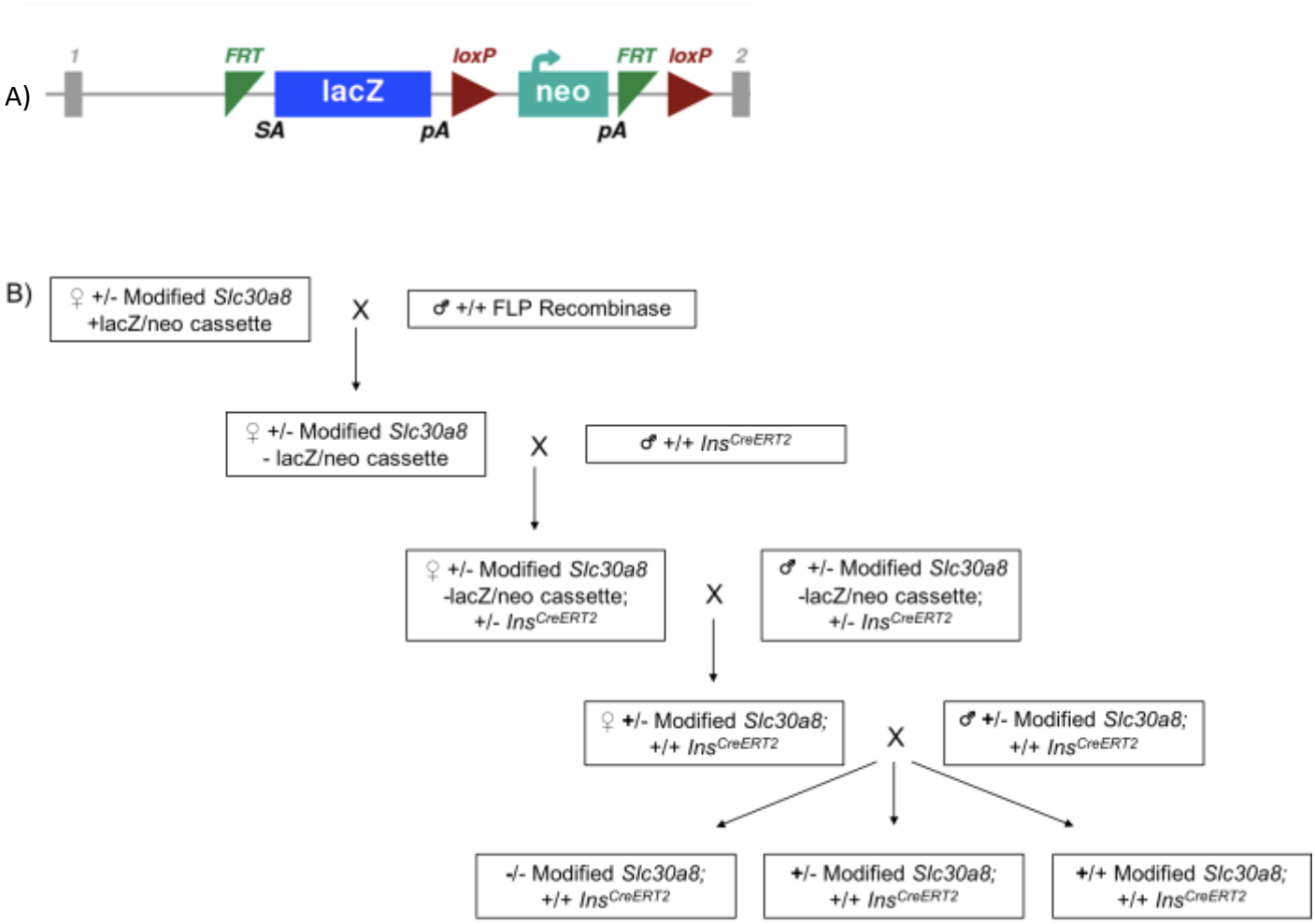

Figure 5.2 Generation and analysis of glucose tolerance and fasting blood glucose in ZnT8 beta cell-specific heterozygously and homozygously expressing the floxed allele. A, Schematic representation of modified *Slc30a8* locus with the intronic LacZ/neo cassette ordered by FRT sites. Exons 2 is surrounded by loxP sites. B, Breeding strategy for generation of ZnT8 WT, HET, and floxed $Cre^{+/+}$ mice.

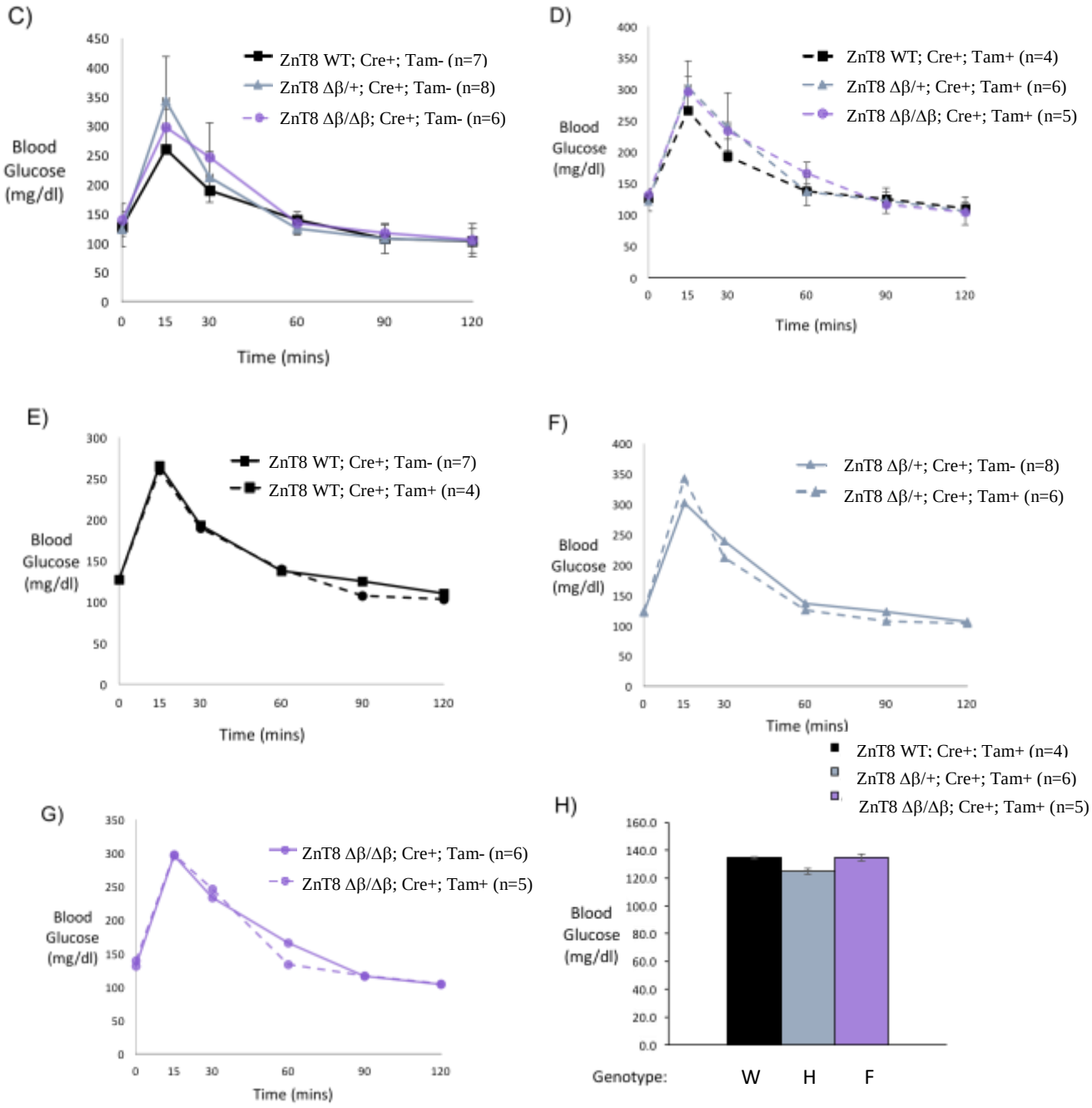

Figure 5.2 Generation and analysis of glucose tolerance and fasting blood glucose in ZnT8 beta cell-specific heterozygously and homozygously expressing the floxed allele. C-G, IPGTTs were performed on 6-hour fasted 8-week-old male conscious (C) Cre+, Tam-, (D) Cre+, Tam+, and 12-week-old (E) ZnT8 WT Cre+, ±Tam, (F) ZnT8 Δβ/+ Cre+, ±Tam, and (G) ZnT8 Δβ/Δβ Cre+, ±Tam mice. Results show the mean glucose concentrations in tail blood ± SEM. H, Blood was collected from 6-hour fasted 13-week-old male conscious Cre+, Tam+ mice. Results show the mean blood glucose concentration in blood isolated from the retro-orbital plexus ± SEM. W, WT; H, Δβ/+; F, Δβ/Δβ.

Finally, interbreeding of these mice resulted in the generation of mice homozygous for the unmodified *Slc30a8* allele, heterozygous for the *Slc30a8* floxed allele, or homozygous for the *Slc30a8* floxed allele, all homozygous for the *Ins1*^{CreERT2} allele. These mice are designated ZnT8 WT, ZnT8 $^{\Delta\beta/+}$, and ZnT8$^{\Delta\beta/\Delta\beta}$; Cre^{+}, respectively. The breeding scheme is depicted in Figure 5.2B.

At 8 weeks of age, there was no difference in glucose tolerance as assessed by IPGTTs between ZnT8 WT, ZnT8 $^{\Delta\beta/+}$, and ZnT8$^{\Delta\beta/\Delta\beta}$; Cre^{+}; Tm^{-} mice (Figure 5.2C). These mice then received injections of 200 mg of tamoxifen on Monday, Wednesday, and Friday of the next week. At 12 weeks of age, there were still no significant differences in glucose tolerance observed between ZnT8 WT, ZnT8 $^{\Delta\beta/+}$, and ZnT8$^{\Delta\beta/\Delta\beta}$; Cre^{+}; Tm^{+} (Figure 5.2D). Additionally, there was no difference in glucose tolerance in mice of the same genotype before or after tamoxifen injections, indicating no genotype-independent effects of tamoxifen on glucose metabolism (Figures 5.2E-G).

FBG did not differ between ZnT8 WT, ZnT8 $^{\Delta\beta/+}$, and ZnT8$^{\Delta\beta/\Delta\beta}$; Cre^{+}; Tm^{+}, matching what was observed in C57BL/6J ZnT8 germline *Slc30a8* KO mice (Figure 5.2H). These results suggest that developmental compensation has not obscured a phenotype in germline *Slc30a8* global KO mouse models.

Heterozygous or Homozygous Global Germline Deletion of ZnT8 Protect Mice on a High Fat Diet from DIO

Based on the design of the studies of Flannick *et al.* [190], we reasoned that a beneficial effect of ZnT8 haploinsufficiency in mice may similarly become apparent in the context of DIO [190]. We therefore placed the global germline ZnT8 WT, HET, and KO mice on a HFD for 15 weeks starting at 10 weeks of age. ZnT8 KO mice were protected from DIO, gaining significantly less weight compared to both ZnT8 WT and HET mice as early as 2 weeks on the diet (Figure 5.3A). ZnT8 HET mice had significantly reduced weight compared to WT mice after 6 weeks on the HFD (Figure 5.3A). After 15 weeks on the HFD, the body composition of these mice was analyzed using an mq10 NMR analyzer (Bruker Optics). The data showed a significant decrease in overall body weight in ZnT8 KO mice compared to WT and

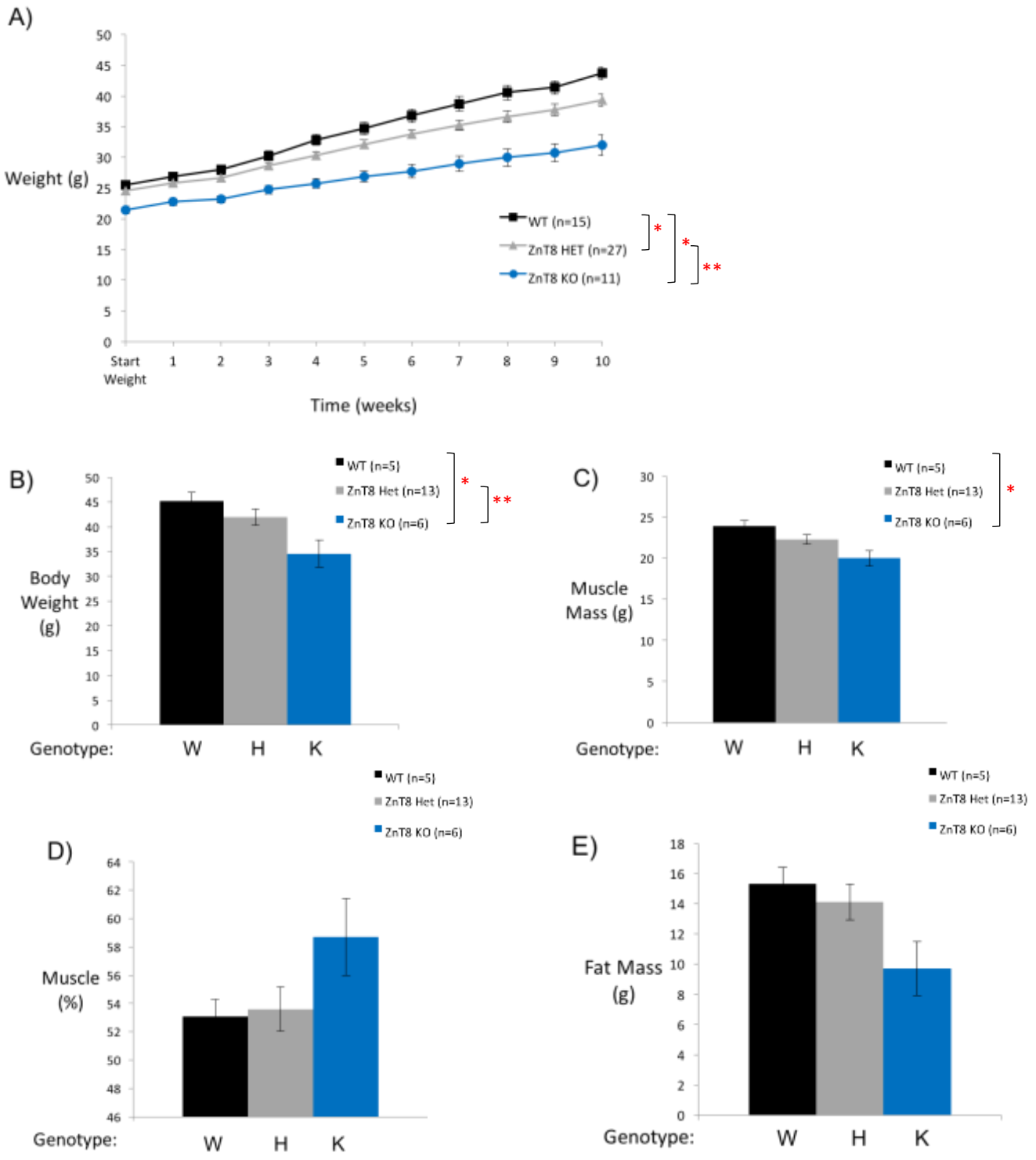

Figure 5.3 Analysis of body weight, body composition, and plasma cholesterol, triglycerides, and free fatty acids in high fat fed ZnT8 HET and KO mice. A, 10-week-old male mice fed a HFD were measured weekly. Results represent the mean ± SEM; P<.0001, two-way ANOVA; *, differences with WT; **, differences between HET and KO. B, Body weights of 6 hour fasted 25-week-old mice were measured. Results represent the mean ± SEM; P<.0145, one-way ANOVA; *, differences with WT; **, differences between HET and KO. C-H, Body composition was assessed by NMR in 6 hour fasted 25-week-old male mice following 15 weeks on a HFD. Results represent the (C, E, G) mean or (D, F, H) percent of body weight ± SEM. C, P=.0139, one-way ANOVA; *, differences with WT.

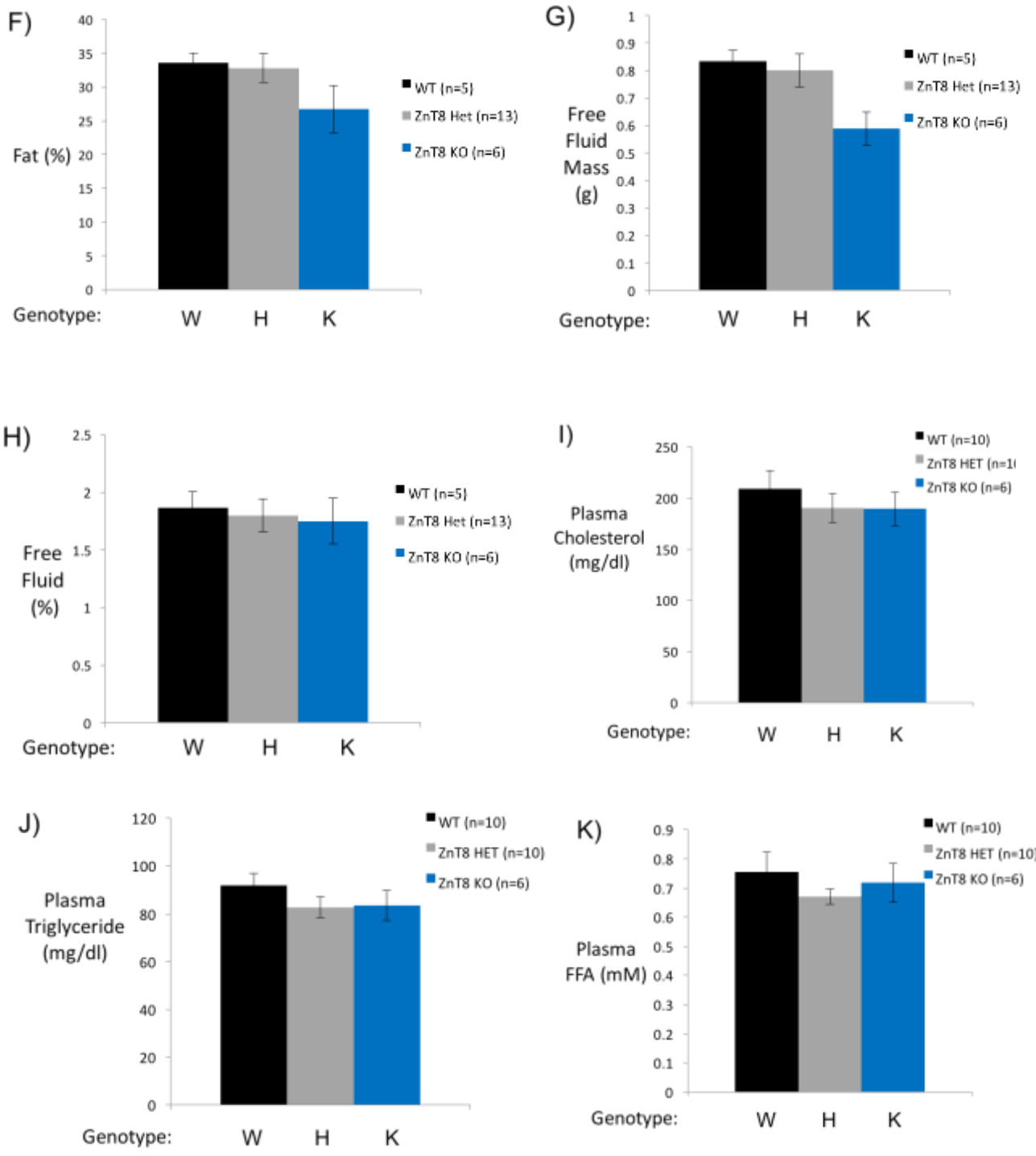

Figure 5.3 Analysis of body weight, body composition, and plasma cholesterol, triglycerides, and free fatty acids in high fat fed ZnT8 HET and KO mice. C-H, Body composition was assessed by NMR in 6 hour fasted 25-week-old male mice following 15 weeks on a HFD. Results represent the (C, E, G) mean or (D, F, H) percent of body weight ± SEM. C, P=.0139, one-way ANOVA; *, differences with WT. I-K, blood was collected from 6-hour fasted 23-week-old male conscious mice. Results show the mean plasma (I) cholesterol, (J) triglyceride, and (K) free fatty acid concentrations from blood isolated from the retro-orbital plexus ± SEM. W, WT; H, HET; K, KO.

HET mice (Figure 5.3B), which could be attributed to the significant decrease in ZnT8 KO muscle mass (Figure 5.3C) compared to WT mice and trends towards reductions in fat (Figure 5.3D) and free fluid (Figure 5.3E) mass. There were no changes in the percentage of muscle, fat, or free fluid mass in these ZnT8 KO mice (Figure 5.3F, G, H), indicating that deletion of ZnT8 does not affect the partitioning of nutrients.

The reduction in body weight in ZnT8 KO mice did not affect plasma cholesterol (Figure 5.3I), triglyceride (Figure 5.3J), or free fatty acid (Figure 5.3K) levels.

Heterozygous or Homozygous Global Germline Deletion of ZnT8 Improves Glucose Tolerance in Mice on a High Fat Diet

We next examined whether the effect of the HFD was associated with altered glucose tolerance in ZnT8 HET or KO mice. Glucose tolerance was assessed using IPGTTs in 20-week-old ZnT8 WT, HET, and KO mice after 10 weeks on a HFD. A significant improvement in glucose tolerance was observed in both ZnT8 HET and KO mice compared to WT mice (Figure 5.4A). FBG was also significantly reduced in ZnT8 KO mice compared to ZnT8 WT and HET mice after 11 weeks on the HFD (Figure 5.4B), and this was associated with a trend towards a reduction in FPI (Figure 5.4C). A comparison of figures 1B and 4A shows that glucose tolerance was markedly impaired in mice on a HFD versus mice on a chow diet. Similarly, a comparison of Figures 5.1E and 5.4C shows that FPI was increased in mice on a HFD versus a chow diet. Both observations are consistent with the presence of insulin resistance. Strikingly, while blood glucose levels rose in mice on a HFD to similar levels regardless of genotype, 15 minutes after IP injection of 2g/kg glucose, there was no further elevation in the already high levels of plasma insulin (Figure 5.4C). The reason why plasma insulin levels do not rise in the ZnT8 KO mice to match those in ZnT8 WT mice is unclear.

The observed reduction in FBG with a similar trend in FPI in ZnT8 KO mice suggests the presence of an improvement in insulin sensitivity. Indeed, after 12 weeks on the HFD, insulin tolerance tests (ITTs)

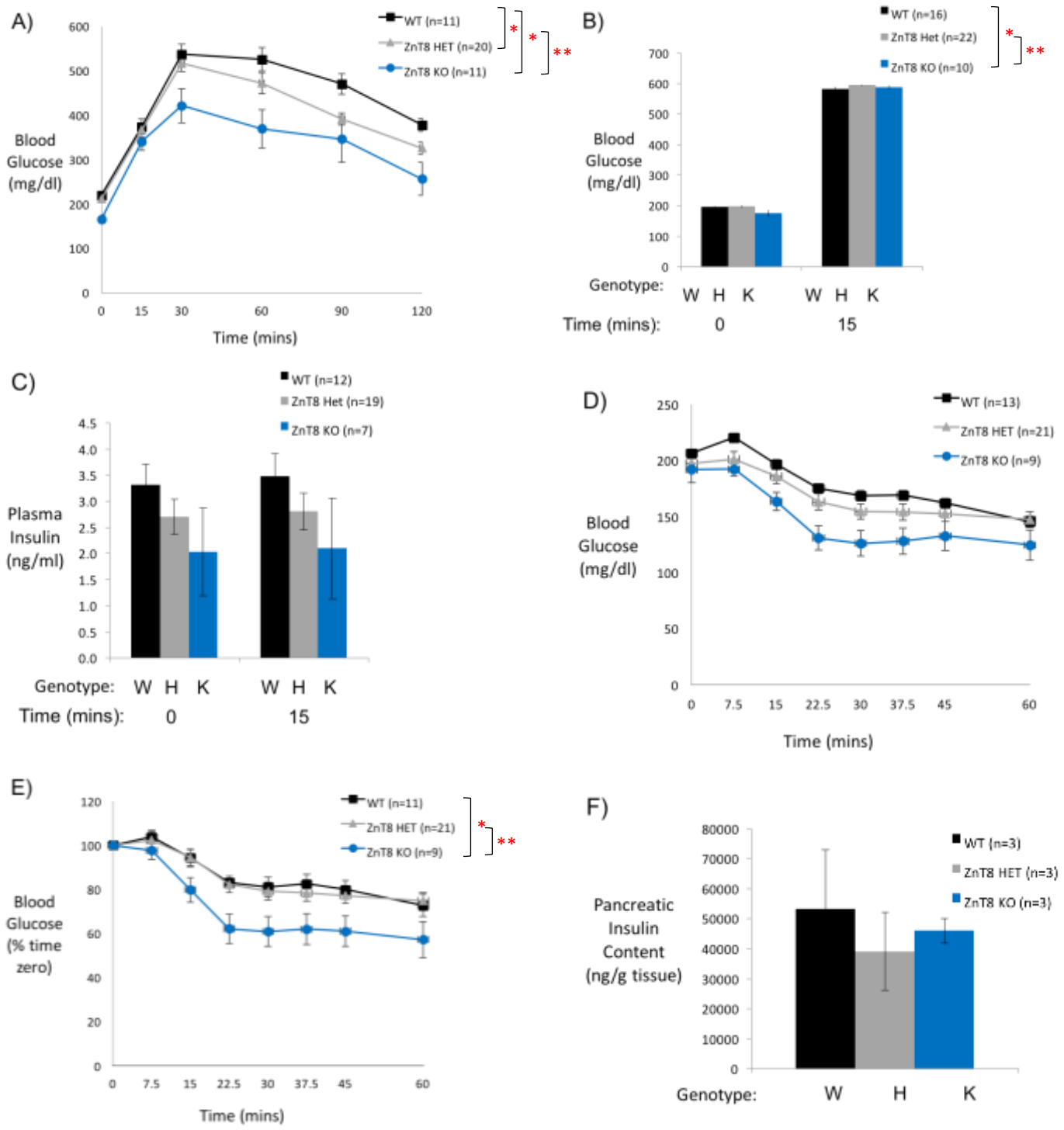

Figure 5.4 Analysis of glucose tolerance, plasma insulin, insulin tolerance and pancreatic insulin content in ZnT8 HET and KO mice. A, IPGTTs were performed on 6-hour fasted 20-week-old male conscious mice after 10 weeks on the HFD. Results show the mean glucose concentrations in tail blood ± SEM; P = .0416, two-way ANOVA; *, differences with WT; **, differences between HET and KO. B-C, IPGTTs were performed on 6-hour fasted 10-week-old male conscious mice. Results show the mean (B) blood glucose and (C) plasma insulin concentrations in blood isolated from the retro-orbital plexus ± SEM. P = .0375, two-way ANOVA; *, differences with WT; **, differences between HET and KO. D-E, ITTs were performed on 22-week-old 5-hour fasted conscious male mice. Results show the mean glucose concentrations in tail blood expressed as (D) mg/dl or as (E) a percentage of blood glucose at t = 0 ± SEM. P = .0248, two-way ANOVA; *, differences with WT; **, differences between HET and KO. F, insulin content was measured in whole pancreas from 25-week-old 6 hour fasted male mice after 15 weeks on the HFD. Results represent the mean ± SEM. W, WT; H, HET; K, KO.

showed improved insulin sensitivity in ZnT8 KO mice compared to WT and HET mice (Figure 5.4D). The difference in FBG at t=0 complicates the interpretation of these data, but when these data were calculated as the percentage of FBG at t=0, this difference was statistically significant (Figure 5.4E). There was no difference in pancreatic insulin content in ZnT8 WT, HET, or KO mice after 15 weeks on the HFD (Figure 5.4F), suggesting that the improvement in glucose tolerance in ZnT8 HET and KO mice is not due to greater insulin secretory capacity.

A comparison of FBG and FPI levels in mice before and after 11 weeks of HFD showed that both parameters rose as expected. However, there were differential effects of this diet and/or aging in ZnT8 WT, HET, and KO mice. ZnT8 WT mice showed nearly a 700% increase in FPI after 11 weeks on the HFD (Figure 5.5A), an increase that was significantly reduced in ZnT8 HET mice and further blunted in ZnT8 KO mice. In contrast to these changes in FPI, FBG only rose moderately in mice on a HFD versus chow diet indicating that these increases in FPI are largely able to overcome the presence of insulin resistance (Figure 5.5B). ZnT8 WT mice on a HFD showed the greatest increases in FBG, which correlates with the greater impairment in glucose tolerance in these mice (Figure 5.4A) compared to chow-fed mice (5.1B).

Heterozygous or Homozygous Global Germline Deletion of *Slc30a8* Does Not Alter Liver Glycogen Content

We recently reported that combined deletion of ZnT7 and ZnT8 resulted in a marked 3.4 fold increase hepatic glycogen content even though ZnT8 mRNA [154] and ZnT7 protein [150] are not detected in the liver. We therefore measured both glycogen content in liver isolated from 25-week-old ZnT8 WT, HET, and KO mice that had been on the HFD for 15 weeks. Figure 5.6 shows that liver glycogen content is unchanged in ZnT8 HET and KO mice compared to WT mice.

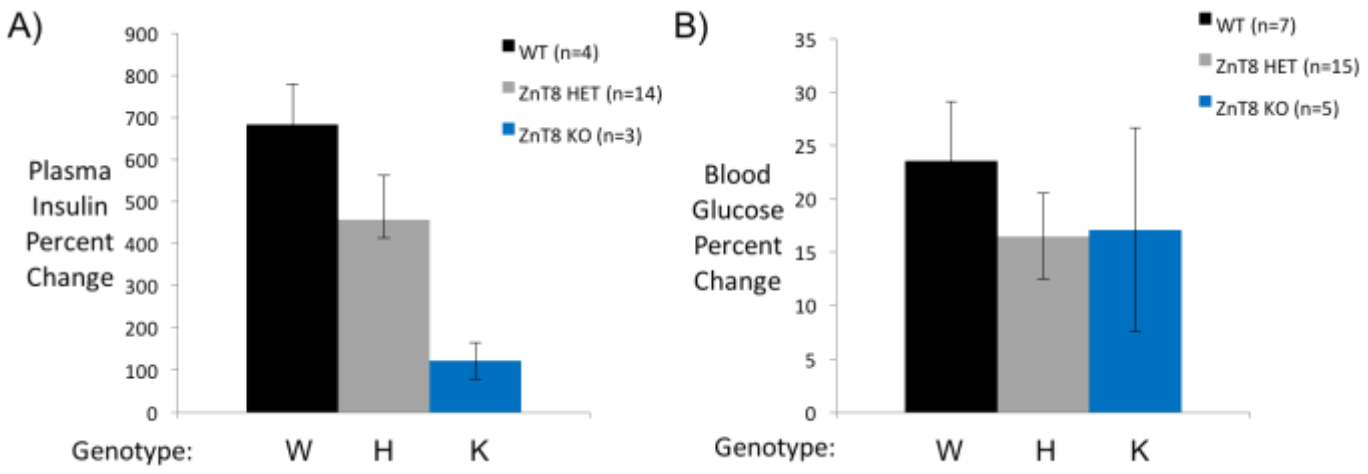

Figure 5.5 Analysis of percent plasma insulin and blood glucose change after 11 weeks of HFD.
A, Percent change of (A) fasting plasma insulin or (B) fasting blood glucose between 10-week-old 6 hour fasted conscious male mice on a chow diet and the same mice after 11 weeks on the HFD. Results show the mean (A) plasma insulin or (B) blood glucose concentrations in tail blood ± SEM. W, WT; H, HET; K, KO.

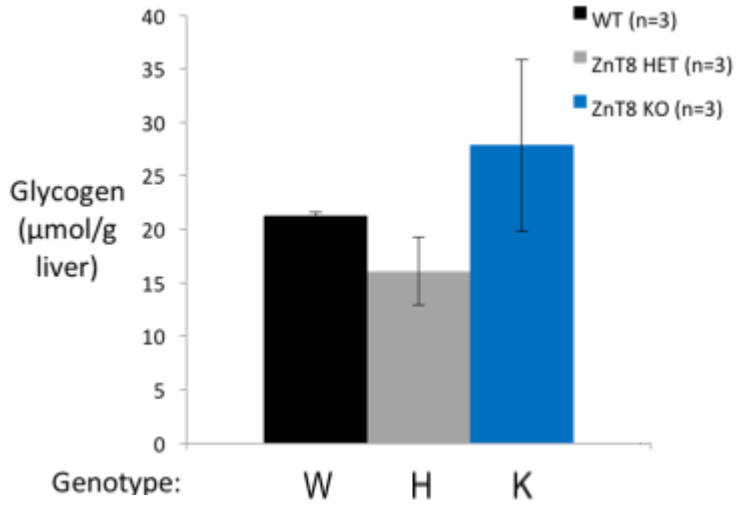

Figure 5.6 Analysis of hepatic glycogen in ZnT8 HET and KO mice. Hepatic glycogen content was measured in livers harvested from 25-week-old 6 hour fasted male mice on the HFD. Results represent the mean ±SEM. W, WT; H, HET; K, KO.

DISCUSSION

As has been shown previously, germline deletion of *Slc30a8* has only a slight transient effect on glucose tolerance (Figure 5.1B) and no effect on plasma insulin levels after glucose administration (Figure 5.1D) or insulin clearance (Figure 5.1E) in mice on a chow diet. We considered the possibility that the lack of phenotype in this, and previous, germline *Slc30a8* KO mouse studies could potentially be due to developmental compensation. However, deletion of *Slc30a8* specifically in the beta cells of 8-week old mice did not alter glucose tolerance (Figure 5.2E) or FBG (Figure 5.2G). This indicates that developmental compensation is not obscuring the identification of a phenotype in *Slc30a8* KO mice. Expression of *Slc30a8* in the testes and pancreas from these mice will be analyzed to ensure deletion from the pancreas specifically upon tamoxifen administration in Cre+ mice. Preliminarily, we see a reduction in *Slc30a8* expression relative to *Ppia* expression in the pancreas of ZnT8$^{\Delta\beta/\Delta\beta}$; Cre^{+}; Tm^{+} mice compared to ZnT8 ZnT8 WT; Cre^{+}; Tm^{+} mice (Figure 5.7). We anticipate that there will be no difference in the pancreatic or testes expression of *Slc30a8* relative to *Ppia* expression between ZnT8 WT; Cre^{-} and ZnT8$^{\Delta\beta/\Delta\beta}$; Cre^{-} mice. Similarly, we do not expect to see differences in pancreatic or testes expression of *Slc30a8* in ZnT8 WT; Cre^{+}; Tm^{-} and ZnT8$^{\Delta\beta/\Delta\beta}$; Cre^{+}; Tm^{-} mice.

Flannick *et al.* reported that *SLC30A8* haploinsufficiency is protective against T2D risk [190]. Here we show that ZnT8 HET and KO mice are protected against DIO (Figure 5.3). This protection from weight gain correlates with secondary improvements in glucose tolerance (Figure 5.4) and insulin sensitivity in ZnT8 KO mice (Figure 5.5). These results largely match a more limited pilot HFD study performed by Dr. Lynley Pound, a previous graduate student in the lab [159]. One difference with that pilot study is that we are currently seeing a difference in body weight between WT and ZnT8 KO mice at 10 weeks of age (Figure 5.3A). We suspect this is a statistical fluke due to the relatively low number of ZnT8 KO mice analyzed to date (n=11) since no difference in weight was observed between WT and ZnT8 KO mice on a chow diet at 4 weeks (Figure 5.8) or in previous studies at 16 weeks [159]. We anticipate that this weight difference will disappear after more ZnT8 KO mice are analyzed.

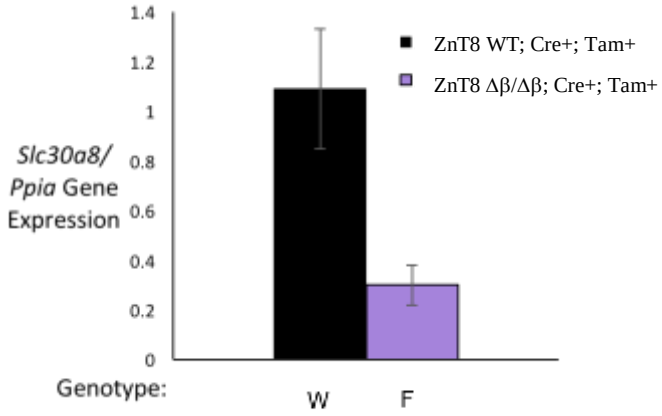

Figure 5.7 Analysis of pancreatic *Slc30a8* expression in ZnT8 WT; Cre^{+}; Tm^{+} and ZnT8$^{\Delta\beta/\Delta\beta}$; Cre^{+}; Tm^{+} mice. *Slc30a8* expression was measured relative to *Ppia* expression in pancreas harvested from 6 hour fasted 13-week-old male mice. Results represent the mean ±SEM (n=4). W, WT; F, floxed.

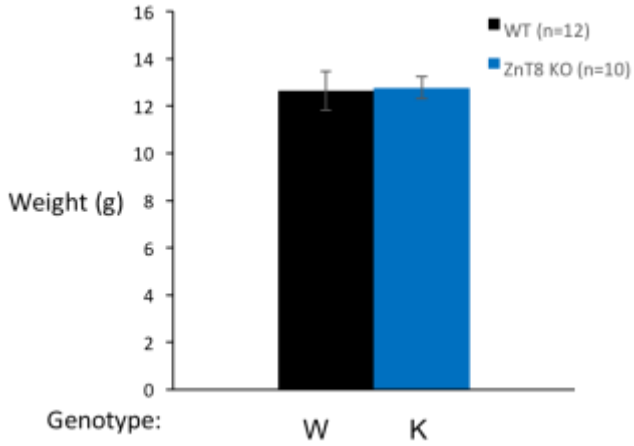

Figure 5.8 Analysis of body weight in ZnT8 HET and KO mice on a chow diet. Body weights of 6 hour fasted 4-week-old mice were measured. Results represent the mean ± SEM. W, WT; K, KO.

In the current study, in ZnT8 HET mice we observe decreased weight gain, a trend towards decreased FPI, and improved glucose tolerance compared to WT mice on a HFD, but there is no difference in insulin sensitivity in ITTs. We speculate that difference in insulin sensitivity between WT and ZnT8 HET mice is too small to be detected in an ITT, but a difference will emerge using more sensitive hyperinsulinemic euglycemic clamps.

Since we observe a phenotype in ZnT8 KO mice on a HFD this implies that developmental compensation does not appear to be at play, or at least is not fully effective, in relation to ZnT8 function in tissues that affect the response to a HFD. In addition, while ZnT7 can compensate for the absence of ZnT8 in mouse islets [176], these data indicate that other ZnT isoforms do not compensate for the absence of ZnT8 in tissues that affect the response to a HFD. The fact that ZnT7 can compensate for the absence of ZnT8 in beta cells also implies that it is the altered function of ZnT8 in a peripheral tissue, not islets, that plays a critical role in the association of ZnT8 with protection against DIO. The potential identity of this tissue is discussed in Chapter 6.

Several groups have previously investigated the effect of both germline and beta cell-specific *Slc30a8* deletion in the context of a diabetogenic environment, namely a HFD [159, 170, 172, 173]. Changes in body weight between WT and *Slc30a8* KO mice on a HFD are difficult to compare between studies given the differences in specific diets used, the length of time the mice were kept on the diet, the ages of the mice placed on the diets, and the genetic backgrounds of the mice studied. An increase [172, 173], decrease [159], and no change [170, 173] in body weight have been reported in *Slc30a8* KO mice compared to controls. Unsurprisingly, the inconsistency of the reported effects of HFD on body weight gain corresponds with conflicting reports on the effect of HFD on FPI, FBG, and glucose tolerance. We hypothesize that the key difference between our data and these other HFD studies is genetic background. Our study is the only to one in which mice were backcrossed onto a pure C57BL/6J background and as a result our WT mice gained more weight than seen in other studies.

In summary, in this study ZnT8 HET and KO mice on a pure C57BL/6J background were protected from impaired glucose tolerance but only in the context of DIO. We hypothesize that decreased ZnT8 activity in a peripheral tissue(s) results in decreased body weight through altered food intake and/or energy expenditure. This then leads to increased insulin sensitivity and improved glucose tolerance, which lowers the demand on the beta cell to hypersecrete insulin to compensate for insulin resistance. A lower demand on insulin production would relieve the stress on the beta cells, lowering the risk of beta cell failure and thereby decreasing the risk of developing T2D.

CHAPTER VI

Summary and Future Directions

Thesis Summary

The work described in this dissertation aimed to elucidate the role of ZnT8 in islet beta cell function and glucose homeostasis. When these studies began in 2013, GWAS had linked a non-synonymous SNP in the *SLC30A8* locus, rs13266634, with altered risk of T2D development [46, 47] and then in 2014 another study had shown that ZnT8 haploinsufficiency was protective against T2D risk [190]. However, despite substantial monetary investment in investigating the function of ZnT8, using *Slc30a8* KO mouse models, no clear role for ZnT8 in the regulation of GSIS or the development of T2D had been defined. The approach taken in this dissertation was to generate a more thorough understanding of the role ZnT8 plays in glucose homeostasis through generation of several mouse models to address three goals: (1) uncover a role for ZnT8 in the islet beta cell; (2) begin to investigate the protective effect of ZnT8 haploinsufficiency on the development of T2D in mice; and (3) indirectly address the disparity between islet zinc concentrations and lack of effects on glucose homeostasis in *Slc30a8* KO mouse models with the reported essential roles for zinc in insulin processing and signaling by exploring the molecular basis for low zinc in Guinea pig islets.

Previous *Slc30a8* KO mouse model studies failed to identify a significant and consistent role for ZnT8 in glucose homeostasis and beta cell function. We expanded these studies through the generation of a novel DKO mouse model. With this mouse model, we were able to demonstrate a significant role for ZnT8 in GSIS (Figure 3.4A). Briefly, although impairments in glucose tolerance (Figure 3.2D & G) and glucose-induced plasma insulin levels (Figure 3.2E & H) were detected in both ZnT7 and DKO animals *in vivo,* GSIS was completely absent only in the DKO isolated islets with no change in the ZnT7 KO islets (Figure 3.4A). The beta cell mass of DKO islets was significantly reduced compared to WT islets (Figure 3.3B), corresponding to the decrease in pancreatic insulin content (Figure 3.3A). These data suggest there

is functional redundancy between ZnT8 and ZnT7 in the beta cell. Additionally, this study led to the hypothesis that decreased *Slc30a8* expression in the peripheral tissues may lead to decreased T2D risk.

While not affecting our conclusions, a limitation of this DKO mouse study involves the interpretation of the *in vivo* data. ZnT7 is ubiquitously expressed [150] and the effects of ZnT7 deletion from tissues other than the islets may influence the overall impact of ZnT7 deletion. For example, the differences in insulin clearance before and after glucose administration were determined by the ratio of plasma C peptide levels to plasma insulin levels. C peptide clearance from the bloodstream occurs, in part, at the kidneys, but differences in C peptide clearance in the different models due to the absence of ZnT7 were not considered in these calculations.

In WT mice, an improvement in glucose tolerance is observed during OGTTs relative to IPGTTs, which is attributed to the release of incretin hormones from the gut following oral gavage of glucose resulting in an enhancement of insulin secretion (Figure 6.1). However, ZnT7 KO mice exhibit no change in glucose tolerance in OGTTs compared to IPGTTs, indicating an impairment in the incretin effect (Figure 6.1), which could be due to impairments in either secretion and/or action of incretin hormones. Interestingly, in DKO mice the incretin effect is at least partially intact since glucose tolerance is improved in OGTTs compared to IPGTTs (Figure 6.1).

Developmental compensation may have obscured a phenotype in previous *Slc30a8* KO mouse models. Therefore, we generated an inducible beta cell-specific ZnT8 KO model. Data from this model suggest that heterozygous or homozygous deletion of *Slc30a8* specifically from the beta cells of adult mice does not alter glucose tolerance compared to control animals. This result contradicts a previously reported impairment in glucose tolerance in beta cell-specific *Slc30a8* KO mice; however, this published study did not use the proper *Cre recombinase*-expressing mice as controls, and so the results are difficult to interpret [128]. Moreover, Hardy *et al.* reported no alteration in glucose tolerance in their mouse model of inducible beta cell-specific *Slc30a8* KO mice with the additional stress of a 16-week HFD intervention,

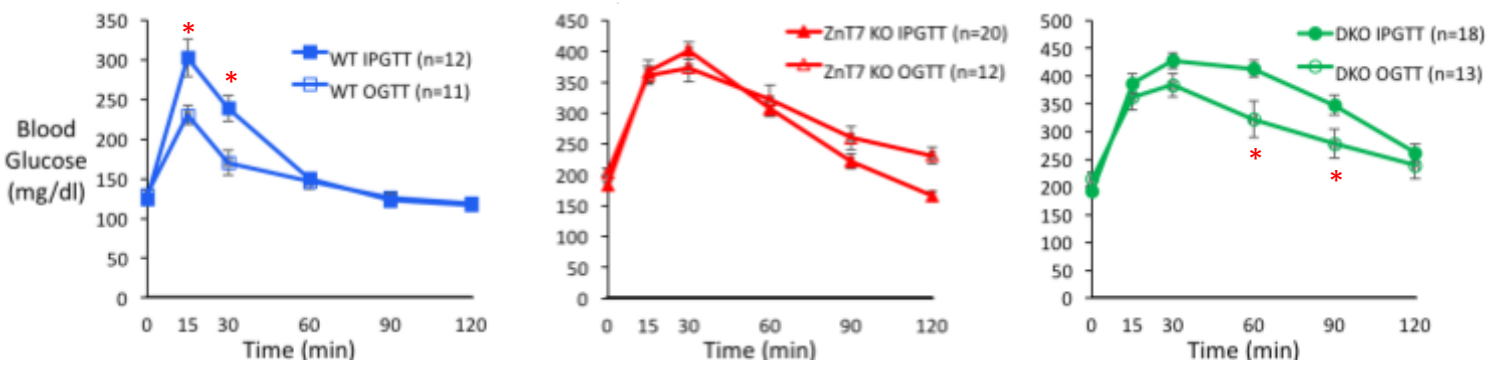

Figure 6.1 Comparison of IP and oral glucose tolerance in WT, ZnT7 KO and DKO mice. IP and OGTTs were performed on 6-hour fasted 10- (IPGTTs) and 20-week-old (OGTTs) male conscious mice. IP and OGTTs are compared within the same genotype. Results show the mean glucose concentrations in tail blood ± SEM; (WT) $P < .0001$; (DKO) $P = .0003$ two-way ANOVA; *, difference between IP and OGTT within the same genotype.

supporting the findings from our beta cell-specific *Slc30a8* KO study [173]. Overall, these studies support the hypothesis that alterations in ZnT8 activity in peripheral tissue leads to altered glucose homeostasis.

The finding that ZnT8 haploinsufficiency is protective against the development of T2D [190] led to a further examination of the effect of *Slc30a8* deletion in the context of a HFD in C57BL/6J mice. First, we were able to confirm that global deletion of *Slc30a8* had no effect on glucose tolerance in C57BL/6J mice fed a chow diet (Figure 5.1B). After the mice were placed on a HFD for 10 weeks, we were able to replicate the previously reported protection from DIO in ZnT8 HET and ZnT8 KO mice (Figure 5.3A) [159]. ZnT8 KO mice also had improved glucose tolerance (Figure 5.4A) and insulin sensitivity (Figure 5.4E) compare to WT mice. The simplest hypothesis is that this protection is secondary to the improvement in body weight. We hypothesize that these data support the human genetic data, which demonstrated a protective effect of ZnT8 haploinsufficiency on the development of T2D [190]. However, our mouse studies have looked at the response to DIO and have not specifically looked at T2D risk. We hypothesize that humans who are haploinsufficient for ZnT8 have decreased weight potentially through improvements in energy expenditure and/or decreased food intake leading to improved, leading to improved insulin sensitivity and therefore decreased beta cell stress, ultimately resulting in decreased T2D risk.

Future Directions

The work described in this dissertation aided in expanding the field's knowledge of the role ZnT8 plays in beta cell function and glucose metabolism. However, although the whole-body alterations in glucose homeostasis and insulin sensitivity have been assessed, the molecular basis for these defects is not fully understood. Continued exploration of the mouse models described in this dissertation can contribute to a greater understanding of the changes in molecular physiology that occur upon *Slc30a8* deletion.

DKO Mouse Model

In our studies on DKO mice, we focused on *in vivo* and *in vitro* glucose-stimulated insulin response and *in vivo* arginine-stimulated insulin response from WT and DKO mice or islets, but additional secretagogues were not investigated. In order to more precisely determine the localization of the molecular defect in the insulin secretion stimulation pathways in DKO mice, the effect of additional secretagogues on insulin secretion could be analyzed. These analyses would reveal which insulin secretory pathways are compromised in DKO islets and to what degree. Secretagogues such as cAMP analogues, KCl, which depolarizes the membrane, the M3 receptor agonist carbachol, the PKC activator PMA, incretin analogs and the calcium ionophore ionomycin could be explored (reviewed in [220]). Each of these secretagogues stimulates insulin secretion from the beta cell in slightly different ways allowing for the identification of specific defects within the signaling pathways. Using static islet incubations, the ability of these secretagogues to stimulate insulin secretion from WT and DKO islets could be compared. Those secretagogues that exhibit a differential effect on insulin secretion from DKO islets relative to WT islets could then be examined in islet perifusion studies [197]. Islet perifusion assays allow for precise and dynamic characterization of insulin secretion, and are more sensitive in detecting abnormalities in insulin secretion than static assays.

Through analysis of *in vivo* plasma insulin levels in DKO mice after arginine administration, we concluded that defects in insulin secretion from the beta cell occur between calcium entry into the beta cell and vesicle fusion and insulin release (Figure 3.4I). Future studies could examine DKO and WT mice for differences in calcium signaling. Using a calcium fluorophore to measure calcium concentration within the islets, basal and glucose-induced changes in intracellular calcium could be determined [221]. If changes in calcium fluctuations are detected, the mechanism by which cytoplasmic calcium is altered could be further examined. Three mechanisms that could potentially explain differences in cytoplasmic calcium levels are: [191] altered calcium release from the ER, (2) altered calcium entry into the ER, or (3) altered calcium entry from the extracellular space into the cytoplasm. Targeted chemical inhibition of

specific ER calcium channels would indicate if these channels were playing a role in the disparity between cytoplasmic calcium concentrations in WT and DKO islets. Specifically, inhibition of the ryanodine receptor (RyR) channels via an inhibitor such as dantrolene would prevent calcium leakage out of the ER [222]. Alternatively, thapsgargin, which inhibits the sarco/endoplasmic reticulum calcium-ATPase (SERCA) pump, blocks the uptake of calcium from the cytoplasm into the ER lumen [223]. The combination of these results would indicate if altered calcium levels detected between WT and DKO islets were due to impaired ER calcium control. Additionally, established electrophysiological methods can be used to measure beta cell calcium influx during glucose stimulation of WT and DKO islets [221]. An alteration in calcium influx detected by these electrophysiological methods would indicate a difference in VGCC activity and therefore a difference in the influx of calcium from the extracellular space. Alterations in calcium flux could lead to altered activation of synaptotagmin [16], [15], and ultimately decreased insulin vesicle fusion and exocytosis.

Defective vesicular secretory machinery could also account for the impaired insulin secretion response detected in DKO islets. If correct, we would observe an impairment in insulin secretion in response to all stimuli tested. Additional experiments to investigate the integrity of the secretory machinery would then aid in identifying the deficit in DKO insulin secretion. Initially, a Western blot of several of the SNARE proteins involved in exocytosis including SNAP-25, VAMP, synaptotagmin IX and syntaxin would indicate if there are changes in SNARE protein expression and availability, which would affect the efficiency of insulin exocytosis.

To further explore vesicle fusion and exocytotic events, transmission electron microscopy could be employed. This technique was previously used in our lab to demonstrate no change in the density of the insulin vesicles [159]. We can use this technique again to expand on these previous studies by obtaining more images and quantifying the insulin vesicles within different pools. Insulin granules can be divided into the readily releasable pool (RRP) and the retention pool within the beta cell [224]. Decreased vesicle concentration in the RRP would suggest decreased fusion of the vesicles with the plasma

membrane. Finally, measuring beta cell membrane capacitance in response to calcium entry using a standard voltage step depolarization protocol can determine whether absence of ZnT7 and ZnT8 modulates the exocytotic process, specifically insulin granule fusion with the plasma membrane [221]. Because of the lack of GSIS in DKO islets, we expect that there will be decreased insulin vesicle docking to the membrane in DKO islets compared to WT islets.

Our arginine tolerance test data indicate that the defect in insulin secretion from DKO islets occurs after glycolysis and depolarization of the plasma membrane (Figure 3.4I). Again, in order to provide further support for this conclusion, metabolic flux of NAD(P)H generation could be examined. Using a combination of two-photon and confocal fluorescence imaging and static isolated islet preparations, the production of NADPH and NADH can be compared between WT and DKO islets [225]. NADPH is mainly generated as a bi-product of the pentose phosphate pathway, a pathway parallel to glycolysis, while NADH is a product of the glycolytic pathway. Alterations in the ratio of these products can provide insight into alterations in the glycolytic response to glucose administration and the production of ATP. Given the function of ZnT7 and ZnT8, no differences in the NADPH and NADH ratio before or after glucose administration between WT and DKO islets would be expected. However, if an unexpected ratio was uncovered, stable isotopes could also be used to further analyze glycolytic flux in these islets [226].

The absence of GSIS in DKO mouse islets indicates an essential role for ZnT8 in mouse islets in the absence of ZnT7. In future experiments, this phenomenon could be examined in human islets using siRNA knock down of *SLC30A8*. After ensuring an effective knockdown of ZnT8 using Western blots, different glucose concentrations would be added to the static islet culture, and the resulting insulin secretory response would be measured. When *Slc30a8* was knocked down in rat beta cell derived line, INS-1, there was a partial impairment in GSIS [227]. However, given that INS-1 cells do not completely replicate islet cell biology, we predict that no difference in GSIS would be detected between control and *SLC30A8* knockdown islets. The islets used for this experiment would exhibit the ‘Group 1’ human islet

GSIS profile, which shows peaks of insulin in response to high glucose and 3-isobutyl-1-methylxanthine (IBMX) [205].

Additionally, this study highlights the role of ZnT8 after additional deletion of ZnT7, but other ZnT isoforms were not examined despite their roles within the beta cell. Therefore, this functional redundancy may not be limited to these two isoforms. Combined deletion of ZnT8 with ZnT3 or 5 could also be examined using similar methods.

ZnT8 KO HFD Mouse Model

The reduced body weight (Figure 5.3A & B) and muscle mass (Figure 5.3C) of ZnT8 KO mice on a HFD must be due to increased energy expenditure and/or decreased food intake. Using the Promethion system, indirect calorimetry, energy expenditure, and physical activity could be analyzed while measuring food and water intake in mice housed separately. Measurement of VO_2 consumption and VCO_2 production in individual mice would be used for the calculation of energy expenditure. These experiments would be performed in mice on a HFD before a difference in weight gain is detected. It is anticipated that a difference in food intake and/or energy expenditure would be found. If food intake were different, follow-up studies would include a pair-fed group to isolate any differences in energy expenditure. Importantly, a yoked feeding system is also available through Vanderbilt's Mouse Metabolic Phenotyping Core. The yoked feeding system would provide food to ZnT8 WT mice at the same times that the ZnT8 KO mice are eating in order to control for differences in overnight feeding behavior that could indirectly affect the outcome of the energy expenditure analysis.

In addition to the decreased body weight, the data suggested a secondary improvement in insulin sensitivity in ZnT8 KO mice on a HFD and a predicted improvement in insulin sensitivity in ZnT8 HET mice that is not detected during ITTs (Figure 5.4D & E). Therefore, hyperinsulinemic-euglycemic clamps could be used to assess insulin sensitivity in these conscious mice. These clamps would also involve tracer technologies to assess tissue-specific glucose uptake, the rate of endogenous glucose appearance, and the

rate of whole-body glucose disappearance. The combination of clamps with tracer technology enable the assessment of insulin action at hepatic and/or peripheral tissue (e.g. muscle and/or adipose).

The effects of heterozygous or homozygous deletion of *Slc30a8* on the response to DIO could be due to the loss of *Slc30a8* expression in the adrenal cortex, adipose and thyroid cells effecting plasma levels of glucocorticoids, leptin, adiponectin and T3/T4. Differences in plasma levels of these hormones have the potential to influence insulin sensitivity, energy expenditure, and food intake leading to an altered response to DIO. In order to assess the effects of these hormones on DIO and not the effect of DIO on hormone levels, these hormones will be measured in chow-fed animals. If differences in plasma hormone levels are detected, deletion from those tissues can also be examined. We hypothesize that there would be no difference in these plasma hormone levels, and the effects of *Slc30a8* deletion on response to DIO is through action in the brain leading to altered food intake and/or energy homeostasis. To further examine the role of ZnT8 the effect of brain-specific deletion of *Slc30a8* could be examined. A mouse model of *Slc30a8* deletion specifically from the brain would be generated by breeding the mouse expressing the floxed *Slc30a8 allele* described previously with a mouse expressing Cre recombinase driven by the *Nestin* promoter [228]. It is expected that these offspring would have improved glucose tolerance and insulin sensitivity as a result of decreased weight gain on a HFD. A caveat of this these experiments is the possibility that concurrent, small changes in multiple tissues contributes to the overall effect of *Slc30a8* deletion in mice fed a HFD such that an individual tissue will not be identified as playing a causative role.

Finally, the Vanderbilt BioVU biobank could be probed with SNPs known to affect ZnT8 function. BioVU is a DNA biobank linked to a de-identified version of Vandebilt health records. Of the over 200,000 DNA samples available in BioVU, 20,000 samples have been genotyped on the Illumina exome chip which contains 260,5775 SNPs. PheWAS analysis could be performed with the non-synonymous ZnT8 SNP, rs13266634. PheWAS is an approach that involves screening the de-identified health records with specific SNPs to identify novel disease-variant associations and plasma hormone/metabolite

associations. This analysis could be used to identify associations between the rs13266634 SNP and plasma hormone levels discussed above.

REFERENCES

1. Tsirigos, K.D., et al., *The TOPCONS web server for consensus prediction of membrane protein topology and signal peptides.* Nucleic Acids Res, 2015. **43**(W1): p. W401-7.
2. Pound, L.D., *Characterization of Islet Genes Implicated in Human Disease.* Vanderbilt University, 2011: p. 163.
3. Jackson, I.J., *A reappraisal of non-consensus mRNA splice sites.* Nucleic Acids Res, 1991. **19**(14): p. 3795-8.
4. Blodgett, D.M., et al., *Novel Observations From Next-Generation RNA Sequencing of Highly Purified Human Adult and Fetal Islet Cell Subsets.* Diabetes, 2015. **64**: p. 3172-3181.
5. Kambe, T., *Molecular architecture and function of ZnT transporters.* Curr Top Membr, 2012. **69**: p. 199-220.
6. Davidson, H.W., J.M. Wenzlau, and R.M. O'Brien, *Zinc transporter 8 (ZnT8) and beta cell function.* Trends Endocrinol Metab, 2014. **25**(8): p. 415-424.
7. Olivares-Reyes, J.A., A. Arellano-Plancarte, and J.R. Castillo-Hernandez, *Angiotensin II and the development of insulin resistance: implications for diabetes.* Mol Cell Endocrinol, 2009. **302**(2): p. 128-39.
8. Chimienti, F., et al., *Identification and cloning of a beta-cell-specific zinc transporter, ZnT-8, localized into insulin secretory granules.* Diabetes, 2004. **53**(9): p. 2330-7.
9. Villasenor, A. and D.Y.R. Stainier, *On the development of the hepatopancreatic ductal system.* Seminars in Cell & Developmental Biology, 2017. **66**: p. 69-80.
10. Dolenšek, J., M.S. Rupnik, and A. Stožer, *Structural similarities and differences between the human and the mouse pancreas.* Islets, 2015. **7**(1): p. e1024405.
11. Fu, Z., E.R. Gilbert, and D. Liu, *Regulation of Insulin Synthesis and Secretion and Pancreatic Beta-Cell Dysfunction in Diabetes.* Current diabetes reviews, 2013. **9**(1): p. 25-53.
12. Steiner, D.F., et al., *A brief perspective on insulin production.* Diabetes Obes Metab, 2009. **11 Suppl 4**: p. 189-96.
13. Komatsu, M., et al., *Glucose-stimulated insulin secretion: A newer perspective.* J Diabetes Investig, 2013. **4**(6): p. 511-6.
14. Palmer, J.P., et al., *Insulin antibodies in insulin-dependent diabetics before insulin treatment.* Science, 1983. **222**(4630): p. 1337-9.
15. Gauthier, B.R. and C.B. Wollheim, *Synaptotagmins bind calcium to release insulin.* Am J Physiol Endocrinol Metab, 2008. **295**(6): p. E1279-86.
16. Gao, Z., et al., *Synaptotagmin III/VII isoforms mediate Ca2+-induced insulin secretion in pancreatic islet beta -cells.* J Biol Chem, 2000. **275**(46): p. 36079-85.
17. Seino, S., et al., *Roles of cAMP signalling in insulin granule exocytosis.* Diabetes Obes Metab, 2009. **11 Suppl 4**: p. 180-8.
18. Shibasaki, T., et al., *Essential role of Epac2/Rap1 signaling in regulation of insulin granule dynamics by cAMP.* PNAS, 2007. **104**(49): p. 19333-19338.
19. Zhao, S., et al., *alpha/beta-Hydrolase domain-6-accessible monoacylglycerol controls glucose-stimulated insulin secretion.* Cell Metab, 2014. **19**(6): p. 993-1007.
20. Pessin, J.E. and A.R. Saltiel, *Signaling pathways in insulin action: molecular targets of insulin resistance.* J Clin Invest, 2000. **106**(2): p. 165-9.
21. Dimitriadis, G., et al., *Insulin effects in muscle and adipose tissue.* Diabetes Research and Clinical Practice, 2011. **93**: p. S52-S59.
22. Satoh, T., *Molecular mechanisms for the regulation of insulin-stimulated glucose uptake by small guanosine triphosphatases in skeletal muscle and adipocytes.* Int J Mol Sci, 2014. **15**(10): p. 18677-92.

23. Niswender, K.D., D.G. Baskin, and M.W. Schwartz, *Insulin and its evolving partnership with leptin in the hypothalamic control of energy homeostasis.* Trends Endocrinol Metab, 2004. **15**(8): p. 362-9.
24. Cone, R., *Anatomy and regulation of the central melanocortin system.* Nt Neurosci, 2005. **8**(5): p. 571-578.
25. Zeggini, E., et al., *Replication of genome-wide association signals in UK samples reveals risk loci for type 2 diabetes.* Science, 2007. **316**(5829): p. 1336-41.
26. Colbran, R.J., et al., *Analysis of specific interactions of native protein phosphatase 1 isoforms with targeting subunits.* Methods Enzymol, 2003. **366**: p. 156-75.
27. Cabrera, S.M., A.M. Henschel, and M.J. Hessner, *Innate inflammation in type 1 diabetes.* Transl Res, 2016. **167**(1): p. 214-27.
28. Bottazzo, G.F., A. Florin-Christensen, and D. Doniach, *Islet-Cell Antibodies in Diabetes Mellitus with Autoimmune Polyendocrine Deficiencies* The Lancet, 1974: p. 1279-1282.
29. Atkinson, M.A., G.S. Eisenbarth, and A.W. Michels, *Type 1 diabetes.* Lancet, 2014. **383**(9911): p. 69-82.
30. Gohlke, H., et al., *SLC30A8 (ZnT8) Polymorphism is Associated with Young Age at Type 1 Diabetes Onset.* The Review of Diabetic Studies. **5**(1): p. 25-27.
31. Hutton, J.C., et al., *Diagnostic and therapeutic target for autoimmune diseases and uses thereof.* 2008.
32. Graham, K.L., et al., *Pathogenic mechanisms in type 1 diabetes: the islet is both target and driver of disease.* Rev Diabet Stud, 2012. **9**(4): p. 148-68.
33. Xiu, Y., et al., *B Lymphocyte Depletion by CD20 Monoclonal Antibody Prevents Diabetes in Nonobese Diabetic Mice despite Isotype-Specific Differences in FcγR Effector Functions.* The Journal of Immunology, 2008. **180**(5): p. 2863-2875.
34. Watkins, R.A., et al., *Established and emerging biomarkers for the prediction of type 1 diabetes: a systematic review.* Transl Res, 2014. **164**(2): p. 110-21.
35. Nyenwe, E.A. and A.E. Kitabchi, *The evolution of diabetic ketoacidosis: An update of its etiology, pathogenesis and management.* Metabolism, 2016. **65**(4): p. 507-21.
36. Nonogaki, K., *New insights into sympathetic regulation of glucose and fat metabolism.* Diabetologia, 2000. **43**(5): p. 533-549.
37. Freeman, R., *Hypoglycemia and the Autonomic Nervous System BT - Diabetic Neuropathy: Clinical Management*, A. Veves and R.A. Malik, Editors. 2007, Humana Press: Totowa, NJ. p. 379-388.
38. Liljenquist, J.E., et al., *Effects of Glucagon on Lipolysis and Ketogenesis in Normal and Diabetic Men.* Journal of Clinical Investigation, 1974. **53**(1): p. 190-197.
39. Todd, J.A. and L.S. Wicker, *Genetic protection from the inflammatory disease type 1 diabetes in humans and animal models.* Immunity, 2001. **15**(3): p. 387-95.
40. Noble, J.A. and H.A. Erlich, *Genetics of type 1 diabetes.* Cold Spring Harb Perspect Med, 2012. **2**(1): p. a007732.
41. Olokoba, A.B., O.A. Obateru, and L.B. Olokoba, *Type 2 Diabetes Mellitus: A Review of Current Trends.* Oman Medical Journal, 2012. **27**(4): p. 269-273.
42. Wild, S.H. and C.D. Byrne, *Risk factors for diabetes and coronary heart disease.* BMJ : British Medical Journal, 2006. **333**(7576): p. 1009-1011.
43. Chang, S.A., *Smoking and type 2 diabetes mellitus.* Diabetes Metab J, 2012. **36**(6): p. 399-403.
44. Castro, A.V.B., et al., *Obesity, insulin resistance and comorbidities – Mechanisms of association.* Arq Bras Endocrinol Metabol, 2014. **58**(6): p. 600-609.
45. Mosser, R.E., et al., *High-fat diet-induced beta-cell proliferation occurs prior to insulin resistance in C57Bl/6J male mice.* Am J Physiol Endocrinol Metab, 2015. **308**(7): p. E573-82.

46. Sladek, R., et al., *A genome-wide association study identifies novel risk loci for type 2 diabetes.* Nature, 2007. **445**(7130): p. 881-5.
47. Yaghootkar, H. and T.M. Frayling, *Recent progress in the use of genetics to understand links between type 2 diabetes and related metabolic traits.* Genome Biol, 2013. **14**(3): p. 203.
48. Muoio, D.M. and C.B. Newgard, *Mechanisms of disease: molecular and metabolic mechanisms of insulin resistance and beta-cell failure in type 2 diabetes.* Nat Rev Mol Cell Biol, 2008. **9**(3): p. 193-205.
49. Samuel, V.T., et al., *Inhibition of protein kinase Cepsilon prevents hepatic insulin resistance in nonalcoholic fatty liver disease.* J Clin Invest, 2007. **117**(3): p. 739-45.
50. Kim, J.K., et al., *PKC-theta knockout mice are protected from fat-induced insulin resistance.* J Clin Invest, 2004. **114**(6): p. 823-7.
51. Eizirik, D.c.L., A.K. Cardozo, and M. Cnop, *The Role for Endoplasmic Reticulum Stress in Diabetes Mellitus.* Endocrine Reviews, 2008. **29**(1): p. 42-61.
52. Goodge, K.A. and J.C. Hutton, *Translational regulation of proinsulin biosynthesis and proinsulin conversion in the pancreaticβ-cell.* Seminars in Cell & Developmental Biology, 2000. **11**(4): p. 235-242.
53. Fonseca, S.G., J. Gromada, and F. Urano, *Endoplasmic reticulum stress and pancreatic beta-cell death.* Trends Endocrinol Metab, 2011. **22**(7): p. 266-74.
54. Ernst, J., et al., *Mapping and analysis of chromatin state dynamics in nine human cell types.* Nature, 2011. **473**(7345): p. 43-9.
55. Wang, M. and R.J. Kaufman, *The impact of the endoplasmic reticulum protein-folding environment on cancer development.* Nat Rev Cancer, 2014. **14**(9): p. 581-597.
56. Xia, J.Y., et al., *Targeted Induction of Ceramide Degradation Leads to Improved Systemic Metabolism and Reduced Hepatic Steatosis.* Cell Metab, 2015. **22**(2): p. 266-78.
57. Holland, W.L., et al., *An FGF21-adiponectin-ceramide axis controls energy expenditure and insulin action in mice.* Cell Metab, 2013. **17**(5): p. 790-7.
58. Konstantynowicz-Nowicka, K., et al., *New evidence for the role of ceramide in the development of hepatic insulin resistance.* PLoS One, 2015. **10**(1): p. e0116858.
59. Koves, T.R., et al., *Mitochondrial overload and incomplete fatty acid oxidation contribute to skeletal muscle insulin resistance.* Cell Metab, 2008. **7**(1): p. 45-56.
60. Shimabukuro, M., et al., *Fatty acid-induced beta cell apoptosis: a link between obesity and diabetes.* Proc Natl Acad Sci U S A, 1998. **95**(5): p. 2498-502.
61. Qiao, L., et al., *Adiponectin Reduces Plasma Triglyceride by Increasing VLDL Triglyceride Catabolism.* Diabetes, 2008. **57**(7): p. 1824 LP-1833.
62. Felig, P., E. Marliss, and J. George F. Cahill, *Plasma Amino Acid Levels and Insulin Secretion in Obesity.* The New England Journal of Medicine, 1969. **281**(15): p. 811-816.
63. Um, S.H., D. D'Alessio, and G. Thomas, *Nutrient overload, insulin resistance, and ribosomal protein S6 kinase 1, S6K1.* Cell Metab, 2006. **3**(6): p. 393-402.
64. Ackermann, A.M. and M. Gannon, *Molecular regulation of pancreatic beta-cell mass development, maintenance, and expansion.* J Mol Endocrinol, 2007. **38**(1-2): p. 193-206.
65. Alfaradhi, M.Z. and S.E. Ozanne, *Developmental programming in response to maternal overnutrition.* Front Genet, 2011. **2**: p. 27.
66. Cheng, D., *Prevalence, predisposition and prevention of type II diabetes.* Nutr Metab (Lond), 2005. **2**: p. 29.
67. Viollet, B., et al., *Cellular and molecular mechanisms of metformin: an overview.* Clin Sci (Lond), 2012. **122**(6): p. 253-70.
68. Hauner, H., *The mode of action of thiazolidinediones.* Diabetes Metab Res Rev, 2002. **18 Suppl 2**: p. S10-5.

69. Cernea, S. and M. Dobreanu, *Diabetes and beta cell function: from mechanisms to evaluation and clinical implications.* Biochemia Medica, 2013: p. 266-280.
70. Sola, D., et al., *Sulfonylureas and their use in clinical practice.* Arch Med Sci, 2015. **11**(4): p. 840-8.
71. Rosengren, A., et al., *Why Treatment Fails in Type 2 Diabetes.* PLoS Med, 2008. **5**(10): p. e215.
72. Kim, W. and J.M. Egan, *The role of incretins in glucose homeostasis and diabetes treatment.* Pharmacol Rev, 2008. **60**(4): p. 470-512.
73. Zou, H., B. Zhou, and G. Xu, *SGLT2 inhibitors: a novel choice for the combination therapy in diabetic kidney disease.* Cardiovascular Diabetology, 2017. **16**(1): p. 65-65.
74. Trujillo, J.M. and W.A. Nuffer, *Impact of Sodium-Glucose Cotransporter 2 Inhibitors on Nonglycemic Outcomes in Patients with Type 2 Diabetes.* Pharmacotherapy, 2017. **37**(4): p. 481-491.
75. Anik, A., et al., *Maturity-onset diabetes of the young (MODY): an update.* J Pediatr Endocrinol Metab, 2015. **28**(3-4): p. 251-63.
76. Pun, P., et al., *Neonatal Diabetes Mellitus: The Impact of Molecular Diagnosis.* NeoReviews, 2010. **11**(6): p. e306.
77. Pearson, E.R., et al., *Switching from Insulin to Oral Sulfonylureas in Patients with Diabetes Due to Kir6.2 Mutations.* New England Journal of Medicine, 2006. **355**(5): p. 467-477.
78. Agha-Jaffar, R., et al., *Gestational diabetes mellitus: does an effective prevention strategy exist?* Nat Rev Endocrinol, 2016. **12**(9): p. 533-46.
79. Lowe, W.L., Jr., et al., *Genetics of Gestational Diabetes Mellitus and Maternal Metabolism.* Curr Diab Rep, 2016. **16**(2): p. 15.
80. Le, T.N., et al., *Prolactin Receptor Gene Polymorphisms Are Associated with Gestational Diabetes.* Genetic Testing and Molecular Biomarkers, 2013. **17**(7): p. 567-571.
81. Barak, Y., et al., *PPARg Is Required for Placental, Cardiac, and Adipose Tissue Development.* Molecular Cell, 1999. **4**: p. 585-595.
82. Das, S.K. and S.C. Elbein, *The Genetic Basis of Type 2 Diabetes.* Cellscience, 2006. **2**(4): p. 100-131.
83. Miki, T., et al., *Defective insulin secretion and enhanced insulin action in KATP channel-deficient mice.* Proc. Natl. Acad. Sci., 1998. **95**: p. 10402-10406.
84. Seghers, V., et al., *Sur1 Knockout Mice: A Model for KATP Channel-Independent Regulation of Insulin Secretion.* Journal of Biological Chemistry, 2000. **275**(13): p. 9270-9277.
85. Odgerel, Z., et al., *Genetic variants in potassium channels are associated with type 2 diabetes in a Mongolian population.* J Diabetes, 2012. **4**(3): p. 238-42.
86. Inoue, H., et al., *Sequence Variants in the Sulfonylurea Receptor (SUR) Gene Are Associated With NIDDM in Caucasians.* Diabetes, 1996. **45**(6): p. 825-830.
87. Hart, L.M., et al., *Variants in the sulphonylurea receptor gene: association of the exon 16–3t variant with Type II diabetes mellitus in Dutch Caucasians.* Diabetologia, 1999. **42**(5): p. 617-620.
88. Meirhaeghe, A., et al., *Impact of Sulfonylurea Receptor 1 Genetic Variability on Non-Insulin-Dependent Diabetes Mellitus Prevalence and Treatment: A Population Study.* American Journal of Medical Genetics, 2001. **101**: p. 4-8.
89. Barroso, I., et al., *Correction: Candidate Gene Association Study in Type 2 Diabetes Indicates a Role for Genes Involved in β-Cell Function as Well as Insulin Action.* PLOS Biology, 2003. **1**(3): p. e92.
90. Hani, E.H., et al., *Missense mutations in the pancreatic islet beta cell inwardly rectifying K+ channel gene (KIR6.2/BIR): a meta-analysis suggests a role in the polygenic basis of Type II diabetes mellitus in Caucasians.* Diabetologia, 1998. **41**(12): p. 1511-5.

91. Laukkanen, O., et al., *Polymorphisms of the SUR1 (ABCC8) and Kir6.2 (KCNJ11) genes predict the conversion from impaired glucose tolerance to type 2 diabetes. The Finnish Diabetes Prevention Study.* J Clin Endocrinol Metab, 2004. **89**(12): p. 6286-90.
92. Nielsen, E.-M.D., et al., *The E23K Variant of Kir6.2 Associates With Impaired Post-OGTT Serum Insulin Response and Increased Risk of Type 2 Diabetes.* Diabetes, 2003. **52**(2): p. 573-577.
93. Hart, L.M.t., et al., *Variations in Insulin Secretion in Carriers of the E23K Variant in the KIR6.2 Subunit of the ATP-Sensitive K Channel in the Beta-Cell.* Diabetes, 2002. **51**(3135-3138).
94. Ahlqvist, E., T.S. Ahluwalia, and L. Groop, *Genetics of type 2 diabetes.* Clin Chem, 2011. **57**(2): p. 241-54.
95. Ishihara, H., et al., *Disruption of the WFS1 gene in mice causes progressive beta-cell loss and impaired stimulus-secretion coupling in insulin secretion.* Hum Mol Genet, 2004. **13**(11): p. 1159-70.
96. Sandhu, M.S., et al., *Common variants in WFS1 confer risk of type 2 diabetes.* Nature Genetics, 2007. **39**(8): p. 951-953.
97. Minton, J.A.L., et al., *Association Studies of Genetic Variation in the WFS1 Gene and Type 2 Diabetes in U.K. Populations.* Diabetes, 2002. **51**: p. 1287-1290.
98. Franks, P.W., et al., *Replication of the association between variants in the WFS1 gene and risk of type 2 diabetes in European populations.* Diabetologia, 2008. **51**(3): p. 458-463.
99. Bush, W.S. and J.H. Moore, *Chapter 11: Genome-wide association studies.* PLoS Comput Biol, 2012. **8**(12): p. e1002822.
100. Baron, M., *The search for complex disease genes: fault by linkage or fault by association?* Molecular Psychiatry, 2001. **6**: p. 143-149.
101. Horikawa, Y., et al., *Replication of genome-wide association studies of type 2 diabetes susceptibility in Japan.* J Clin Endocrinol Metab, 2008. **93**(8): p. 3136-41.
102. Elbein, S.C., et al., *Role of Calpain-10 Gene Variants in Familial Type 2 Diabetes in Caucasians.* The Journal of Clinical Endocrinology & Metabolism, 2002. **87**(2): p. 650-654.
103. Song, Y., et al., *Common genetic variation in calpain-10 gene (CAPN10) and diabetes risk in a multi-ethnic cohort of American postmenopausal women.* Hum Mol Genet, 2007. **16**(23): p. 2960-71.
104. Shao, W., et al., *The Wnt Signaling Pathway Effector TCF7L2 Controls Gut and Brain Proglucagon Gene Expression and Glucose Homeostasis.* Diabetes, 2013. **62**: p. 789-800.
105. Marfil, V., et al., *Interaction between Hhex and SOX13 modulates Wnt/TCF activity.* J Biol Chem, 2010. **285**(8): p. 5726-37.
106. Zhang, J., et al., *The diabetes gene Hhex maintains delta-cell differentiation and islet function.* Genes Dev, 2014. **28**(8): p. 829-34.
107. Dina, C., et al., *Variation in FTO contributes to childhood obesity and severe adult obesity.* Nat Genet, 2007. **39**(6): p. 724-726.
108. Frayling, T.M., et al., *A common variant in the FTO gene is associated with body mass index and predisposes to childhood and adult obesity.* Science, 2007. **316**(5826): p. 889-94.
109. Grarup, N., et al., *Association Testing of Novel Type 2 Diabetes Risk Alleles in the JAZF1, CDC123/CAMK1D, TSPAN8, THADA, ADAMTS9, and NOTCH2 Loci With Insulin Release, Insulin Sensitivity, and Obesity in a Population-Based Sample of 4,516 Glucose-Tolerant Middle-Aged Danes.* Diabetes, 2008. **57**(9): p. 2534-2540.
110. Tartaglia, L.A., *The Leptin Receptor.* The Journal of Biological Chemistry, 1997. **272**(10): p. 6093-6096.
111. Klok, M.D., S. Jakobsdottir, and M.L. Drent, *The role of leptin and ghrelin in the regulation of food intake and body weight in humans: a review.* Obes Rev, 2007. **8**(1): p. 21-34.

112. Pandit, R., S. Beerens, and R.A.H. Adan, *Role of leptin in energy expenditure: the hypothalamic perspective.* Am J Physiol Regul Integr Comp Physiol, 2017. **312**(6): p. R938-R947.
113. King, A.J., *The use of animal models in diabetes research.* Br J Pharmacol, 2012. **166**(3): p. 877-94.
114. Kjørholt, C., et al., *Chronic Hyperglycemia, Independent of Plasma Lipid Levels, Is Sufficient for the Loss of β-Cell Differentiation and Secretory Function in the db/db Mouse Model of Diabetes.* Diabetes, 2005. **54**(9): p. 2755 LP-2763.
115. Shafrir, E., E. Ziv, and L. Mosthaf, *Nutritionally Induced Insulin Resistance and Receptor Defect Leading to β-Cell Failure in Animal Models.* Annals of the New York Academy of Sciences, 1999. **892**(1): p. 223-246.
116. Song, J., et al., *Brain expression of Cre recombinase driven by pancreas-specific promoters.* Genesis: The Journal of Genetics and Development, 2010. **48**(11): p. 628-634.
117. Wang, Y., et al., *Recombinase technology: applications and possibilities.* Plant Cell Rep, 2011. **30**(3): p. 267-85.
118. Thorens, B., et al., *Ins1Cre knock-in mice for beta cell-specific gene recombination.* Diabetologia, 2015. **58**: p. 558-565.
119. Kelleher, S.L., et al., *Zinc in specialized secretory tissues: roles in the pancreas, prostate, and mammary gland.* Adv Nutr, 2011. **2**(2): p. 101-11.
120. Hutton, J.C., E.J. Penn, and M. Peshavaria, *Low-molecular-weight constituents of isolated insulin-secretory granules: Bivalent cations, adenine nucleotides and inorganic phosphate.* Biochem. J., 1983(210): p. 297-305.
121. Rutter, G.A. and F. Chimienti, *SLC30A8 mutations in type 2 diabetes.* Diabetologia, 2015. **58**(1): p. 31-6.
122. Chausmer, A.B., *Zinc, insulin and diabetes.* J Am Coll Nutr, 1998. **17**(2): p. 109-15.
123. Cunningham, L.W., R.L. Fischer, and C.S. Vestling, *A Study of the Binding of Zinc and Cobalt by Insulin.* Journal of the American Chemical Society, 1955. **77**(21): p. 5703-5707.
124. Foster, M.C., et al., *Elemental composition of secretory granules in pancreatic islets of Langerhans.* Biophysical Journal, 1993. **64**(2): p. 525-532.
125. Aspinwall, C.A., et al., *Effects of Intravesicular H1 and Extracellular H1 and Zn21 on Insulin Secretion in Pancreatic Beta Cells.* The Journal of Biological Chemistry, 1997. **272**(50): p. 31308-31314.
126. Ranasinghe, P., et al., *Zinc and diabetes mellitus: understanding molecular mechanisms and clinical implications.* Daru, 2015. **23**: p. 44.
127. Bēgin-Heick, N., et al., *Zinc Supplementation Attenuates Insulin Secretory Activity in Pancreatic Islets of the ob/ob Mouse.* Diabetes, 1985. **34**(2): p. 179-184.
128. Tamaki, M., et al., *The diabetes-susceptible gene SLC30A8/ZnT8 regulates hepatic insulin clearance.* J Clin Invest, 2013. **123**(10): p. 4513-24.
129. Chimienti, F., *Zinc, pancreatic islet cell function and diabetes: new insights into an old story.* Nutr Res Rev, 2013. **26**(1): p. 1-11.
130. Zhou, H., et al., *Zinc, not insulin, regulates the rat alpha-cell response to hypoglycemia in vivo.* Diabetes, 2007. **56**(4): p. 1107-12.
131. Andersson, K.-E., H.D. L. Bratt, and E. Lanner, *Some Aspects of the Intestinal Absorption of Zinc in Man.* European Journal of Clinical Pharmacology, 1976. **9**: p. 423-428.
132. Cameron, A.R., et al., *Zinc-dependent effects of small molecules on the insulin-sensitive transcription factor FOXO1a and gluconeogenic genes.* Metallomics, 2010. **2**(3): p. 195-203.
133. Myers, S.A., *Zinc transporters and zinc signaling: new insights into their role in type 2 diabetes.* Int J Endocrinol, 2015. **2015**: p. 167503.
134. Song, Y., et al., *Zinc deficiency affects DNA damage, oxidative stress, antioxidant defenses, and DNA repair in rats.* J Nutr, 2009. **139**(9): p. 1626-31.

135. Prasad, A.S., *Zinc is an Antioxidant and Anti-Inflammatory Agent: Its Role in Human Health.* Front Nutr, 2014. **1**: p. 14.
136. Scott, D.A. and A.M. Fisher, *The Insulin and the Zinc Content of Normal and Diabetic Pancreas.* Journal of Clinical Investigation, 1938. **17**(6): p. 725-728.
137. S, P., S. Pasula, and K. Sameera, *Trace elements in diabetes mellitus.* J Clin Diagn Res, 2013. **7**(9): p. 1863-5.
138. Al-Timimi, D.J., D.M. Sulieman, and K.R. Hussen, *Zinc status in type 2 diabetic patients: relation to the progression of diabetic nephropathy.* J Clin Diagn Res, 2014. **8**(11): p. CC04-8.
139. Jayawardena, R., et al., *Effects of zinc supplementation on diabetes mellitus: a systematic review and meta-analysis.* Diabetology & Metabolic Syndrome, 2012. **4**(13).
140. Simon, S.F. and C.G. Taylor, *Dietary zinc supplementation attenuates hyperglycemia in db/db mice.* Exp Biol Med (Maywood), 2001. **226**(1): p. 43-51.
141. Wang, X., et al., *Effect of zinc supplementation on type 2 diabetes parameters and liver metallothionein expressions in Wistar rats.* J Physiol Biochem, 2012. **68**(4): p. 563-72.
142. Borovansky, J. and P.A. Riley, *CYTOTOXICITY OF ZINC IN VITRO.* Chem-Biol Interactions, 1989. **69**: p. 279-291.
143. Hennigar, S.R. and S.L. Kelleher, *Zinc networks: the cell-specifi c compartmentalization of zinc for specialized functions.* Biol Chem, 2012. **393**: p. 565-578.
144. Maret, W., *The Function of Zinc Metallothionein: A Link between Cellular Zinc and Redox State.* Journal of Nutrition, 2000. **130**: p. 1455S-1458S.
145. Cherezov, V., et al., *Insights into the mode of action of a putative zinc transporter CzrB in Thermus thermophilus.* Structure, 2008. **16**(9): p. 1378-88.
146. Martel, G., et al., *Zinc transporter ZnT3 is involved in memory dependent on the hippocampus and perirhinal cortex.* Behav Brain Res, 2011. **223**(1): p. 233-8.
147. Smidt, K., et al., *The zinc transporter ZNT3 co-localizes with insulin in INS-1E pancreatic beta cells and influences cell survival, insulin secretion capacity, and ZNT8 expression.* Biometals, 2016. **29**(2): p. 287-98.
148. Inoue, K., et al., *Osteopenia and male-specific sudden cardiac death in mice lacking a zinc transporter gene, Znt5.* Human Molecular Genetics, 2002. **11**(15): p. 1775-1784.
149. Sheline, C.T., et al., *Dietary zinc reduction, pyruvate supplementation, or zinc transporter 5 knockout attenuates beta-cell death in nonobese diabetic mice, islets, and insulinoma cells.* J Nutr, 2012. **142**(12): p. 2119-27.
150. Kirschke, C.P. and L. Huang, *ZnT7, a novel mammalian zinc transporter, accumulates zinc in the Golgi apparatus.* J Biol Chem, 2003. **278**(6): p. 4096-102.
151. Huang, L., et al., *Znt7 (Slc30a7)-deficient mice display reduced body zinc status and body fat accumulation.* J Biol Chem, 2007. **282**(51): p. 37053-63.
152. Huang, L., et al., *Znt7-null mice are more susceptible to diet-induced glucose intolerance and insulin resistance.* J Biol Chem, 2012. **287**(40): p. 33883-96.
153. Huang, L., M. Yan, and C.P. Kirschke, *Over-expression of ZnT7 increases insulin synthesis and secretion in pancreatic beta-cells by promoting insulin gene transcription.* Exp Cell Res, 2010. **316**(16): p. 2630-43.
154. Chimienti, F., A. Favier, and M. Seve, *ZnT-8, a pancreatic beta-cell-specific zinc transporter.* Biometals, 2005. **18**(4): p. 313-7.
155. Chimienti, F., et al., *In vivo expression and functional characterization of the zinc transporter ZnT8 in glucose-induced insulin secretion.* J Cell Sci, 2006. **119**(Pt 20): p. 4199-206.
156. Pound, L.D., et al., *Deletion of the mouse Slc30a8 gene encoding zinc transporter-8 results in impaired insulin secretion.* Biochem J, 2009. **421**(3): p. 371-376.
157. Nica, A.C., et al., *Cell-type, allelic, and genetic signatures in the human pancreatic beta cell transcriptome.* Genome Res, 2013. **23**(9): p. 1554-62.

158. Pound, L.D., et al., *Characterization of the human SLC30A8 promoter and intronic enhancer.* J Mol Endocrinol, 2011. **47**(3): p. 251-9.
159. Pound, L.D., et al., *The physiological effects of deleting the mouse slc30a8 gene encoding zinc transporter-8 are influenced by gender and genetic background.* PLoS One, 2012. **7**(7): p. e40972.
160. Eizirik, D.L., et al., *The human pancreatic islet transcriptome: expression of candidate genes for type 1 diabetes and the impact of pro-inflammatory cytokines.* PLoS Genet, 2012. **8**(3): p. e1002552.
161. Mohanasundaram, D., et al., *Ultrastructural analysis, zinc transporters, glucose transporters and hormones expression in New world primate (Callithrix jacchus) and human pancreatic islets.* Gen Comp Endocrinol, 2011. **174**(2): p. 71-9.
162. Schweiger, M., M. Steffl, and W.M. Amselgruber, *The zinc transporter ZnT8 (slc30A8) is expressed exclusively in beta cells in porcine islets.* Histochem Cell Biol, 2013. **140**(6): p. 677-84.
163. Leung, K.W., et al., *Expression of ZnT and ZIP zinc transporters in the human RPE and their regulation by neurotrophic factors.* Invest Ophthalmol Vis Sci, 2008. **49**(3): p. 1221-31.
164. Deniro, M. and F.A. Al-Mohanna, *Zinc transporter 8 (ZnT8) expression is reduced by ischemic insults: a potential therapeutic target to prevent ischemic retinopathy.* PLoS One, 2012. **7**(11): p. e50360.
165. Smidt, K., et al., *Zinc-transporter genes in human visceral and subcutaneous adipocytes: lean versus obese.* Mol Cell Endocrinol, 2007. **264**(1-2): p. 68-73.
166. Liu, B.Y., et al., *Down-regulation of zinc transporter 8 in the pancreas of db/db mice is rescued by Exendin-4 administration.* Mol Med Rep, 2011. **4**(1): p. 47-52.
167. Murgia, C., et al., *Diabetes-linked zinc transporter ZnT8 is a homodimeric protein expressed by distinct rodent endocrine cell types in the pancreas and other glands.* Nutr Metab Cardiovasc Dis, 2009. **19**: p. 431-439.
168. Zhong, M.L., et al., *Widespread expression of zinc transporter ZnT (SLC30) family members in mouse endocrine cells.* Histochem Cell Biol, 2012. **138**(4): p. 605-16.
169. Pound, L.D., et al., *The pancreatic islet beta-cell-enriched transcription factor Pdx-1 regulates Slc30a8 gene transcription through an intronic enhancer.* Biochem J, 2011. **433**(1): p. 95-105.
170. Lemaire, K., et al., *Insulin crystallization depends on zinc transporter ZnT8 expression, but is not required for normal glucose homeostasis in mice.* Proc Natl Acad Sci U S A, 2009. **106**(35): p. 14872-7.
171. Wijesekara, N., et al., *Beta cell-specific Znt8 deletion in mice causes marked defects in insulin processing, crystallisation and secretion.* Diabetologia, 2010. **53**(8): p. 1656-68.
172. Nicolson, T.J., et al., *Insulin storage and glucose homeostasis in mice null for the granule zinc transporter ZnT8 and studies of the type 2 diabetes-associated variants.* Diabetes, 2009. **58**: p. 2070-2083.
173. Hardy, A.B., et al., *Effects of high-fat diet feeding on Znt8-null mice: differences between beta-cell and global knockout of Znt8.* Am J Physiol Endocrinol Metab, 2012. **302**(9): p. E1084-96.
174. Mitchell, R.K., et al., *Molecular Genetic Regulation of Slc30a8/ZnT8 Reveals a Positive Association With Glucose Tolerance.* Mol Endocrinol, 2016. **30**(1): p. 77-91.
175. Lee, J.Y., et al., *RIP-Cre revisited, evidence for impairments of pancreatic beta-cell function.* J Biol Chem, 2006. **281**(5): p. 2649-53.
176. Syring, K.E., et al., *Combined Deletion of Slc30a7 and Slc30a8 Unmasks a Critical Role for ZnT8 in Glucose-Stimulated Insulin Secretion.* Endocrinology, 2016. **157**(12): p. 4534-4541.
177. Windelov, J.A., J. Pedersen, and J.J. Holst, *Use of anesthesia dramatically alters the oral glucose tolerance and insulin secretion in C57Bl/6 mice.* Physiol Rep, 2016. **4**(11).

178. Feng, C., et al., *Isoflurane anesthesia exacerbates learning and memory impairment in zinc-deficient APP/PS1 transgenic mice.* Neuropharmacology, 2016. **111**: p. 119-129.
179. Rij, A.M.V. and M.T. Hall, *The Effect of Anesthetic Agents on Zinc Metabolism in the Rat Liver.* Biological Trace Element Research, 1985. **8**: p. 231-235.
180. Beintema, J.J. and R.N. Campagne, *Molecular evolution of rodent insulins.* Mol Biol Evol, 1987. **4**(1): p. 10-8.
181. Zimmerman, A.E. and C.C. Yip, *Guinea pig insulin. I. Purification and physical properties.* J Biol Chem, 1974. **249**(13): p. 4021-5.
182. Scott, L.J., et al., *A genome-wide association study of type 2 diabetes in Finns detects multiple susceptibility variants.* Science, 2007. **316**(5829): p. 1341-5.
183. Saxena, R., et al., *Genome-wide association analysis identifies loci for type 2 diabetes and triglyceride levels.* Science, 2007. **316**(5829): p. 1331-6.
184. Kirchhoff, K., et al., *Polymorphisms in the TCF7L2, CDKAL1 and SLC30A8 genes are associated with impaired proinsulin conversion.* Diabetologia, 2008. **51**(4): p. 597-601.
185. Xu, K., et al., *Association between rs13266634 C/T polymorphisms of solute carrier family 30 member 8 (SLC30A8) and type 2 diabetes, impaired glucose tolerance, type 1 diabetes--a meta-analysis.* Diabetes Res Clin Pract, 2011. **91**(2): p. 195-202.
186. Boesgaard, T.W., et al., *The common SLC30A8 Arg325Trp variant is associated with reduced first-phase insulin release in 846 non-diabetic offspring of type 2 diabetes patients--the EUGENE2 study.* Diabetologia, 2008. **51**(5): p. 816-20.
187. Faccinetti, N.I., et al., *Characterization of zinc transporter 8 (ZnT8) antibodies in autoimmune diabetic patients from Argentinian population using monomeric, homodimeric, and heterodimeric ZnT8 antigen variants.* Eur J Endocrinol, 2016. **174**(2): p. 157-65.
188. Merriman, C., et al., *Lipid-tuned Zinc Transport Activity of Human ZnT8 Protein Correlates with Risk for Type-2 Diabetes.* J Biol Chem, 2016. **291**(53): p. 26950-26957.
189. Wong, W.P., et al., *Exploring the Association Between Demographics, SLC30A8 Genotype, and Human Islet Content of Zinc, Cadmium, Copper, Iron, Manganese and Nickel.* Sci Rep, 2017. **7**(1): p. 473.
190. Flannick, J., et al., *Loss-of-function mutations in SLC30A8 protect against type 2 diabetes.* Nat Genet, 2014. **46**(4): p. 357-63.
191. Orban, T., et al., *Pancreatic islet autoantibodies as predictors of type 1 diabetes in the Diabetes Prevention Trial-Type 1.* Diabetes Care, 2009. **32**(12): p. 2269-74.
192. Wattler, S., M. Kelly, and M. Nehls, *Construction of gene targeting vectors from lambda KOS genomic libraries.* Biotechniques, 1999. **26**(6): p. 1150-6, 1158, 1160.
193. Brouwers, B., et al., *Impaired islet function in commonly used transgenic mouse lines due to human growth hormone minigene expression.* Cell Metab, 2014. **20**(6): p. 979-90.
194. Boortz, K.A., et al., *G6PC2 Modulates Fasting Blood Glucose In Male Mice in Response to Stress.* Endocrinology, 2016. **157**: p. 3002-3008.
195. Boortz, K.A., et al., *G6PC2 Modulates the Effects of Dexamethasone on Fasting Blood Glucose and Glucose Tolerance.* Endocrinology, 2016. **157**: p. 4133-4145.
196. Sambrook, J., Fritsch, EF and Maniatis T, *Molecular Cloning: A Laboratory Manual*. 2nd ed. 1989, Plainview, NY: Cold Spring Harbor Laboratory Press.
197. Dai, C., et al., *Islet-enriched gene expression and glucose-induced insulin secretion in human and mouse islets.* Diabetologia, 2012. **55**(3): p. 707-18.
198. Livak, K.J. and T.D. Schmittgen, *Analysis of relative gene expression data using real-time quantitative PCR and the 2(-Delta Delta C(T)) Method.* Methods, 2001. **25**(4): p. 402-8.
199. Zhang, H., et al., *Efficient recombination in pancreatic islets by a tamoxifen-inducible Cre-recombinase.* Genesis, 2005. **42**(3): p. 210-7.

200. Adkins, B.A., et al., *Importance of the route of intravenous glucose delivery to hepatic glucose balance in the conscious dog.* J Clin Invest, 1987. **79**(2): p. 557-65.
201. Wang, Y., et al., *Deletion of the gene encoding the ubiquitously expressed glucose-6-phosphatase catalytic subunit-related protein (UGRP)/glucose-6-phosphatase catalytic subunit-beta results in lowered plasma cholesterol and elevated glucagon.* J Biol Chem, 2006. **281**(52): p. 39982-9.
202. Hassid, W.Z. and S. Abraham, *Determination of Glycogen with anthrone reagent.* Methods Enzymol, 1957. **3**: p. 34-38.
203. Bruss, M.L. and A.L. Black, *Enzymatic microdetermination of glycogen.* Analytical Biochemistry, 1978. **84**(1): p. 309-312.
204. Kunst, A., B. Dreager, and J. Ziegenhorn, *UV methods with Hexokinase and Glucose-6-phosphate Dehydrogenase.* Methods of Enzymatic Analysis, 1981. **VI Metabol**: p. 163-172.
205. Kayton, N.S., et al., *Human Islet Preparations Distributed for Research Exhibit a Variety of Insulin Secretory Profiles.* Am J Physiol Endocrinol Metab, 2015. **308**: p. E592-602.
206. Golson, M.L., et al., *High Fat Diet Regulation of beta-Cell Proliferation and beta-Cell Mass.* Open Endocrinol J, 2010. **4**.
207. Golson, M.L., et al., *Activated FoxM1 Attenuates Streptozotocin-Mediated beta-Cell Death.* Mol Endocrinol, 2014. **28**(9): p. 1435-47.
208. Golson, M.L., W.S. Bush, and M. Brissova, *Automated quantification of pancreatic beta-cell mass.* Am J Physiol Endocrinol Metab, 2014. **306**(12): p. E1460-7.
209. Hohmeier, H.E., et al., *Isolation of INS-1-derived cell lines with robust ATP-sensitive K+ channel-dependent and -independent glucose-stimulated insulin secretion.* Diabetes, 2000. **49**(3): p. 424-30.
210. Tuli, J.S., J.A. Smith, and D.B. Morton, *Corticosterone, adrenal and spleen weight in mice after tail bleeding, and its effect on nearby animals.* Lab Anim, 1995. **29**(1): p. 90-5.
211. Teilmann, A.C., et al., *Physiological and pathological impact of blood sampling by retro-bulbar sinus puncture and facial vein phlebotomy in laboratory mice.* PLoS One, 2014. **9**(11): p. e113225.
212. Zavaroni, I., et al., *Renal metabolism of C-peptide in man.* J Clin Endocrinol Metab, 1987. **65**(3): p. 494-8.
213. Henquin, J.C., *The dual control of insulin secretion by glucose involves triggering and amplifying pathways in beta-cells.* Diabetes Res Clin Pract, 2011. **93 Suppl 1**: p. S27-31.
214. Huang, Q., et al., *Coupling of Insulin Secretion and Display of a Granule-resident Zinc Transporter ZnT8 on the Surface of Pancreatic beta-Cells.* J Biol Chem, 2017.
215. Li, L., S. Bai, and C.T. Sheline, *hZnT8 (slc30a8) Transgenic Mice Which Overexpress the R325W Polymorph Have Reduced Islet Zn2+ and Proinsulin Levels, Increased Glucose Tolerance After a High-Fat Diet, and Altered Levels of Pancreatic Zinc Binding Proteins.* Diabetes, 2016.
216. Muller, U., *Ten years of gene targeting: targeted mouse mutants, from vector design to phenotype analysis.* Mech Dev, 1999. **82**(1-2): p. 3-21.
217. Gingrich, J.A. and R. Hen, *The broken mouse: the role of development, plasticity and environment in the interpretation of phenotypic changes in knockout mice.* Curr Opin Neurobiol, 2000. **10**(1): p. 146-52.
218. Bockamp, E., et al., *Of mice and models: improved animal models for biomedical research.* Physiol Genomics, 2002. **11**(3): p. 115-32.
219. Barbaric, I., G. Miller, and T.N. Dear, *Appearances can be deceiving: phenotypes of knockout mice.* Brief Funct Genomic Proteomic, 2007. **6**(2): p. 91-103.
220. Prentki, M., F.M. Matschinsky, and S.R. Madiraju, *Metabolic signaling in fuel-induced insulin secretion.* Cell Metab, 2013. **18**(2): p. 162-85.

221. Dadi, P.K., et al., *Inhibition of pancreatic beta-cell Ca2+/calmodulin-dependent protein kinase II reduces glucose-stimulated calcium influx and insulin secretion, impairing glucose tolerance.* J Biol Chem, 2014. **289**(18): p. 12435-45.
222. Palnitkar, S.S., et al., *Pharmacological distinction between dantrolene and ryanodine binding sites: evidence from normal and malignant hyperthermia-susceptible porcine skeletal muscle.* Biochemistry Journal, 1997. **326**: p. 847-852.
223. Lytton, J., M. Westlin, and M.R. Hanley, *Thapsigargin Inhibits the Sarcoplasmic or Endoplasmic Reticulum Ca-ATPase Family of Calcium Pumps.* The Journal of Biological Chemistry, 1991. **266**(26): p. 17067-17071.
224. Hou, J.C., L. Min, and J.E. Pessin, *Chapter 16 Insulin Granule Biogenesis, Trafficking and Exocytosis.* 2009. **80**: p. 473-506.
225. Rocheleau, J.V., W.S. Head, and D.W. Piston, *Quantitative NAD(P)H/flavoprotein autofluorescence imaging reveals metabolicmechanisms of pancreatic islet pyruvate response.* Journal of Biological Chemistry, 2004. **279**(30): p. 31780-31787.
226. Wall, M.L., et al., *Novel Stable Isotope Analyses Demonstrate Significant Rates of Glucose Cycling In Mouse Pancreatic Islets.* Diabetes, 2015. **64** (6): p. 2129-2137.
227. Fu, Y., et al., *Down-regulation of ZnT8 expression in INS-1 rat pancreatic beta cells reduces insulin content and glucose-inducible insulin secretion.* PLoS One, 2009. **4**(5): p. e5679.
228. Bates, B., et al., *Neurotrophin-3 is required for proper cerebellar development.* Nature Neuroscience, 1999. **2**(2): p. 115-117.